1992

Finite element and boundary element analysis of electromagnetic NDE phenomena

Shridhar Nath
Iowa State University

Order Number 9311520

Finite element and boundary element analysis of electromagnetic NDE phenomena

Nath, Shridhar, Ph.D.

Iowa State University, 1992

U·M·I
300 N. Zeeb Rd.
Ann Arbor, MI 48106

Finite element and boundary element analysis of electromagnetic NDE phenomena

by

Shridhar Nath

A Dissertation Submitted to the

Graduate Faculty in Partial Fulfillment of the

Requirements for the Degree of

DOCTOR OF PHILOSOPHY

Department: Electrical Engineering and Computer Engineering
Major: Electrical Engineering (Electromagnetics)

Approved:

Signature was redacted for privacy.

In Charge of Major Work

Signature was redacted for privacy.

For the Major Department

Signature was redacted for privacy.

For the Graduate College

Members of the Committee:

Signature was redacted for privacy.

Iowa State University
Ames, Iowa
1992

TABLE OF CONTENTS

LIST OF TABLES

LIST OF FIGURES

ACKNOWLEDGMENTS

It has been a great honor and privilege for me to have the guidance, support and encouragement of Dr William Lord the last few years. In spite of his busy schedule, he has always found the time and patience to listen and show me different avenues to continue with this research. His encouragement to teach during my graduate program and to attend conferences contributed greatly to my professional maturity.

I would also like to thank Professor Tom Rudolphi for being a patient teacher. His willingness to discuss my research at all hours of the day has played a key role in its development. I would also like to acknowledge the use of the boundary element software developed by Dr. Rudolphi.

I would like to thank my committee, Professors J.P. Basart, A.A. Read and V. Vittal for their interest and support in my work. A special thanks to the graduate students in the NDE lab, especially Zhongqing You for their helpful suggestions.

The ever present support and encouragement of my family helped me through the rough times. Last but not the least, I am indebted to my wife Shrilata as she has always been there for me when I needed her. Her friendship, support and marathon editing efforts made all this possible.

Finally, I would like to acknowledge the financial support from the Palmer Endowment, and NASA during my graduate program.

ABSTRACT

The endeavor to produce quality products coupled with a drive to minimize failure in major industries such as aerospace, power and transportation is the driving force behind studies of electromagnetic nondestructive evaluation (NDE) methods. Popular domain and integral methods used for the purpose of modeling electromagnetic NDE phenomena include the finite element and boundary element methods. However no single numerical modeling technique has emerged as the optimal choice for all electromagnetic NDE processes. In a computer aided design environment, where the choice of an optimum modeling technique is critical, an evaluation of the various aspects of different numerical approaches is extremely helpful.

In this dissertation, a comparison is made of the relative advantages and disadvantages of the finite element (FE) and boundary element (BE) methods as applied to the DC and AC Potential drop (DCPD and ACPD) methods for characterizing fatigue cracks. The comparison covers aspects of robustness, computer resource requirements and ease of numerically implementing the methods. Two dimensional FE and BE models are used to model an infinitely thin fatigue crack using the ACPD method, and a two and three dimensional FE and BE model is used to study the compact tension and single edge notch specimen using the DCPD method. Calibration curves and field plots in the specimen are compared to experimental and analytical

data. The FE and BE methods are complementary numerical techniques and are combined to exploit their individual merits in the latter part of this dissertation. A three dimensional hybrid formulation to model eddy current NDE is then developed which discretizes the interior with finite elements and the exterior with boundary elements. The three dimensional model is applied to an absolute eddy current coil over a finite block. A feasibility study to confirm the validity of the formulation is undertaken by comparing the numerical results for probe lift-off and coil impedance measurements with published data.

This comparative study outlined above indicates that when the solution is required at discrete points, as in the potential drop methods, or the model needs to handle infinite boundaries, as in eddy current NDE, the boundary element model is more suitable. Since it is based on the Green's function, the BE method is limited to linear problems. Finite element analysis gives full field solutions, making it ideal for studying energy/defect interactions. The hybrid FE/BE formulation handles non-linearity and infinite boundaries naturally, thus utilizing the *best of both worlds.*

CHAPTER 1. INTRODUCTION

Mathematical Modeling of NDE Phenomena

The endeavor to produce quality products coupled with a drive to minimize failure in major industries such as power, aerospace and transportation has provided the major impetus for new developments in nondestructive evaluation (NDE). This past decade has seen the rapid growth in computer technology, and resources, with increased usage of a computer aided design (CAD) environment. The increased demands on industry to provide reliable methods for detecting flaws is making NDE an integral part of the design process.

Any nondestructive testing (NDT) system consists of an energy source, the input transducer coupled to the material, the energy/defect interaction in the material, an output transducer and finally interpretation of the output signal. The *forward* problem deals with the input transducer, the energy/defect interaction and the output signal, while the *inversion* process interprets the output signal as it carries all the information relating to the defect. The size, shape and location of the flaw, and changes in material properties, affect the output signal. To fully characterize a defect, all this information needs to be extracted and decoded from the signal.

NDE research is concerned with the total picture, from the physics of the energy/defect interaction, to the transducer response characteristics. A number of NDE

techniques are employed to detect, characterize and size defects. These include visual inspection, radiography, ultrasonics, electromagnetic methods, acoustic emission among others. The technique adopted for a particular application depends on the material, geometry, type and size of flaw, and other factors. These different techniques can be classified mathematically by the governing partial differential equation (PDE) [1, 2, 3], or even by the excitation or energy source frequency.

In the area of electromagnetic NDE, elliptic PDEs describe flux leakage and DCPD methods, parabolic PDE's govern eddy current methods and the ACPD method, and hyperbolic PDE's describe microwave NDE. The ideal *forward* model in electromagnetic NDE should be capable of handling complex geometries and changes in the material properties, such as conductivity and permeability, and should predict the electric and magnetic fields in the vicinity of defects or inhomogeneities. This model can be achieved by solving the three dimensional (3D) field equations.

Over the years, mathematical modeling has played a key role in interpreting complex experimental signals and providing insight into the physical processes that govern all the various NDE techniques [4-8]. A good mathematical model can be used as a *test bed* to duplicate an experimental situation too difficult or expensive to replicate in the laboratory. The models can also generate training data sets for signal processing and calibration signals needed in NDT instrumentation. In contrast to numerical models, analytical approaches to model field/defect interaction or transducer responses have been limited to simple defect shapes and sizes. Numerical models overcome these limitations and are thus employed extensively in studying NDE systems.

Popular domain, numerical methods utilized to model NDE systems are the finite

difference and finite element method (FEM) while the integral methods commonly used are the moment method and the boundary element method (BEM). The FEM has proven to be superior to the finite difference scheme in accuracy and discretization flexibility. Similarly, the BEM is favored over the moment method as the number of unknowns in the system is relatively small. Though the FEM is very versatile in handling many problems, it may not be the most effective method for all electromagnetic NDE processes. Therefore it is left to the discretion of the user to choose the most suitable technique. In a CAD environment, choosing the optimum modeling technique is essential which neccesiates an evaluation of the various aspects of the different numerical techniques.

Scope of the Thesis

The main thrust of this dissertation is to develop a multiformulation strategy involving he FEM and BEM as applied to electromagnetic NDE. This involves developing and implementing finite element, boundary element and hybrid finite-boundary element formulation for specific applications and then comparing and contrasting the FEM and BEM as applied to electromagnetic NDE. One of the goals is then to identify which strategy or method is suitable for a particular application. This dissertation is restricted to static and quasi-static electromagnetic NDE applications. The DCPD method and the ACPD method are adopted as representative examples to illustrate the task of comparing the FEM and BEM in two and three dimensional models. The FEM and BEM are complementary techniques, each having its own merits and drawbacks. To compare these two methods, a number of aspects of these techniques are studied to obtain a complete picture. The study discusses the effectiveness of each

method, an essential element in the modeling of NDE phenomena. This is due to the fact that NDE is unique in its requirements for both in understanding the physics of the energy/defect interaction and in computing the sensor response.

Another important issue discussed in this dissertation is modeling implementation considerations, a prominent factor in the users decision process. For example, the computer storage and execution time requirements are compared, as such resources are crucial to the success of these models.

Considerable success has been achieved in two dimensional (2D) modeling of NDE phenomena. Modeling of steady state eddy currents has been extensively treated and reported as part of a practical defect characterization scheme [9-11] while moving eddy current coils have also been successfully modeled [12-14]. A number of three dimensional models have also been reported in the literature using finite elements and boundary elements independently [15-20]. The major considerations for a good three dimensional model are the establishment of the correct formulation and derivation of the quantities of interest such as eddy current densities, flux densities and coil impedance from the solution. Many different formulations [21-25] have been presented and used, each having its own advantages and disadvantages. Three dimensional modeling is concerned not only with the problem of discretization difficulties, but also with the vector nature of the application. There are certain problems where neither the FEM or BEM is suitable, but a combination of the two techniques is more appropriate. Thus, in the latter part of this dissertation, the salient features of both the FEM and BEM are extracted and combined in a new three dimensional hybrid formulation for eddy current NDE applications.

A detailed background study on finite elements and boundary elements pertain-

ing to low frequency electromagnetic NDE applications is presented in Chapter 2. This covers some historical information and the use of these numerical techniques in electromagnetics.

Chapter 3 covers the basic theory for the DCPD and ACPD methods and their applications. A generic finite element formulation of the Helmholtz equation is presented which covers both these cases.

The BEM, which is based on the theory of Green's functions, is the numerical implementation of a boundary integral equation (BIE). Chapter 4 discusses the significance of Greens' functions, their importance and derivation. Other integral methods such as the moment method and the indirect boundary element method are also discussed. Starting from Green's second theorem, the boundary integral equation is developed for the DCPD and ACPD methods. The DCPD method is governed by Laplace's equation, while the governing equation for the ACPD method is the diffusion equation. The Green's functions for these two specific cases are derived.

The three dimensional hybrid finite-boundary element method is discussed in detail in Chapter 5. This chapter starts with the derivation of the eddy current diffusion equation from Maxwell's equations. While alternate formulations for the field equation are reviewed, the magnetic vector potential formulation is shown to be general and most easy to use. Following this are the derivation of the finite element formulation and the boundary integral equation.

Chapter 6 is dedicated to discussing the results obtained from the two dimensional DCPD and ACPD modeling of the single edge notch and compact tension specimens for fatigue crack characterization. Results from the three dimensional model of the compact tension specimen for the DCPD method are also presented.

All of these results are compared to experimental, analytical or other numerical data cited in the literature in order to validate these models.

The motivation for studying a two and three dimensional finite element and boundary element model is to compare the two methods as applied to electromagnetic NDE. In Chapter 7, the results obtained in Chapter 6 are compared and contrasted. Tables are presented showing the computing times, memory requirements and the discretization needed to solve those problems. Recommendations are made regarding: 1. the ease of using these algorithms, and 2. applications where a certain modeling technique is preferred over another and 3. the advantages and disadvantages of both the FEM and BEM.

Chapter 8 deals with the results obtained from the feasibility study of the hybrid finite-boundary element model. The model is applied to an absolute coil scanning over an aluminum block. Lift-Off studies, probe impedance measurements and eddy current densities are computed for this situation. These results are compared to experimental and analytical data to validate the model.

To conclude this dissertation, Chapter 9 presents some final thoughts on this research and recommendations for future work in the area.

CHAPTER 2. NUMERICAL MODELING

In the evolution and application of numerical techniques a stage of development is reached when a method cannot be stretched any further to gain additional benefits. At this stage, a thorough study is required to review the method. Demerdash and Nehl [26] compared the FEM and the finite difference method (FDM) as applied to electrical machines. They concluded that the FEM was superior to FDM in accuracy, storage and computer time. Tortschanoff [27] discussed the field equations for eddy current problems and compared the FEM and FDM by using different solution techniques to solve the system of equations. Beasley et al. [28] tested the Monte Carlo method, FEM, and the charge simulation method for calculating electrostatic fields and potential. Krawczyk and Turkowski [29] stressed the necessity for choosing the technique that would satisfy the needs of the problem in the most efficient manner. Girdinio and Molinari [30] suggested the development of a multiformulation approach to the numerical computation of electromagnetic problems. The idea was to develop a single flexible tool or code, capable of managing a wide variety of formulations which are of practical interest and at the same time are user friendly. Salon and Schneider [31] compared the FEM and BEM in two dimensions by applying them to electrostatic and eddy current problems at power frequencies. Molinari [32] has presented an excellent article on the guidelines for an effective usage and considera-

tions for the development of computer codes for CAD analysis. Trowbridge [33, 34] discussed the future of electromagnetic computing and the state of the art of domain and integral methods as it was in 1990.

Finite Elements

Finite element (FE) analysis originated in the structural and civil engineering disciplines, where it was utilized to compute stresses and strains in beams with various constraints [35]. It is a powerful numerical technique for solving boundary value problems (BVP). The procedure involves: 1. functional minimization that satisfies the original differential equation, or a weighted residual approach; 2. *volume* discretization of the geometry; 3. interpolation of the unknown using specific functions; and 4. solving a set of linear equations. The method can inherently handle complex shapes, anisotropy and non-linearities and easily incorporates the boundary conditions. A major disadvantage of this method is the large memory requirements due to the volume discretization, especially when modeling unbounded problems. It was initially adapted by the electrical engineering community to study magnetic fields in electrical machines such as motors, transformers and others [36-40]. Since the governing PDEs are the same for electromagnetic NDE, the FEM has been successfully applied to static and quasi-static NDE phenomena.

In the static modeling area, Ritchie and Bathe [41] and Aaronson and Ritchie [42] predicted the fatigue crack growth in metallic specimens via the DCPD method using the FEM in 2D. The governing equation solved was Laplace's equation. This model has been accepted as a standard in fracture mechanics. Leakage field profiles have been predicted by Lord and Hwang [43,44] and Satish [45,46] by modeling Poisson's

equation in 2D. Lord, et al [47] took the process one step further and studied leakage field profiles for 3D pipeline structures. There is a wealth of information on the study of eddy currents in transformers, motors and other electrical machinery where the diffusion equation is solved. Silvester and Chari [36,48] are credited with introducing the FEM in studying electric and magnetic field interaction in machines. Lord [49-51], Palanisamy [14,52,53], and Ida [15,54] utilized the FEM to study electromagnetic field interaction in heat exchanger tubing using eddy current NDE. Their research has shown great consistency with experimental data for 2D, axisymmetric and 3D models. The physics of the remote field eddy current phenomenon was much better understood due to the FE models of Lord [55] , Sun [56], Atherton [57] and Hoshikawa [58]. One of Lord's key observations was that FE models can simulate electromagnetic NDE situations too difficult or expensive to replicate in the laboratory. Though pulsed eddy current NDE is not popular in industry, attempts have been made by researchers [59] to study the transient nature of the phenomenon. Considerable amount of effort has been devoted by Rodger [60,61], Shin [62] and others in accounting for the velocity induced field term in the diffusion equation.

A key application of the FEM is to use the technique to design transducers [63,64] by observing the magnetic fields. Since the method is versatile, it has the capability to model various parameters and study their effects. Various formulations have been used to solve both the static and quasi-static problems using the FEM. Each formulation has its advantages and disadvantages, and their use in eddy current NDE is discussed in a later chapter.

Boundary Elements

Along with FE models, integral methods are being used for the simulation of electromagnetic NDE phenomena. The development of integral methods has been advanced mainly by researchers in the antenna area. This is due to the fact that scattering and radiation problems involve unbounded regions, where integral methods are ideal techniques. Numerically these equations are solved directly by the moment method, or converted to a Fredholm equation and solved by standard iteration solvers, or converted to a boundary integral equation and solved by the boundary element method (BEM). The method of moments has been pioneered by Harrington [65] for solution of antenna patterns or electromagnetic scattering from conducting bodies. Similar to the FEM, the BEM has also been developed by researchers in the structural and civil engineering field to look at stresses and strains in beams and other structures. Brebbia [66] was one of the first researchers to introduce the BEM in the early 1970's. The first step for the BEM is the scalar or vector Green's second theorem. Identifying the appropriate Green's function and computing the fundamental solution is the next step. The *surface* of the geometry is then discretized, the unknown function interpolated using specific functions, and finally a linear set of equations is solved. A major advantage of this method is that the boundary at infinity need not be modeled since the radiation conditions are satisfied. Since it is based on a Green's function, the principle of superposition is applied, thus making the method unusable for handling non-linearities. Extensive research is underway at various institutions to develop BE algorithms for non-linear and anisotropic problems.

Simkin [67], Mayergoyz [68] and others capitalized on the benefits of integral methods and applied them to solve for magnetostatic and quasi-static problems in

electrical machinery. McWhirter [69] developed computational methods for solving 2D quasi-static problems by solving the Fredholm equation of the second kind. Lean [70-72] used the BEM to solve eddy current problems in 2D, and gave a good overview of boundary integral methods in electromagnetics [73]. Trowbridge solved the integral equations for computing eddy currents in both the accelerator and Tokamak magnets in 2D and 3D [74]. Rucker and Richter [75-77] formulated a three dimensional code for both magnetostatic and eddy current applications, while Tsuboi [78] and Tsuboi and Tanaka [79] developed an eddy current code using the BEM. Nicolas [80] developed a surface impedance formulation in conjunction with the BEM to solve both low frequency and high frequency 3D eddy current problems. In the field of NDE, Beissner [81-83], initially used the indirect integral method to compute fields around a flaw, but later used the BEM to calculate the fields around a 3D defect. Dunbar [84] solved a volume integral (similar to the indirect method) to obtain fields everywhere in the flaw volume and also emphasized the need for a hybrid approach for complicated geometries. Kahn [85] used the BEM to study the flaw interaction in 2D crack problems. Tsuboi and Misaki [86] computed the 3D field distribution in steel pipes using the BEM. All these researchers solve the diffusion equation in the integral form. Conolly [87] applied the BEM to predict flaws from the potential computed by the ACPD. With numerical methods gaining popularity, there is more research being published on the techniques themselves and their applications to electromagnetic NDE phenomena.

There is a continuous effort by various researchers to improve the various aspects of the differential and integral techniques to make them more attractive. With parallel processing gaining momentum, researchers are experimenting with various computer

architectures to implement the FEM and BEM [88-90]. Both Single Instruction Multiple Data (SIMD) and Multiple Instruction Multiple Data (MIMD) machines with distributed memory are being used to solve these problems. Much research is still necessary, however, to answer many unsolved questions which will ultimately benefit the NDE community as modern numerical methods offer the opportunity to model more complex and larger geometries and obtain solutions in near real time.

Hybrid Methods

A Hybrid method is a combination of two or more techniques applied to solve a given problem. Hybrid methods can be used to solve time dependent problems using a finite difference scheme to tackle the temporal domain and finite elements for the spatial domain. They can also be used to combine analytical methods for the exterior region with finite elements for the interior region to solve steady state problems. This dissertation is concerned with only the hybrid finite-boundary element method applied to quasi-static eddy current phenomena. In many practical electromagnetic situations, there are homogeneous infinite regions coupled with complicated inhomogeneous or non-linear regions. Similar to the FE and BE formulations the hybrid methods used in the electromagnetic power engineering area seem to have preceded those used in the NDE area.

McDonald and Wexler [91] used the FEM in the interior region of a parallel plate capacitor and a boundary integral equation for the outer boundary. In their method, elements from each region overlap at the interface to avoid any singularity problems, but this technique requires more elements for the purpose of linking the two methods. Over the decade, D'Angelo [92], Salon and D'Angelo [93], Schneider [94] and Peng

and Salon [95] generated a series of algorithms for solving 2D, axisymmetric and 3D electrostatic and quasi-static problems involving power devices using the FE-BE hybrid method. Matsuko [96] solved the eddy current problem in 3D combining the FEM and BEM and compared it to analytical methods. In addition to these, traditional FE codes have been used in conjunction with some special modifications to solve problems. Bettess [97] used infinite elements, Silvester implemented the ballooning [98] approach, and Chari [99] developed an algorithm using an analytical solution for the exterior, with FE in the interior, to solve infinite region problems. The applications in all these cases were the study of power devices. In the last five years, researchers in the NDE community have utilized the benefits of hybrid methods to solve various problems.

Researchers from all over the world involved in numerical analysis of electromagnetic fields have set up a TEAM workshop [100]. This group has identified fifteen standard problems involving static, quasi-static and high frequency fields, linear and non-linear material problems. The aim of this workshop is for different groups or individuals to use these problems as *standards* to validate their numerical models. These groups meet every year and exchange notes on the various modeling schemes used. This has the potential to give a tremendous boost to the numerical modeling efforts in electromagnetic NDE because of the involvement of researchers from around the globe in trying to generate optimal models.

CHAPTER 3. POTENTIAL DROP METHODS: FINITE ELEMENT FORMULATION

Fracture analysis is usually performed only after gathering accurate information on the size and shape of a crack. Accurate determination, therefore, of crack dimensions is of extreme importance in many critical structural components. In certain materials, such as high toughness steels, crack initiation and growth may occur prior to failure. Under dynamic loading, fatigue can lead to crack propagation before the component fails. Thus, crack monitoring systems are utilized to identify the initiation point, crack growth rate and the final size of the crack.

Potential Drop methods are used widely in the fracture mechanics area to monitor fatigue crack growth and predict crack length. The methods are the DC potential drop method (DCPD) and the AC potential drop method (ACPD), which use dc and ac excitation, respectively.

As mentioned in Chapter 1, this dissertation deals with the finite and boundary element modeling of the DCPD and ACPD method. This Chapter discusses the theory, analytical modeling techniques reported in the literature, and the finite element formulation of the potential drop methods.

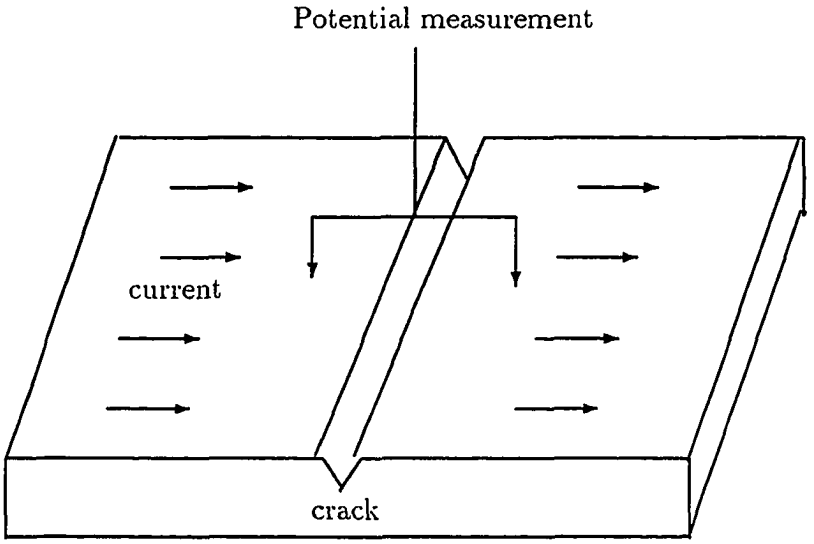

Figure 3.1: DCPD measurement

DCPD Method

Principle

In the DCPD method, a constant current is passed through a cracked specimen (Figure 3.1), and the electric potential drop which results across the crack is then monitored. As the crack length increases, the uncracked cross-sectional area of the test piece decreases, causing an increase in current path resistance and a subsequent rise in potential. In practice, for a particular geometry, plots are made of the potential in the form of $\frac{U}{U_0}$ as a function of $\frac{A}{W}$ where U_0 is the reference potential drop across the initial crack, U is the potential drop as the crack length increases, and $\frac{A}{W}$ is the crack length to specimen width ratio. These plots are called *calibration curves.*

The DCPD method generates *calibration curves* for various geometries, mate-

rials and current input. Johnson [101] and others have shown that the *calibration curves* are independent of material properties and thickness, but sensitive to the geometry of the initial crack. Schwalbe and Hellman [102] and Aronson and Ritchie [42] have investigated different configurations of placing input current leads and voltage monitoring leads. An optimized configuration was agreed upon by undertaking experimental measurements [103] and numerical analysis [42]. The input leads determine the uniform current distribution over the cross-section, while the potential measuring leads measure very small changes in the potential as the crack grows.

Three types of experimental specimens are used in fatigue crack growth monitoring ; i) the center-cracked tension specimen (CCT), ii) the single-edge notched specimen (SEN) and iii) the compact tension specimen (CT). To ensure that cracking occurs predictably, the specimen contains a starter notch (initial crack). The American Society for Testing Materials (ASTM) has standardized the specimen dimensions and crack size. Figure 3.2 shows the SEN and CT specimens with the appropriate input and output leads.

The accuracy of predicting fatigue crack length is vital to the study of fracture mechanics. Knott [103,104], Romilly [105] and others have studied the calibration techniques of the DCPD method extensively, since the accuracy in predicting crack length relies on calibration standards. They developed an electrolyte bath, in the shape of a specimen, with models of the defect made of non-conducting material inserted into the electrolyte. The voltage drop anywhere across the crack plane was measured using a set of insulated probes inserted into the electrolyte.

The next few sections are devoted to the analytical and numerical modeling of the Potential Drop methods.

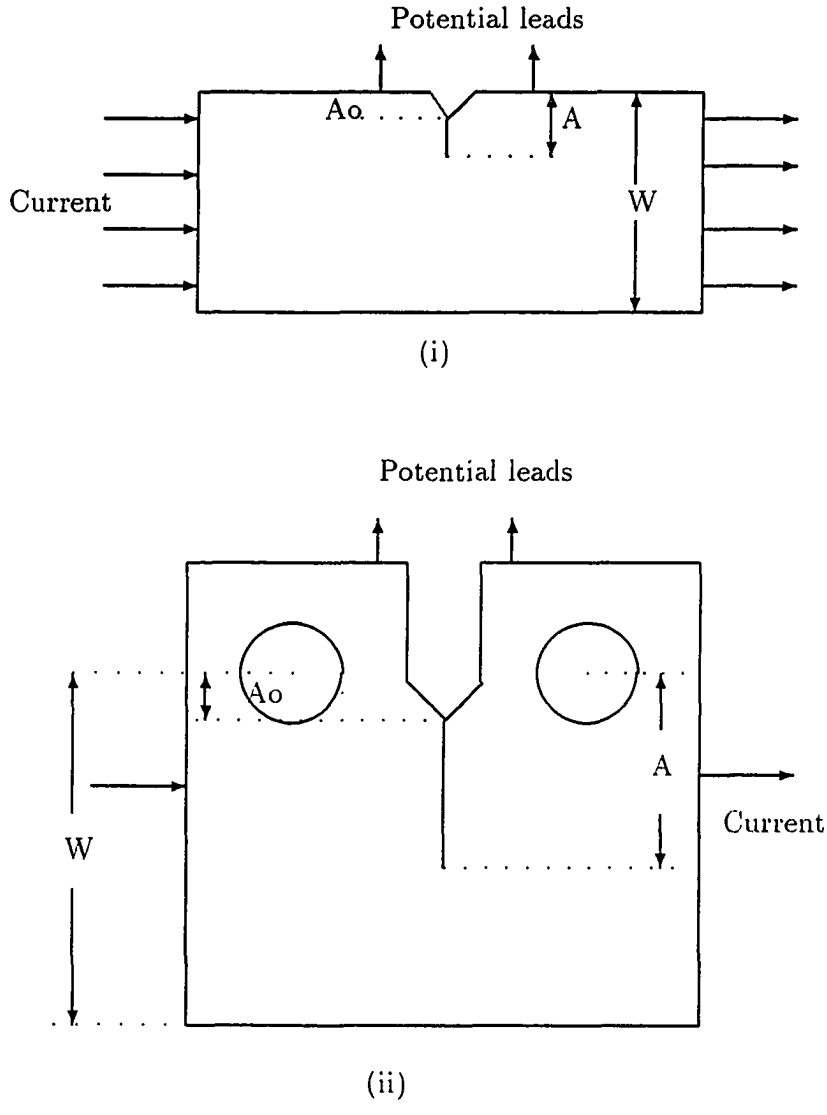

Figure 3.2: Experimental specimens for the DCPD measurements i) SEN specimen and ii) CT specimen

Modeling

The governing PDE for the DCPD method is Laplace's equation

$$\nabla^2 V = 0 \tag{3.1}$$

where V is the steady state voltage in the specimen geometry with a constant current in the plane of the geometry. The boundary conditions are $V = 0$ over the uncracked portion and $V = V_{reference}$ at the current injection point.

As part of the early modeling work of the DCPD method, Johnson modeled the CCT specimen using the theory of conjugate functions to compute the potential arising from a crack. The expression for the calibration curves obtained by Johnson is universally used for the CCT and SEN specimens and was confirmed by Li and Wei [106] and Schwalbe and Hellman. The equation is

$$\frac{U}{U_0} = \cosh^{-1} \frac{[\cosh(\frac{\pi x}{2W}) \cos(\frac{\pi A}{2W})]}{[\cosh(\frac{\pi x}{2W}) \cos(\frac{\pi A_0}{2W})]} \tag{3.2}$$

where U_0 and A_0 denote the initial value of the potential and the crack length, $2x$ is the distance between measurement probe leads, and U is the potential as the crack length A increases. The potential distribution due to a crack is similar to modeling irrotational, incompressible fluid flow as stated by Clark and Knott [107]. These authors used conformal mapping techniques in the complex domain to study the potential distribution of various crack shapes (V-notch, elliptical etc). Orazem and Ruch [108] have applied the Schwarz Christoffel transformation in the complex domain to determine the potential and to plot the *calibration curves*. They have suggested a single-parametric logarithmic equation for the CT specimen which is valid for cracks of varying lengths. Two dimensional finite element modeling of

the DCPD method has been reported in literature. Aronson and Ritchie used the model to optimize the test configurations and measure the probe sensitivity and reproducibility. Ritchie and Bathe have provided calibration curves for the SEN and CT specimens. All the results were confirmed with experimental data.

In this dissertation the DCPD method is studied to model an infinite thickness specimen (2D) and finite thickness specimen (3D). The results are compared and discussed in a later chapter.

ACPD Method

Principle

The operating principle of the ACPD method is similar to that of the DCPD method with one major variation. The difference lies in the fact that the excitation is a uniform alternating current which is carried in only a thin layer of the metal surface due to the skin effect phenomenon. Thus the current required to produce a given field strength at the surface is much less than with dc excitation, as the effective cross-section carrying the current is of a smaller area [109-111].

An instrument called the *Crack Microgauge* was developed for laboratory and inservice inspection at the University College, London based on the principle of the ACPD method. The instrument has a frequency range of 600 Hz to 6 kHz to operate on various ferrous and non-ferrous metals. The ACPD method is used for measuring fatigue cracks in standard CT and other specimens. Other major applications where the technique has been successfully applied are: 1) monitoring surface cracks at welded joints of different structures [109], 2) detecting and sizing fatigue cracks in threaded connections such as bolts [111], 3) detecting surface cracks underwater in

the structure of an offshore oil platform and 4) measurement of thickness of metallic coating [113].

Modeling

Maxwell's equations govern electromagnetic fields at all frequencies. Where the displacement current can be neglected, the electric field $\vec{E}$ and the magnetic field $\vec{H}$ can be derived from the low frequency Maxwell-Ampere and Maxwell-Faraday equations, which are

$$\nabla \times \vec{E} = -\frac{\partial \vec{B}}{\partial t} \tag{3.3}$$

$$\nabla \times \vec{H} = \vec{J} \tag{3.4}$$

where $\vec{B}$ is the magnetic flux density and $\vec{J}$ is the current density. Assuming steady state alternating current, using the vector identity $\nabla \times \nabla \times \vec{E} = \nabla(\nabla \cdot \vec{E}) - \nabla^2 \vec{E}$, and combining equations 3.3 and 3.4, the governing PDE is obtained as

$$\nabla^2 \vec{E} = j\omega\mu\sigma\vec{E} \tag{3.5}$$

or

$$\nabla^2 \vec{E} = k^2 \vec{E} \tag{3.6}$$

where $k^2 = j\omega\mu\sigma$, ω is the angular frequency, μ is the permeability and σ is the conductivity. For the problem of a one dimensional crack with a uniform depth and infinitesimal thickness (Figure 3.3), the $\vec{E}$ field is solenoidal. Introducing the stream function ψ, where

$$E_x = \frac{\partial \psi}{\partial y}$$

$$E_y = -\frac{\partial \psi}{\partial x}$$

and substituting into equation 3.6 gives

$$\frac{\partial^2}{\partial x^2}(\hat{i}\frac{\partial \psi}{\partial y} - \hat{j}\frac{\partial \psi}{\partial x}) + \frac{\partial^2}{\partial y^2}(\hat{i}\frac{\partial \psi}{\partial y} - \hat{j}\frac{\partial \psi}{\partial x}) = k^2(\hat{i}\frac{\partial \psi}{\partial y} - \hat{j}\frac{\partial \psi}{\partial x}) \tag{3.7}$$

where $\hat{i}$ and $\hat{j}$ are the unit vectors in the x and y direction in the cartesian coordinate system. By equating each component in the above equation and integrating appropriately, the governing equation reduces to

$$\nabla^2 \psi = k^2 \psi \tag{3.8}$$

The potential across the probe is given by

$$V_{ab} = -\int_a^b \vec{E} \cdot \vec{dl} \tag{3.9}$$

In Figure 3.3, the potential V_1 is obtained when the probe is away from the crack, while V_2 is the reading when the probe straddles the crack. The dimensional estimate of the crack depth is given by

$$d = \frac{1}{2}\Delta\frac{V_2 - V_1}{V_1} \tag{3.10}$$

with Δ being the probe width. For a particular geometry and set of calculations the probe width is fixed. The nature of the problem for the ACPD method depends on the ratio of the crack length (d) to the skin depth (δ). When $|d| >> \delta$, the classical skin effect phenomenon occurs in which the current flow is confined to the top thin layer of the specimen and is called the *thin skin limit*. When $|d| << \delta$, the field behaves as if a dc current is applied and is called the *thick skin limit*[112].

Dover et al [109] introduced the theory of the ACPD method about twelve years ago. The authors formulated the problem in terms of the stream function ψ and conjugate function ϕ with boundary conditions on the crack surface and a surface

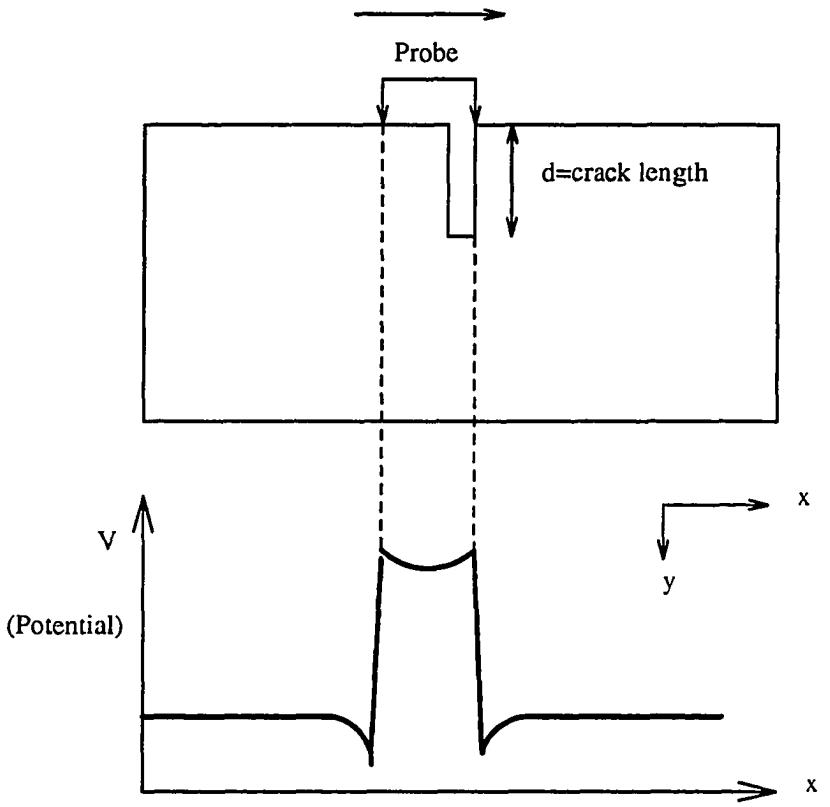

Figure 3.3: ACPD measurement setup

at infinity. The functions ϕ and ψ satisfy the Cauchy Riemann conditions with ϕ satisfying Laplace's equation (Figure 3.4). This is due to the fact that when a plane symmetrical crack is unfolded [111], a 2D Laplace problem is produced. The theory is called the *unfolding theory.* Using the *unfolding theory* and the Schwarz. Christoffel transformation, exact solutions were obtained for circular cracks [109], elliptical cracks [114], triangular and rectangular cracks [115].

A general solution for arbitrary skin depth was obtained by Mirshekhar, et al.[116]. The potential was computed in terms of Mathieu functions which allow for accurate interpretation of surface breaking crack depths from voltage readings taken by the instrument. Michael [117] considered higher order terms in the analytical solution and gave a more accurate expression for the depth of a surface flaw in the thin skin limit, which is

$$d = d_0[1.- \frac{d_0}{\Delta} + \frac{1}{\pi}\frac{d_0}{\delta}] \tag{3.11}$$

where d_0 is given by equation (3.10). On the other hand, modeling in the thick skin limit the depth of the flaw is given by [118]

$$d = d_0[1 - \frac{1}{\pi}\frac{\delta}{d_0}\frac{d_0}{\Delta} + \frac{4-\pi}{4\pi}\frac{\delta}{d_0}] \tag{3.12}$$

The surface distribution of the electromagnetic fields varies with the parameter $m = \frac{d}{\mu_r \delta}$, especially for ferromagnetic materials. Lewis [119] reported how the fields vary for different crack shapes in mild steel and aluminum.

More recently Connolly [87], McIver [120] and Takahashi and Miya [121] have used numerical methods to characterize cracks. In Connolly's method an initial guess of the crack shape is made by equation (3.10). The exact potential distribution for this estimated crack is determined using the BEM. A comparison is made between

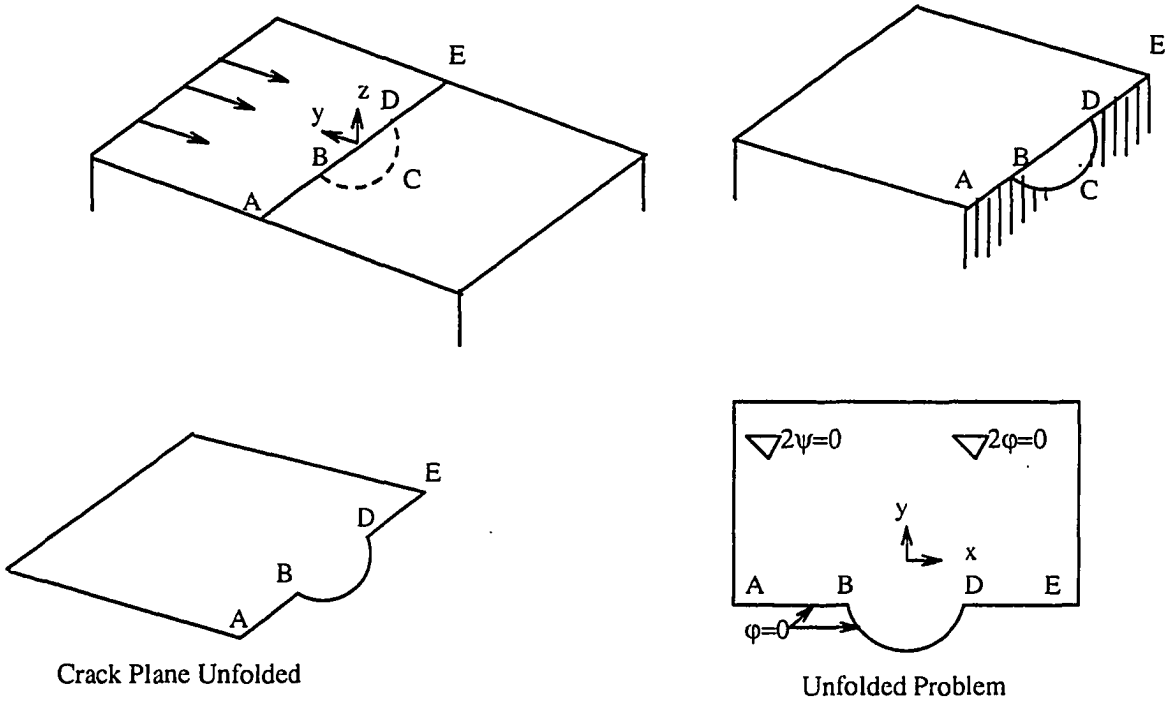

Figure 3.4: A crack of finite aspect ratio and the *unfolded problem* [111].

the calculated and given potential until the difference is minimized to a prescribed level. McIver modeled the crack using the stream function and the potential as independent variables. A Fredholm equation was solved to determine the shape of the crack. Takahashi and Miya extended McIver's work to apply it to magnetic field measurements instead of potential measurements. The authors validated their method with experimental results obtained on a steel plate.

The next section describes the finite element formulation for the Helmholtz equation. When the frequency term is present ($k^2 \neq 0$), the formulation is valid for the ACPD method, and when ($k^2 = 0$), the equation reduces to Laplace's equation which models the DCPD method.

Finite Element Formulation

The classical FEM proceeds by deriving an energy functional of the system or by using the weighted residual approach. Next, the entire region is discretized into triangular or rectangular subregions over which the unknown function varies linearly or quadratically using interpolation functions. These interpolation functions are substituted in the functional which is subsequently minimized at each of the nodes to obtain an element matrix associated with every element in the region. The element matrix is generated by performing numerical integration of the shape functions over each element. These element matrices and the forcing function vector of each element are incorporated into a global stiffness matrix by an appropriate mapping scheme. The solution of the matrix equation yields the variable of interest at each node. In the next section each of these steps discussed above is outlined briefly.

Energy functional

The energy functional corresponding to the ACPD method governing equation (3.8) is

$$F = \int_v \frac{1}{2\mu}[(\frac{\partial\psi}{\partial x})^2 + (\frac{\partial\psi}{\partial y})^2 + (\frac{\partial\psi}{\partial z})^2]dv + \int_v \frac{1}{2} j\omega\sigma\psi^2 dv \qquad (3.13)$$

If we replace μ by $\frac{1}{\sigma}$, ψ by V and set $\omega = 0$ in equation (3.13), the functional F will represent that corresponding to Laplace's equation. The Euler form of this equation is the governing equation, which ensures that minimizing the functional will give the correct solution.

Discretization

In 2D, first order three node triangular elements are used while in 3D, 8 node isoparametric block elements are utilized (Figure 3.5). The interpolation functions or shape functions for these elements are given in Appendix A. Criteria for discretization are

- An element cannot cover more than one material.
- To have a high accuracy for the solution, the discretization must be dense where the expected gradient of the variable is larger. The only restriction to the number of elements is governed by available computer resources.
- The conductivity and permeability are constant in an element.

By computing the variable ψ or V at each of the nodes of the mesh, ψ or V can be calculated at any point within the element. Thus either variable can be represented

by

$$V = \sum_{i=1}^{n} N_i(x,y,z)v_i \tag{3.14}$$

$$\psi = \sum_{i=1}^{n} N_i(x,y,z)\psi_i \tag{3.15}$$

where N_i are the shape functions and v_i and ψ_i are the nodal values at each element and n is the total number of nodes for each element in the mesh. To calculate the partial derivatives, one operates on the shape functions,

$$\frac{\partial \psi}{\partial k} = \sum_{i=1}^{n} \frac{\partial N_i}{\partial k}\psi_i \tag{3.16}$$

$$\frac{\partial V}{\partial k} = \sum_{i=1}^{n} \frac{\partial N_i}{\partial k}v_i \tag{3.17}$$

where k=x,y,z.

Finite element equation

The exact solution of the variable ψ corresponds to the minimum value of the energy functional. This is achieved by taking the first variation of the functional with respect to ψ and setting it to zero. Thus

$$\delta F_f = \int_v \frac{1}{\mu}((\frac{\partial \psi}{\partial x})\delta(\frac{\partial \psi}{\partial x}) + (\frac{\partial \psi}{\partial y})\delta(\frac{\partial \psi}{\partial y}) + (\frac{\partial \psi}{\partial z})\delta(\frac{\partial \psi}{\partial z}))dv + \int_v j\omega\sigma\psi\delta\psi\, dv \tag{3.18}$$

In matrix form

$$\delta F_f = \int_v (\begin{bmatrix} \delta(\frac{\partial \psi}{\partial x}) & \delta(\frac{\partial \psi}{\partial y}) & \delta(\frac{\partial \psi}{\partial z}) \end{bmatrix} \begin{bmatrix} \frac{1}{\mu} & 0 & 0 \\ 0 & \frac{1}{\mu} & 0 \\ 0 & 0 & \frac{1}{\mu} \end{bmatrix} \begin{bmatrix} \frac{\partial \psi}{\partial x} \\ \frac{\partial \psi}{\partial y} \\ \frac{\partial \psi}{\partial z} \end{bmatrix} + j\omega\sigma\psi\delta\psi)dv \tag{3.19}$$

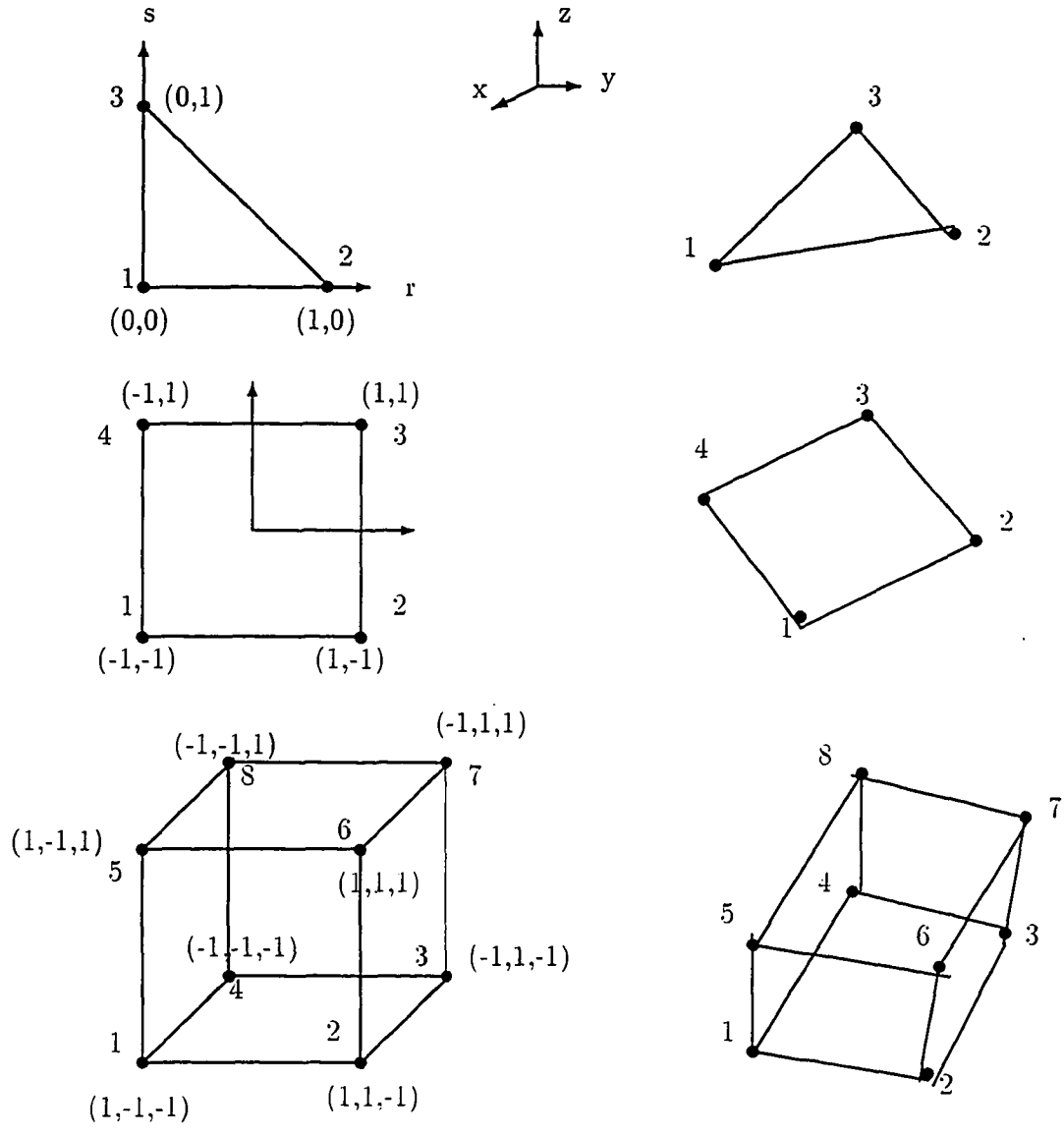

Local elements Global elements

Figure 3.5: Typical 3, 4 and 8 node elements used in finite elements and boundary elements. Figure shows both the local and global elements

Substituting equations (3.14-3.17) in equation (3.18) and defining

$$[\psi] = \begin{bmatrix} \psi_1 \\ \psi_2 \\ \psi_3 \\ \psi_4 \\ \psi_5 \\ \psi_6 \\ \psi_7 \\ \psi_8 \end{bmatrix}, [K] = \begin{bmatrix} \frac{1}{\mu} & 0 & 0 \\ 0 & \frac{1}{\mu} & 0 \\ 0 & 0 & \frac{1}{\mu} \end{bmatrix}, [N] = \begin{bmatrix} N_1 N_2 N_3 N_4 N_5 N_6 N_7 N_8 \end{bmatrix}$$

$$\text{and } \Delta N = \begin{bmatrix} \frac{\partial N}{\partial x} \\ \frac{\partial N}{\partial y} \\ \frac{\partial N}{\partial z} \end{bmatrix}$$

the variation equation is now

$$\delta F_f = \int_v \delta[\psi]_e^T [\Delta N]^T [K][\Delta N][\psi]_e dv + \int_v j\omega\sigma\delta[\psi]_e^T [N]^T [N][\psi]_e dv \qquad (3.20)$$

Integrating over the total volume, element by element, the expression for the first integral in equation (3.20) is

$$\int_v \delta[\psi]_e^T [\Delta N]^T [K][\Delta N][\psi]_e = \delta[\psi]_e^T [S]_e [\psi]_e \qquad (3.21)$$

where subscript e stands for element and

$$[S]_e = \int_v [\Delta N]^T [K][\Delta N] dv \qquad (3.22)$$

and the second integral is

$$\int_v j\omega\sigma\delta[\psi]_e^T [N]^T [N][\psi]_e = j\delta[\psi]_e^T [R][\psi]_e \qquad (3.23)$$

where

$$[R] = \int_v \sigma\omega[N]^T[N]dv \tag{3.24}$$

Thus the contribution from every element is

$$\delta F_{fe} = \delta[\psi]_e^T[S]e[\psi]e + j\delta[\psi]e[R]e[\psi]e \tag{3.25}$$

The total variation is the sum of all the elements in the volume and is given by

$$\delta F_f = \delta[\psi]^T[S][\psi] + j\delta[\psi]^T[R][\psi] \tag{3.26}$$

To minimize the functional, the variation has to be equal to zero. Therefore setting $\delta F_f = 0$, one obtains the *finite element equation*

$$([S] + j[R])[\psi] = [Q] \tag{3.27}$$

or

$$[G][\psi] = [Q] \tag{3.28}$$

where [G] is the global stiffness matrix which is sparse, banded, symmetric and diagonally dominant, and $[\psi]$ is a vector of the unknown potential at all the nodes in the volume. The right hand side [Q] is a vector of boundary conditions, which is zero everywhere except at the current injection points. To minimize the computer memory usage, only the diagonal and upper banded portion of the global matrix is stored in 2D. In 3D, the diagonal and non-zero elements of the upper banded portion of the stiffness matrix is stored. To solve this set of linear equations, a standard Gaussian elimination technique is used for the 2D case, while in 3D, an iterative incomplete Cholesky conjugate gradient (ICCG) algorithm is used.

The next chapter discusses Green's functions and derives the boundary integral equation for the potential drop methods.

CHAPTER 4. POTENTIAL DROP METHODS : BOUNDARY ELEMENT FORMULATION

The general concept of integral methods to solve PDE's starts when the original problem, which is most often expressed in differential form, is cast into integral form. The integral equation is normally defined over the boundary of the domain, and therefore all the variables are defined as boundary variables. The Green's function approach is then to solve a given PDE with a closed function representing the solution. Introduction of the Green's function is both the strength and the weakness of integral methods.

The boundary integral equation (BIE) is obtained from Green's second theorem and the corresponding Green's function. The boundary element method is the numerical approach used in this dissertation to solve the BIE. In this chapter a brief discussion of Green's functions; their significance and derivation, and the development of the BIE for the DCPD and ACPD method are presented.

Green's Functions

Green's functions are defined as the solution to a PDE using a unit source as the forcing function. In other words, the *Green's function* is a solution of a system which is homogeneous everywhere except at one point. The solution to the actual forcing

function is then the superposition of the solution obtained with the unit source at the different locations representing the actual source distribution. Thus, the Green's function is the *impulse response* of a system [122]. The Green's function for a given problem can be expressed as a finite explicit function, or as an infinite series, or even in integral form. All these solutions, although different in form yield the same result.

In electrical engineering, the Green's function concept is used very often without ever mentioning it. A classic example is the potential measured at a point $\vec{r_1}$, due to a unit point charge placed at the origin. In electrostatics the electric field is irrotational, and if there are no surface charges present, the electric potential V is governed by Laplace's equation. From Coloumb's law, the electric field is given as

$$\vec{E} = \frac{1}{4\pi\epsilon r^3}\vec{r}$$

then the potential is obtained from the relation

$$V = -\int \vec{E} \cdot \vec{dl}$$

Thus

$$V = -\int_{\infty}^{r} \frac{dr}{4\pi\epsilon r^2}$$

which gives $V = \frac{1}{4\pi\epsilon r}$. This is the Green's function of the system. Thus, the Green's function of this system is the same as the potential due to a unit point charge. Another point to be clarified at this stage is that the temporal impulse response of a system is normally the response of the system at time t due to a unit source applied at time t'. The Green's function is normally the response of the system at a point in space due to a spatial impulse applied at another point in space. Thus the impulse

response is in the temporal domain, while the Green's function as described here is in the spatial domain.

Typical properties of *Green's functions* are:

- the solution of the equation is

$$L(G(r,s)) = \delta(s) \tag{4.1}$$

  where L is the Sturm Liouville operator [123], *G(r,s)* is the two point Green's function, $\delta(s)$ is the Dirac delta function (unit source) and r and s are the field and the source point in space for the system, respectively. Appendix B gives the properties of the Dirac delta function.

- it has continuous first and second derivatives except at $r = s$
- it satisfies the boundary conditions of the problem
- in general they are symmetric in nature ($G(r,s) = G(s,r)$)

Thus, to solve an inhomogeneous equation

$$L(u) = f \tag{4.2}$$

where L is the second order Sturm-Liouville operator

$$L(u) = pu'' + ru' - qu \tag{4.3}$$

the solution for u can be given by

$$u(r) = \int_{r0}^{r1} G(r,s)f(s)ds \tag{4.4}$$

where *f(s)* is some known source distribution in the system. For linear operators with simple geometries the Green's function is well documented and so the solution is easily computable. Generating the Green's function in the case of complex geometries is tedious. Since the Green's function solution is based on the principle of superposition, it is not readily available for non-linear operators. The next section develops the BIE for the Potential Drop methods.

Boundary Integral Equation

The governing PDE for the ACPD method is the scalar Helmholtz equation given by

$$\nabla^2\psi = k^2\psi \tag{4.5}$$

where $k^2 = j\omega\mu\sigma$, while for the DCPD method the governing PDE is

$$\nabla^2 V = 0 \tag{4.6}$$

The BIE for Helmholtz and Laplace's equation is identical except for the different Green's function used in the formulation.

Green's second theorem is the starting point for the BIE:

$$\int_v (G\nabla^2 F - F\nabla^2 G)dv = \int_s (G\frac{\partial F}{\partial n} - F\frac{\partial G}{\partial n})ds \tag{4.7}$$

where F and G are functions continuous in the domain v including the boundary or surface s (Figure 4.1) and n is the normal at any point on the surface. The next step is to let G satisfy

$$\nabla^2 G = \delta(\vec{x} - \vec{\xi}) \tag{4.8}$$

$\vec{x}$ is the field point and $\vec{\xi}$ is the source point and $\delta(\vec{x}-\vec{\xi})$ is the Dirac delta function. From the previous discussion on Green's functions, one can say that G is the Green's function for the governing PDE. In 2D, $G(\vec{x},\vec{\xi})$ is

$$G(\vec{x},\vec{\xi}) = -\frac{1}{2\pi}\ln(r) \tag{4.9}$$

$$G(\vec{x},\vec{\xi}) = \frac{1}{2\pi}K_0(kr) \tag{4.10}$$

K_0 is the modified Bessel function of the second kind and $r = \sqrt{(x_1-\xi_1)^2+(x_2-\xi_2)^2+(x_3-\xi_3)^2}$. In 3D, the Green's function for Laplace's equation is

$$G(\vec{x},\vec{\xi}) = \frac{1}{4\pi r} \tag{4.11}$$

The Green's function is derived in Appendix C for the scalar Helmholtz equation and shows that $\nabla^2 G = 0$ for $r \neq 0$. Thus, letting F be V or ψ, and substituting the corresponding PDE in equation (4.7) results in the equations,

$$k^2\int_v G(\vec{x},\vec{\xi})\psi(\vec{x})dv = \int_s (G(\vec{x},\vec{\xi})\frac{\partial\psi}{\partial n}(\vec{x}) - \psi(\vec{x})\frac{\partial G}{\partial n}(\vec{x},\vec{\xi}))ds \tag{4.12}$$

$$0 = \int_s (G(\vec{x},\vec{\xi})\frac{\partial V}{\partial n}(\vec{x}) - V(\vec{x})\frac{\partial G}{\partial n}(\vec{x},\vec{\xi}))ds \tag{4.13}$$

for the Helmholtz and Laplace's equation respectively. These integral equations are valid at every single point in the domain v and so these must be integrable. Since $G(\vec{x},\vec{\xi})$ needs to be a continuous function in the domain, but is a singular function at $\vec{x}=\vec{\xi}$, this singularity needs to be eliminated. To illustrate the process of removing the singularity, the following section will discuss this issue using the 2D Laplace's equation.

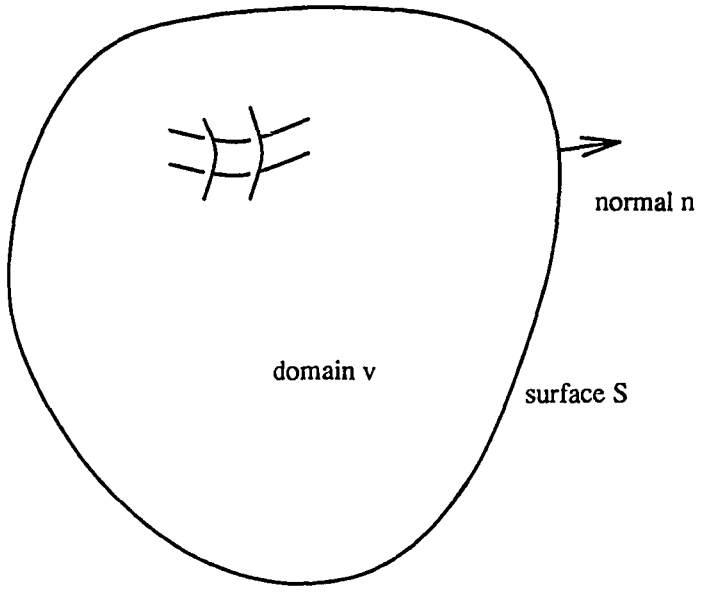

Figure 4.1: Typical domain with volume v and surface S

Singularity removal [124]

The Green's function is a two point kernel function, and when $\vec{x} = \vec{\xi}$ the function blows up or is singular. The point $\vec{\xi}$ can be located inside the domain, on the boundary of the domain, or outside the domain. Each of these cases is studied separately. Figure 4.2 shows the domain and the three cases where the field point is located.

Case I: Point $\vec{\xi}$ is inside the domain v:

Since $G(\vec{x}, \vec{\xi}) = -\frac{1}{2\pi} \ln(r)$, then

$$\frac{\partial G}{\partial n}(\vec{x}, \vec{\xi}) = -\frac{1}{2\pi}(\frac{1}{r})\vec{e} \cdot \vec{n} \tag{4.14}$$

where $\vec{e}$ is the unit vector amongst the spatial coordinate directions and $\vec{n}$ is the usual unit normal to the surface at a point. For all the cases the right hand side of

equation (4.13) can be written as

$$\int_{S'+S_1+S_\epsilon+S_2}(G(\vec{x},\vec{\xi})\frac{\partial V}{\partial n}(\vec{x})-V(\vec{x})\frac{\partial G}{\partial n}(\vec{x},\vec{\xi}))ds \tag{4.15}$$

The contributions due to S_1 and S_2 cancel as they are oriented in opposite directions as $\epsilon \rightarrow 0$. Consider the contributions due to S_ϵ, the integrand of 4.15 is,

$$\int_{S_\epsilon}(G(\vec{x},\vec{\xi})\frac{\partial V}{\partial n}(\vec{x})-V(\vec{x})\frac{\partial G}{\partial n}(\vec{x},\vec{\xi}))ds \tag{4.16}$$

Substituting for $G(\vec{x},\vec{\xi}) = -\frac{1}{2\pi}\ln(r)$, the first integral can be written as

$$\int_{S_\epsilon}(G(\vec{x},\vec{\xi})\frac{\partial V}{\partial n}(\vec{x}))ds = -\frac{1}{2\pi}\int \ln(\epsilon)\frac{\partial V}{\partial n}\epsilon d\theta \tag{4.17}$$

As $\epsilon \rightarrow 0$, $\epsilon\ln(\epsilon) \rightarrow 0$ and so

$$\lim_{\epsilon\rightarrow 0}\int_{S_\epsilon} G(\vec{x},\vec{\xi})\frac{\partial V}{\partial n}(\vec{x})ds = 0 \tag{4.18}$$

The second integral is

$$\int_{S_\epsilon} V(\vec{x})\frac{\partial G}{\partial n}(\vec{x},\vec{\xi})ds = \int_{\pi}^{-\pi} -\frac{1}{2\pi\epsilon}\vec{e}\cdot\vec{n}V(\vec{x})\epsilon d\theta \tag{4.19}$$

Since $V(\vec{x})$ is continuous near $\vec{x} = \vec{\xi}$ and setting $\vec{e}\cdot\vec{n} = -1$, the integral is

$$\lim_{\epsilon\rightarrow 0}\int_{S_\epsilon} V(\vec{x})\frac{\partial G}{\partial n}(\vec{x},\vec{\xi})\epsilon d\theta = V(\vec{\xi}) \tag{4.20}$$

Thus the singular integral picks out the value of the potential function at the source point $(\vec{\xi})$.

Case II: Point $\vec{\xi}$ is on the boundary or the surface:

$$\int_{S_\epsilon} V(\vec{x})\frac{\partial G}{\partial n}(\vec{x},\vec{\xi})ds = -\int_0^{\pi} V(\vec{x})\frac{1}{2\pi\epsilon}\vec{e}\cdot\vec{n}\epsilon d\theta \tag{4.21}$$

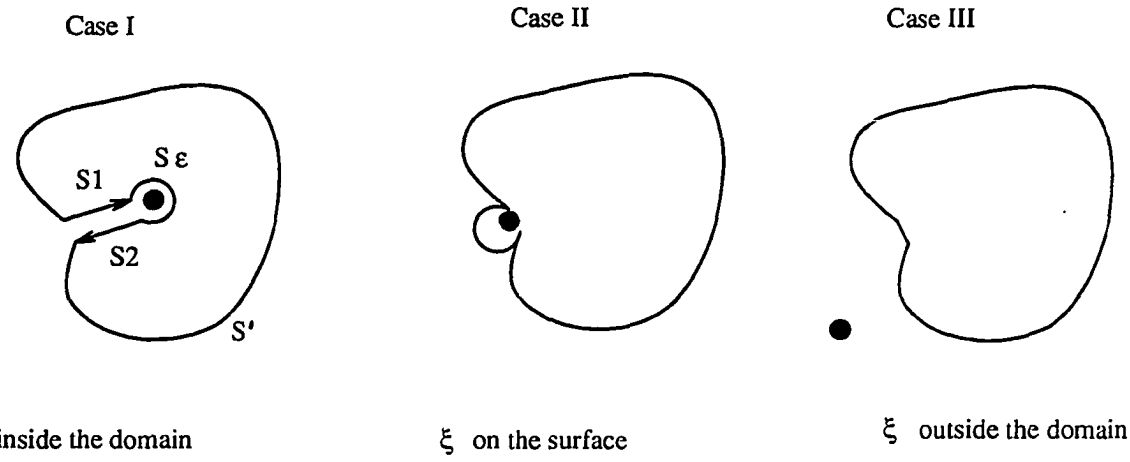

Figure 4.2: Singular integration showing $\vec{\xi}$ inside the domain, on the surface of the domain and outside the domain

Thus, in the limit, the integral is

$$\lim_{\epsilon \to 0} \int_{S_\epsilon} V(\vec{x}) \frac{\partial G}{\partial n}(\vec{x}, \vec{\xi}) = \frac{1}{2} V(\vec{\xi}) \tag{4.22}$$

Case III: Point $\vec{\xi}$ is outside the domain, and therefore the contribution from both integrals is zero.

Thus, after removing the singularity at the point $\vec{x} = \vec{\xi}$, the *boundary integral equation* is

$$C(\vec{\xi}) V(\vec{\xi}) = \int (G(\vec{x}, \vec{\xi}) \frac{\partial V}{\partial n}(\vec{x}, \vec{\xi}) - V(\vec{x}) \frac{\partial G}{\partial n}(\vec{x}, \vec{\xi})) ds \tag{4.23}$$

where $C(\vec{\xi}) = 1, 0.5, 0$ depending on the location of point $(\vec{\xi})$. To solve this BIE, one needs to know either the potential or its normal derivative, as boundary conditions, at all points on the boundary.

There are many different techniques to solve the BIE (4.23). The prominent methods are the method of moments, indirect boundary element method and the

direct boundary element method. A brief discussion of the techniques follows.

Boundary Integral Techniques

Method of moments [65]

This technique is used frequently in the solution of high frequency electromagnetic problems including antenna design, scattering due to an incident electromagnetic wave and others. The general procedure is outlined below:
Consider the inhomogeneous equation (4.2), where u is unknown and f is known. u is expanded in a series form using some basis functions k_n in the domain, as

$$u = \sum_n \alpha_n k_n \tag{4.24}$$

where α_n are constants. Substituting in equation (4.2) yields

$$\sum_n \alpha_n L(k_n) = f \tag{4.25}$$

The next step is to define a set of weighting functions w_m and take the inner product of equation (4.25) with every w_m. The result is

$$\sum_n \alpha_n < w_m, L\, k_n >=< w_m, f > \; m = 0, 1, .. \tag{4.26}$$

This gives rise to a linear set of equations and in matrix form it is,

$$[\, l_{mn} \,][\, \alpha_n \,] = [\, f_m \,] \tag{4.27}$$

The final solution is then given by

$$[\, u \,] = [\, k_n \,][\, l_{mn}^{-1} \,][\, f_m \,] \tag{4.28}$$

The accuracy of the solution depends on the choice of k_n and w_m.

Indirect boundary element method [124]

In this method the solution $V(\vec{\xi})$ in equation (4.23) is approximated by

$$V(\vec{\xi}) = \int_{\gamma} G(\vec{x}, \vec{\xi}) \sigma(\vec{x}) d\gamma \tag{4.29}$$

where γ is either the surface S enclosing the domain or another surface just outside S. The function $\sigma(\vec{x})$ is an unknown distribution or *density function* in the domain which is determined by enforcing the boundary conditions of the problem. The other term $\frac{\partial V}{\partial n}$ in equation (4.23) is given by

$$\frac{\partial V}{\partial n}(\vec{\xi}) = \int_{\gamma} \frac{\partial G}{\partial n}(\vec{x}, \vec{\xi}) \sigma(\vec{x}) d\gamma(\vec{x}) \tag{4.30}$$

One advantage of this method is that if the surface γ is chosen to lie just outside the domain, the singularity problem is avoided and a closed form solution is obtained. The major disadvantage lies in the computation of the correct *density function* $\sigma(\vec{x})$ for a given problem, causing many researchers to avoid this method.

Direct boundary element method [124]

This is the approach used in this dissertation for solving the BIE for the DCPD and ACPD NDE methods, and later for the eddy current NDE problem.

The numerical procedure for this approach, similar to the FEM, is summarized below:

- The domain surface is discretized into a number of line segments in 2D or surfaces in 3D. Each line segment has three nodes, while the surfaces are 4 node quadrilaterals. The discretization is varied depending on the expected solution gradient.

- Along each element the potential and its normal derivative are assumed to vary linearly using standard shape functions. These shape functions are given in Appendix A.

- Substituting these shape functions into the BIE gives,

$$C(\vec{\xi})V(\vec{\xi}) = \sum_{i=1}^{nelements} (\int_S G(\vec{x},\vec{\xi})H_i(\vec{x})ds\frac{\partial V_i}{\partial n}(\vec{x}) - \int_S H_i(\vec{x})\frac{\partial G}{\partial n}(\vec{x},\vec{\xi})dsV_i(\vec{x})) \tag{4.31}$$

  In 2D the Green's function contains a weak singularity $O(\ln(r))$ while its normal derivative has a strong singularity $O(\frac{1}{r})$ as $\vec{x} \rightarrow \vec{\xi}$. Due to these singularities, the discretized BIE must be interpreted as an improper Cauchy integral. In 3D the strong singularity is $O(\frac{1}{r^2})$. For both cases, the strong singularity is analytically removed and then solved numerically.

- A global matrix equation is obtained,

$$[T]\{V\} - [P]\{\frac{\partial V}{\partial n}\} = \{0\} \tag{4.32}$$

  where $\{V\}$ and $\{\frac{\partial V}{\partial n}\}$ are the unknowns at every node point on the domain boundary. These coefficient matrices $[T]$ and $[P]$ are non-symmetric and fully populated.

- After incorporating the appropriate boundary conditions, the set of linear equation is solved using Gaussian elimination.

CHAPTER 5. EDDY CURRENT NDE: HYBRID FINITE-BOUNDARY ELEMENT FORMULATION

The previous two chapters describe the FEM and the BEM as applied to the potential drop methods. The governing equations for the DCPD and the ACPD method are Laplace's, and the scalar Helmholtz equation respectively. Eddy current methods are governed by the diffusion equation and are quasi-static in nature.

The FEM is a domain method, needs a volume discretization, and handles non-linearities and awkward geometries easily. On the other hand, the BEM is an integral method and requires only surface or boundary discretization. A major feature of the BEM is it's ease of handling infinite boundaries and the inherent 3D nature of its formulation and application.

These two methods have entirely different features, but complement each other, and can be combined to exploit their individual merits. A typical geometry for eddy current NDE is shown in Figure 5.1. The three regions that need to be considered are: 1) probe, 2) conducting specimen, and 3) free space region extending to infinity. It is assumed that eddy currents in the probe are neglected. Using only the FEM, all the three region volumes need to be discretized, a condition that puts heavy demands on the computation resources. If the BEM is used exclusively, then only the surface of the probe and conducting region need to be discretized. Since radiation conditions are

satisfied at infinity, the free space region need not be modeled. In the hybrid method, the probe and specimen volume are discretized using finite elements, while the surface of the probe and specimen are discretized using boundary elements. Thus, the effect of the free space region is embedded in the boundary element formulation. It must be noted that the surface nodes of both the discretizations used in the computations in this dissertation are identical.

This chapter describes a hybrid finite-boundary element formulation for solving the 3D eddy current diffusion equation. The governing equations for eddy current NDE are developed from first principles. Then a background study on various formulations to solve the eddy current problem using finite elements is briefly described.

Governing Equation

The low frequency Maxwell's equations for electromagnetic fields where the displacement current can be neglected are

$$\nabla \times \vec{E} = -\frac{\partial \vec{B}}{\partial t} \tag{5.1}$$

$$\nabla \times \vec{H} = \vec{J}_s + \vec{J}_{induced} \tag{5.2}$$

$$\nabla \cdot \vec{B} = 0 \tag{5.3}$$

$$\nabla \cdot \vec{D} = \rho v \tag{5.4}$$

The magnetic vector potential (MVP) $\vec{A}$ is defined as

$$\vec{B} = \nabla \times \vec{A} \tag{5.5}$$

The constitutive relations for a linear, homogeneous, isotropic medium are

$$\vec{J} = \sigma \vec{E} \tag{5.6}$$

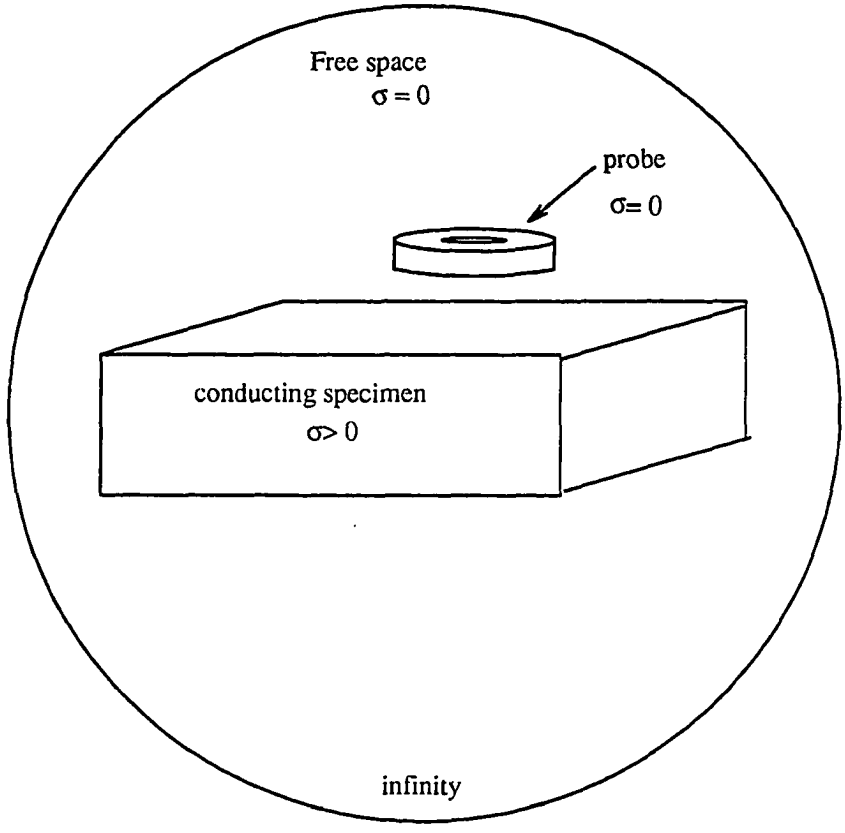

Figure 5.1: Typical eddy current geometry showing the probe, conducting specimen and free space region to infinity

$$\vec{B} = \mu\vec{H} \tag{5.7}$$

$$\vec{D} = \epsilon\vec{E} \tag{5.8}$$

Substituting equation (5.5) in (5.1) yields

$$\nabla \times (\vec{E} + \frac{\partial \vec{A}}{\partial t}) = 0 \tag{5.9}$$

Using the vector identity $\nabla \times \nabla S = 0$ for any scalar S, the electric field intensity can be defined as

$$\vec{E} = -\frac{\partial \vec{A}}{\partial t} - \nabla\phi$$

where ϕ is the electric scalar potential. Finally substituting equations (5.9), (5.5) and (5.7) in (5.2), the governing equations for the eddy current phenomenon is obtained as,

$$\nabla \times \frac{1}{\mu}\nabla \times \vec{A} + \sigma\frac{\partial \vec{A}}{\partial t} + \sigma\nabla\phi = \vec{J_s} \tag{5.10}$$

Taking the divergence of the above equation while maintaining current continuity $\nabla \cdot \vec{J}_{induced} = 0$, ϕ must satisfy

$$\nabla \cdot \sigma(\frac{\partial \vec{A}}{\partial t} + \nabla\phi) = 0 \tag{5.11}$$

Assuming steady state alternating current, the governing PDE's are

$$\begin{aligned} \nabla \times \frac{1}{\mu}\nabla \times \vec{A} + j\sigma\omega\vec{A} + \sigma\nabla\phi &= \vec{J_s} \\ \nabla \cdot \sigma(j\omega\vec{A} + \nabla\phi) &= 0 \end{aligned} \tag{5.12}$$

Assuming a homogeneous medium, and substituting the vector identity $\nabla \times \nabla \times \vec{A} = \nabla(\nabla \cdot \vec{A}) - \nabla^2\vec{A}$, the governing PDE's can be written as

$$\begin{aligned} -\nabla^2\vec{A} + \nabla(\nabla \cdot \vec{A}) + j\omega\mu\sigma\vec{A} + \mu\sigma\nabla\phi &= \vec{J} \\ \nabla \cdot \sigma(j\omega\vec{A} + \nabla\phi) &= 0 \end{aligned} \tag{5.13}$$

The divergence of $\vec{A}$ or the *gauge* condition is arbitrarily chosen. This is an important parameter and so the next paragraph discusses possible choices of $\nabla \cdot \vec{A}$.

The gauge condition

According to Helmholtz's theorem, any vector is uniquely defined if its curl and divergence are specified. The curl of $\vec{A}$ is defined, while it's divergence is arbitrary. Possible choices are:

- $\nabla \cdot \vec{A} = -\mu\epsilon\frac{\partial \phi}{\partial t}$
- $\nabla \cdot \vec{A} = 0$

The first condition is called the *Lorentz gauge*. If the displacement current density is not neglected, the governing PDE can be written as

$$\nabla \times \nabla \times \vec{A} = \mu(\vec{J} + \frac{\partial \vec{D}}{\partial t}) \tag{5.14}$$

Substituting equations (5.8) and (5.10) in (5.14) yields

$$\nabla(\nabla \cdot \vec{A} + \mu\epsilon\frac{\partial \phi}{\partial t}) - \nabla^2\vec{A} = \mu\vec{J}_s - \mu\epsilon\frac{\partial^2 \vec{A}}{\partial t^2} \tag{5.15}$$

Substituting the *Lorentz gauge* in (5.15) the governing PDE assumes the form of

$$\nabla^2\vec{A} - \mu\epsilon\frac{\partial^2 \vec{A}}{\partial t^2} = -\mu\vec{J} \tag{5.16}$$

This is a simplified wave equation. Thus for high frequency applications where the wave phenomenon is considered, the *Lorentz gauge* is ideal because it uncouples the two potentials from the wave equations. Bryant et al. [125] and others have discussed the *Lorentz gauge* for eddy current problems and the uniqueness of $\vec{A}$ in these formulations.

The second condition is called the *Coloumb gauge* and is implemented in this dissertation. Assuming a homogeneous medium and enforcing the Coloumb gauge the governing PDE can be written as

$$\nabla^2 \vec{A} - j\omega\mu\sigma\vec{A} - \mu\sigma\nabla\phi = -\mu\vec{J}_s \tag{5.17}$$

This is a vector Poisson's equation.

Since the FEM has no restriction in modeling non-linear materials, the curl-curl equation (5.12) is maintained as the governing equation. Thus to insure uniqueness an additional term $\frac{1}{\mu}\nabla\cdot\vec{A}$ is added. When the governing equations are discretized to form the FEM global matrix, the scalar potential term makes the matrix non-symmetric [21]. To restore symmetry, Biro and Preis [23] and Rodger [21] have defined $\phi = \frac{\partial\phi'}{\partial t}$. Thus with this substitution in equation (5.12), the actual governing equation for the FEM in this dissertation can be stated as

$$\begin{aligned} \nabla\times\frac{1}{\mu}\nabla\times\vec{A} - \frac{1}{\mu}\nabla\cdot\vec{A} + j\omega\sigma\vec{A} + j\omega\sigma\nabla\phi' &= \vec{J}_s \\ \nabla\cdot\sigma(j\omega\vec{A} + j\omega\nabla\phi') &= 0 \end{aligned} \tag{5.18}$$

A number of researchers have discussed the *Coloumb gauge* in detail. Chari et al [5] have proven that for 3D magnetostatic problems, adoption of the Coloumb gauge is mandatory. Morisue [126] states that the $\vec{A}$ is unique by using the Coloumb gauge in conjunction with certain boundary conditions for the eddy current problem. A similar conclusions is made by Hasebe and Kano [127] for the magnetostatic case.

The BEM is used to model only the free space region, and so the governing equation is

$$\nabla\times\nabla\times\vec{A} = 0 \tag{5.19}$$

There are many different formulations for solving the eddy current problem. A brief discussion on these formulations is presented in the next few sections.

Alternate Formulations

The introduction of the magnetic vector potential is but one choice of the available potential functions that can be used. The use of the electric vector potential, scalar potential, stream functions and others offer a variety of formulations. Formulations which solve for the electric field intensity ($\vec{E}$) or magnetic field intensity ($\vec{H}$) directly are also used.

Potential function formulation

The motivation to use potential functions to represent the electric and magnetic fields is in the ease of applying boundary conditions and in the reduction of dependent variables, which reduce the computational effort [15]. For example, in the solution of the 2D ACPD method, the calculation of the x and y components of the $\vec{E}$ field uniquely solves the problem everywhere. Introducing the scalar potential φ , one needs to solve a single scalar quantity, from which $\vec{E}$ can be computed.

In eddy current problems the current distribution cannot be restricted to one or two dimensions in space, or cannot be easily calculated analytically. The scalar potential is unable to specify current distributions and thus needs to be coupled with a vector potential or a primary field quantity ($\vec{E}$ or $\vec{H}$).

Magnetic vector potential $\vec{A}$

The use of the MVP to solve eddy current problems is a very popular approach. The equations in (5.18) are coupled, making it necessary to solve for the three components of $\vec{A}$ and the scalar potential ϕ. Publications by Sarma [131], Trowbridge [34], Rodger [21] and Biro and Preis [23] have discussed the various formulations using the MVP.

Demerdash [132], Biddlecombe et al [128], Chari et al [5] and others proposed the use of the MVP both in conductors and free space as well as the electric scalar potential ϕ in conductors. Demerdash used the curl-curl equation without a gauge condition, Chari discretized the vector Poisson's equation while Biddlecombe proposed that using isoparametric elements with the curl curl equation guarantees the uniqueness of $\vec{A}$.

Later Emson and Simkin [129], Rodger and Eastham [17] and others proposed the elimination of ϕ in conductors and the introduction of the magnetic scalar potential Ω in the homogeneous free space region. This leads to

$$\frac{\partial \vec{A}^*}{\partial t} = \frac{\partial \vec{A}}{\partial t} + \sigma \nabla \varphi \tag{5.20}$$

where $\vec{A}^*$ is the modified vector potential. This reduces the governing equation to

$$\nabla \times \frac{1}{\mu} \nabla \times \vec{A}^* + j\omega\sigma\vec{A}^* = \vec{J} \tag{5.21}$$

This has been successfully implemented by a number of researchers [15,17], but it has some weaknesses. Equation (5.20) implies $\nabla \cdot \sigma\vec{A}^* = 0$ which produces a continuity condition

$$\sigma_1 \vec{A}^* \cdot \vec{n} = \sigma_2 \vec{A}^* \cdot \vec{n} \tag{5.22}$$

for two conductors with different conductivities as compared to

$$\vec{A_1^*} \cdot \vec{n} = \vec{A_2^*} \cdot \vec{n} \tag{5.23}$$

from equation (5.21). Also for regions with $\sigma = 0$, Emson and Simkin's formulation gives rise to a number of difficulties during its implementation [21,23].

In the proposed hybrid finite-boundary element model, the BEM mesh is superimposed on the FEM mesh and so the electric scalar potential is essential to maintain the continuity between regions of different conductivities.

Electric vector potential $\vec{T}$

By defining $\vec{J} = \nabla \times \vec{T}$, where $\vec{T}$ is the electric vector potential, and letting $\vec{H} = \vec{T} - \nabla\Omega$, the governing PDE can be stated as

$$\nabla \times (\frac{1}{\sigma}\nabla \times \vec{T}) + \mu\frac{\partial \vec{T}}{\partial t} - \mu\nabla\frac{\partial \Omega}{\partial t} = 0 \tag{5.24}$$

$$\nabla \cdot (\mu\nabla\Omega) = \nabla \cdot (\mu\vec{T}) \tag{5.25}$$

where Ω is obtained from the second equation. By suitably defining the divergence of $\vec{T}$, one obtains the solution of the above equations. A problem with this technique is that cancellation errors occur in calculating the magnetic field since $\vec{T}$ and $\nabla\Omega$ could be of similar magnitude in highly permeable materials. This method is called the $T - \Omega$ method.

Magnetic scalar potential Ω

In free space, curl of $\vec{H}$ is zero and so the $\vec{H}$ field can be written as the gradient of a magnetic scalar potential Ω

$$\vec{H} = -\nabla\Omega \tag{5.26}$$

For regions containing current distributions, the field is written as a sum of two parts,

$$\vec{H} = \vec{H_c} + \vec{H_m} \tag{5.27}$$

where $\vec{H_c}$ is due to the currents in the region and $\vec{H_m}$ is due to the rest of the field. Thus $\vec{H_m} = -\nabla\Omega$. Since $\vec{H_c}$ cannot be represented by a scalar potential, it is calculated analytically using the Biot-Savart law. This method has been implemented by Trowbridge [74] and others. The approach is similar to the $T - \Omega$ method and has similar cancellation problems when calculating the magnetic flux density.

With most electromagnetic problems, researchers are interested in knowing the electric and magnetic field distributions in the material. This is accomplished by solving Maxwell's equation using potential functions and then computing the field quantity. Ferrari [24] and others show that certain problems with simple boundary and interface conditions can be solved by directly solving Maxwell's equations for the $\vec{E}$ and $\vec{H}$ fields.

Nakata, et al [130] have discretized the various eddy current formulations discussed above and compared the accuracy, computer storage and cpu time for each method. They applied the formulations to the Bath cube problem [100] and compared the magnetic flux density at certain points in the material.

The MVP, although not the easiest and most economical to implement, is general and applicable to most situations. The MVP is essential to describe the current distribution and the scalar potential is necessary to maintain continuity among different conducting regions. This is the reason for the magnetic vector potential and electric scalar potential being used in this dissertation.

The next section describes the development of the finite element and boundary element equations for the eddy current problem

Formulation

Finite element

The procedure for generating the finite element equation is similar to that described in Chapter 3. Instead of using the energy functional as the starting point, the Galerkin weighted residual approach is used.

The governing equations are

$$\begin{aligned} \nabla \times \frac{1}{\mu} \nabla \times \vec{A} - \nabla(\frac{1}{\mu} \nabla \cdot \vec{A}) + j\omega\sigma\vec{A} + j\omega\sigma\nabla\phi' &= \vec{J_s} \\ \nabla \cdot \sigma(j\omega\vec{A} + j\omega\nabla\phi') &= 0 \end{aligned} \tag{5.28}$$

There are four unknowns to be determined; three components of $\vec{A}$ and the scalar potential ϕ'. In further derivations, the prime on ϕ' will be dropped for simplicity. Using the Galerkin weighted residual method, with the weighting functions being the shape function, the equations are

$$\begin{aligned} \int_v N_i(\nabla \times \frac{1}{\mu} \nabla \times \vec{A} - \nabla(\frac{1}{\mu} \nabla \cdot \vec{A}) + j\omega\sigma\vec{A} + j\omega\sigma\nabla\phi)dv &= \int_v N_i \vec{J_s} dv \\ \int_v N_i \nabla \cdot \sigma(j\omega\vec{A} + j\omega\nabla\phi)dv &= 0 \end{aligned} \tag{5.29}$$

The volume v consists of the conducting specimen and probe coil, while the surface s is the surface enclosing this volume. Using the vector identities

$$\begin{aligned} \nabla \times (\phi\vec{a}) &= \nabla\phi \times \vec{a} + \phi\nabla \times \vec{a} \\ \int(\nabla \times \vec{a})dv &= \int(\vec{n} \times \vec{a})ds \\ \phi\nabla\psi &= \nabla(\phi\psi) - \psi\nabla\phi \\ \nabla \cdot (\phi\vec{a}) &= \vec{a} \cdot \nabla\phi + \phi\nabla \cdot \vec{a} \end{aligned} \tag{5.30}$$

and Gauss's theorem, equations in (5.29) can be rewrittten as

$$\int_v \left(-\nabla N_i \times \frac{1}{\mu}\nabla \times \vec{A} + \nabla N_i \frac{1}{\mu}\nabla \cdot \vec{A} + j\omega\sigma N_i \vec{A} + j\omega\sigma N_i \nabla\phi\right) dv$$
$$- \int_s N_i(\vec{n} \times \frac{1}{\mu}\nabla \times \vec{A})ds - \int_v \vec{J}_s dv = 0 \qquad (5.31)$$

$$-\int_v (j\omega\sigma\vec{A} + j\omega\sigma\nabla\phi)\cdot\nabla N_i dv + \int_s (j\omega\sigma N_i\vec{A} + j\omega\sigma N_i\nabla\phi)\cdot\vec{n}ds = 0 \qquad (5.32)$$

This is the finite element equation to be discretized and integrated over the specified domain. The surface integral in equation (5.31) is the linking term between the FEM and the BEM.

Isoparametric discretization

Eight node hexahedral linear elements are used for the volume discretization. The shape functions in local coordinates are given in Appendix A. The global coordinates are mapped by the shape functions

$$x = \sum_{i=1}^{8} N_i(r,s,t)x_i \qquad (5.33)$$

$$y = \sum_{i=1}^{8} N_i(r,s,t)y_i \qquad (5.34)$$

$$z = \sum_{i=1}^{8} N_i(r,s,t)z_i \qquad (5.35)$$

and similarly the potential functions $\vec{A}$ and ϕ are expressed as

$$A_x(x,y,z) = \sum_{i=1}^{8} N_i(r,s,t)A_{xi} \qquad (5.36)$$

$$A_y(x,y,z) = \sum_{i=1}^{8} N_i(r,s,t)A_{yi} \qquad (5.37)$$

$$A_z(x,y,z) = \sum_{i=1}^{8} N_i(r,s,t)A_{zi} \tag{5.38}$$

$$\phi(x,y,z) = \sum_{i=1}^{8} N_i(r,s,t)\phi \tag{5.39}$$

These approximations are introduced into the integral equations. However these equations contain the derivatives of the potential functions which must be evaluated in terms of the global coordinates.

$$\frac{\partial A_k}{\partial x} = \sum_{i=1}^{8} \frac{\partial N_i}{\partial x} A_{xi} \tag{5.40}$$

$$\frac{\partial A_k}{\partial y} = \sum_{i=1}^{8} \frac{\partial N_i}{\partial y} A_{yi} \tag{5.41}$$

$$\frac{\partial A_k}{\partial z} = \sum_{i=1}^{8} \frac{\partial N_i}{\partial z} A_{zi} \qquad k = x,y,z \tag{5.42}$$

As the shape functions are derived in local coordinates, their derivatives are determined in these coordinates by using the chain rule

$$\begin{aligned}
\frac{\partial N_i}{\partial r} &= \frac{\partial N_i}{\partial x}\frac{\partial x}{\partial r} + \frac{\partial N_i}{\partial y}\frac{\partial y}{\partial r} + \frac{\partial N_i}{\partial z}\frac{\partial z}{\partial r} \\
\frac{\partial N_i}{\partial s} &= \frac{\partial N_i}{\partial x}\frac{\partial x}{\partial s} + \frac{\partial N_i}{\partial y}\frac{\partial y}{\partial s} + \frac{\partial N_i}{\partial z}\frac{\partial z}{\partial s} \\
\frac{\partial N_i}{\partial t} &= \frac{\partial N_i}{\partial x}\frac{\partial x}{\partial t} + \frac{\partial N_i}{\partial y}\frac{\partial y}{\partial t} + \frac{\partial N_i}{\partial z}\frac{\partial z}{\partial t}
\end{aligned} \tag{5.43}$$

These equations can be written in matrix form as

$$\begin{bmatrix} \frac{\partial N_i}{\partial r} \\ \frac{\partial N_i}{\partial s} \\ \frac{\partial N_i}{\partial t} \end{bmatrix} = \begin{bmatrix} \frac{\partial x}{\partial r} & \frac{\partial y}{\partial r} & \frac{\partial z}{\partial r} \\ \frac{\partial x}{\partial s} & \frac{\partial y}{\partial s} & \frac{\partial z}{\partial s} \\ \frac{\partial x}{\partial t} & \frac{\partial y}{\partial t} & \frac{\partial z}{\partial t} \end{bmatrix} \begin{bmatrix} \frac{\partial N_i}{\partial x} \\ \frac{\partial N_i}{\partial y} \\ \frac{\partial N_i}{\partial z} \end{bmatrix} = [J] \begin{bmatrix} \frac{\partial N_i}{\partial x} \\ \frac{\partial N_i}{\partial y} \\ \frac{\partial N_i}{\partial z} \end{bmatrix}$$

where [J] is the Jacobian of the transformation. The global derivatives can be derived

by

$$\begin{bmatrix} \frac{\partial N_i}{\partial x} \\ \frac{\partial N_i}{\partial y} \\ \frac{\partial N_i}{\partial z} \end{bmatrix} = [J]^{-1} \begin{bmatrix} \frac{\partial N_i}{\partial r} \\ \frac{\partial N_i}{\partial s} \\ \frac{\partial N_i}{\partial t} \end{bmatrix}$$

Similarly the volume can be written as

$$dv = dxdydz = |J|drdsdt$$

where $|J|$ is the determinant of the Jacobian.

To evaluate the elemental contributions to the final global form, equations (5.31 and 5.32) must be integrated over the element. Since isoparametric elements are used, all the quantities are mapped into the local coordinate system. This transformation simplifies the integration limits, but due to the complex shapes involved numerical integration is performed. A Gauss quadrature method is used where the integrations are reduced to

$$\int_{-1}^{1}\int_{-1}^{1}\int_{-1}^{1} f'(r,s,t)drdsdt \tag{5.44}$$

where f' is the transformed integrand. Appendix D discusses the process of numerical integration.

Global matrix

Equations (5.31 and 5.32) are integrated over the entire domain to form the final matrix. Instead of performing this process over the entire region, it is convenient to integrate it over each element and then sum all the individual contributions. This

gives $4 \times N$ simultaneous linear equations or a $4N \times 4N$ global coefficient matrix where N is the total number of nodes in the domain. Thus at each node, the variables to be determined are the 3 components of $\vec{A}$ and the scalar potential ϕ. Eight node linear elements are used for discretization which yield 32 equations. The size of the element matrix is 32×32. Substituting the shape functions and their derivatives into equation (5.31) the following submatrix is obtained for every node in the element.

$$\begin{bmatrix} S_{4i-3,4i-3} & 0 & 0 & 0 \\ 0 & S_{4i-2,4i-2} & 0 & 0 \\ 0 & 0 & S_{4i-1,4i-1} & 0 \\ 0 & 0 & 0 & 0 \end{bmatrix}$$

$$+j\omega\sigma \begin{bmatrix} R_{4i-3,4i-3} & 0 & 0 & R_{4i-3,4i} \\ 0 & R_{4i-2,4i-2} & 0 & R_{4i-2,4i} \\ 0 & 0 & R_{4i-1,4i-1} & R_{4i-1,4i} \\ R_{4i,4i-3} & R_{4i,4i-2} & R_{4i,4i-1} & R_{4i,4i} \end{bmatrix} \begin{bmatrix} A_{xi} \\ A_{yi} \\ A_{zi} \\ \phi \end{bmatrix} = \begin{bmatrix} Q_{4i-3} \\ Q_{4i-2} \\ Q_{4i-1} \\ 0 \end{bmatrix}$$

where the coefficients are

$$S_{4i-3,4i-3} = \int_v \left(\frac{\partial N_i}{\partial x}\frac{1}{\mu_y}\frac{\partial N_j}{\partial x} + \frac{\partial N_i}{\partial y}\frac{1}{\mu_z}\frac{\partial N_j}{\partial y} + \frac{\partial N_i}{\partial z}\frac{1}{\mu_x}\frac{\partial N_j}{\partial z}\right) dxdydz \qquad (5.45)$$

$$S_{4i-2,4i-2} = S_{4i-3,4i-3} \qquad (5.46)$$

$$S_{4i-1,4i-1} = S_{4i-3,4i-3} \qquad (5.47)$$

$$R_{4i-3,4i-3} = \int_v N_i N_j \, dxdydz \qquad (5.48)$$

$$R_{4i-2,4i-2} = R_{4i-3,4i-3} \qquad (5.49)$$

$$R_{4i-1,4i-1} = R_{4i-3,4i-3} \qquad (5.50)$$

$$R_{4i,4i-3} = \int_v N_i \frac{\partial N_j}{\partial x} dxdydz \tag{5.51}$$

$$R_{4i,4i-2} = \int_v N_i \frac{\partial N_j}{\partial y} dxdydz \tag{5.52}$$

$$R_{4i,4i-1} = \int_v N_i \frac{\partial N_j}{\partial z} dxdydz \tag{5.53}$$

$$R_{4i-3,4i} = R_{4i,4i-3} \tag{5.54}$$

$$R_{4i-2,4i} = R_{4i,4i-2} \tag{5.55}$$

$$R_{4i-1,4i} = R_{4i,4i-1} \tag{5.56}$$

$$R_{4i,4i} = -\int_v (\frac{\partial N_i}{\partial x}\frac{\partial N_j}{\partial x} + \frac{\partial N_i}{\partial y}\frac{\partial N_j}{\partial y} + \frac{\partial N_i}{\partial z}\frac{\partial N_j}{\partial z}) dxdydz \tag{5.57}$$

$$Q_{4i-3} = \int_v J_x N_i dxdydz \tag{5.58}$$

$$Q_{4i-2} = \int_v J_y N_i dxdydz \tag{5.59}$$

$$Q_{4i-1} = \int_v J_z N_i dxdydz \tag{5.60}$$

In addition to the volume integrals, two surface integrals are involved in equation (5.32). They are added to equations (5.51 to 5.53) as follows:

$$R_{4i-3,4i-3} = R_{4i-3,4i-3} - \int_s N_i N_j n_x ds \tag{5.61}$$

$$R_{4i-2,4i-2} = R_{4i-2,4i-2} - \int_s N_i N_j n_y ds \tag{5.62}$$

$$R_{4i-1,4i-1} = R_{4i-1,4i-1} - \int_s N_i N_j n_z ds \tag{5.63}$$

$$R_{4i,4i} = R_{4i,4i} - \int_s (N_i \frac{\partial N_j}{\partial x} n_x + N_i \frac{\partial N_j}{\partial y} n_y + N_i \frac{\partial N_j}{\partial z} n_z) ds \tag{5.64}$$

Here, $\vec{n}$ is the unit normal vector, and n_x, n_y and n_z are the components of the unit normal in the x,y and z directions respectively.

The surface integral of equation (5.31), which is the linking term, is treated separately. The integrand $\vec{n} \times \frac{1}{\mu} \nabla \times \vec{A}$ is considered as a secondary variable $\hat{B}$. Thus, this integral gives a nodal matrix of the form,

$$\begin{bmatrix} T_{4i-3,4i-3} & 0 & 0 \\ 0 & T_{4i-2,4i-2} & 0 \\ 0 & 0 & T_{4i-1,4i-1} \end{bmatrix}$$

where,

$$T_{4i-3,4i-3} = \int_s N_i N_j \, ds \tag{5.65}$$

$$T_{4i-2,4i-2} = \int_s N_i N_j \, ds \tag{5.66}$$

$$T_{4i-1,4i-1} = \int_s N_i N_j \, ds \tag{5.67}$$

In this formulation, the conductivity is assumed to be spatially independent while the permeability is allowed spatial variation. Each coefficient (equations (5.45-5.67)) for each node in the element is numerically integrated using Gauss quadrature and summed into a complex elemental matrix equation of the form

$$\{[S] + j\omega\sigma[R]\}A + [T]\{\hat{B}\} = \{Q\} \tag{5.68}$$

[S] and [R] are the real and imaginary part of the 32×32 elemental matrix. [T] is a 24×24 matrix which links the two formulations, $\{A\}$ and $\{Q\}$ are the 32×1 vectors of the unknown and source terms respectively, and $\{\hat{B}\}$ is the 24×1 vector of the secondary variable which is later eliminated.

The elemental matrices are summed over the total number of elements to provide a global system of $4 \times N$ simultaneous linear system of algebraic equations.

$$[G]\{A\} + [T]\{\hat{B}\} = \{Q\} \tag{5.69}$$

[G] is the global coefficient matrix which is sparse, banded and diagonally dominant. *Skyline storage* [140] gives a compact form to store this matrix, which reduces the storage requirements tremendously. Since this matrix equation has to be coupled with the boundary element equation, it is discussed after the boundary element formulation.

The next section discusses the boundary element formulation.

Boundary element

The boundary integral is applied to the free space around the probe and conducting specimen. Thus the governing equation is

$$\begin{aligned} \nabla \times \frac{1}{\mu} \nabla \times \vec{A} &= 0 \\ \nabla \times \nabla \times \vec{A} &= 0 \end{aligned} \tag{5.70}$$

with the Coloumb gauge $\nabla \cdot \vec{A} = 0$.

Green's second identity for vectors is

$$\begin{aligned} &\int_v (\vec{Q} \cdot \nabla \times \nabla \times \vec{P} - \vec{P} \cdot \nabla \times \nabla \times \vec{Q}) dv = \\ &\quad \int_s \left((\vec{P} \times \nabla \times \vec{Q}) - (\vec{Q} \times \nabla \times \vec{P}) \right) \cdot \vec{n} ds \end{aligned} \tag{5.71}$$

In 3D, the Green's function that satisfies equation (5.70) is

$$G = \frac{1}{4\pi r}$$

while the fundamental solution is

$$\vec{F} = \nabla(\frac{1}{4\pi r}) \times \hat{a}$$

where $\hat{a}$ is an arbitrary unit vector, and $r = \sqrt{(x'-x)^2+(y'-y)^2+(z'-z)^2}$. Identifying $\vec{P} = \vec{A}$ and $\vec{Q} = \frac{\hat{a}}{4\pi r}$, and applying equation (5.70) and Gauss's theorem, equation (5.71) is transformed as [138,139]:

$$-\hat{a}\int_s(\vec{A}\cdot\vec{n})\nabla(\frac{1}{4\pi r})ds = \hat{a}\cdot\int_s\nabla(\frac{1}{4\pi r})\times(\vec{A}\times\vec{n})ds - \hat{a}\cdot\int_s(\frac{\nabla\times\vec{A}}{4\pi r})\times\vec{n}ds$$

Since $\hat{a}$ is an arbitrary unit vector, it is eliminated to obtain,

$$0 = \int_s(\vec{A}\cdot\vec{n})\nabla(\frac{1}{4\pi r})ds + \int_s\nabla(\frac{1}{4\pi r})\times(\vec{A}\times\vec{n})ds - \int_s\frac{(\nabla\times\vec{A})\times\vec{n}}{4\pi r}ds \qquad (5.72)$$

This integral equation is valid for regions where the functions are continuous and possesses continuous first and second derivatives. Since $\vec{Q}$ has a singularity at $r = 0$, this point has to be excluded.

Singularity removal

About the point (x', y', z') a small sphere of surface s_ϵ and radius r_1 is circumscribed such that $r_1 \to 0$. Now the domain volume is bounded by $s = s' + s_\epsilon$.

Over s_ϵ, $\nabla(\frac{1}{4\pi r}) = \frac{1}{4\pi}(\frac{\vec{r_0}}{r_1^2})$. Thus equation (5.69) over s_ϵ can be written as

$$0 = \frac{1}{4\pi r_1^2}\int_{s_\epsilon}\vec{r_0}(\vec{A}\cdot\vec{n})ds_\epsilon + \frac{1}{4\pi r_1^2}\int_{s_\epsilon}\vec{r_0}\times(\vec{A}\times\vec{n})ds_\epsilon + \frac{1}{4\pi r_1}\int_{s_\epsilon}(\nabla\times\vec{A})\times\vec{n}ds_\epsilon \qquad (5.73)$$

$\vec{r_0}$ is the unit vector in the direction of $\vec{r}$. Using various identities and assuming $\vec{r_0}\cdot\vec{n} = 1$, $\vec{r_0}\times\vec{n} = 0$ and in the limit as $r_1 \to 0$, the above equation is reduced to

$$\frac{1}{4\pi r_1^2}\int_{s_\epsilon}\vec{A}ds_\epsilon$$

In the limit as $r_1 \rightarrow 0$, $ds_\epsilon = 4\pi r_1^2$, thus

$$\int_{s_\epsilon} = \vec{A}(x', y', z') \tag{5.74}$$

Thus in the limit analysis, the value of the function at the source point is obtained. The *boundary integral equation* (BIE) is then

$$\vec{A}(x', y', z') = -\int_s (\vec{A} \cdot \vec{n}) \nabla(\frac{1}{4\pi r}) ds + \int_s \nabla(\frac{1}{4\pi r}) \times \vec{n} \times \vec{A} ds + \int_s \frac{(\nabla \times \vec{A}) \times \vec{n}}{4\pi r} ds \tag{5.75}$$

The third integral on the right hand side is the linking term. This BIE can be written in a more compact form as

$$\vec{A}(x', y', z') = -\int_s \tilde{T} \vec{A} ds + \int_s \tilde{U} \hat{B} ds \tag{5.76}$$

where the kernels that operate on the variables $\vec{A}$ and $\hat{B}$ are:

$$\begin{aligned} \tilde{T} &= -\nabla(\frac{1}{4\pi r}) \times \vec{n} \times + \nabla(\frac{1}{4\pi r}) \vec{n} \cdot \\ \tilde{U} &= \frac{\mu}{4\pi r} \end{aligned} \tag{5.77}$$

$\hat{B}$ is the secondary variable $\frac{1}{\mu} \nabla \times \vec{A} \times \vec{n}$

Since the kernels in these integrals need to be regularized, they are written in a convenient form as

$$\vec{A}(x', y', z') + \int_{s'} \tilde{T} \vec{A} ds + \int_{s_\epsilon} \tilde{T} \vec{A} ds = \int_{s'} \tilde{U} \hat{B} ds + \int_{s_\epsilon} \tilde{U} \hat{B} ds \tag{5.78}$$

The kernels under the s' domain are non-singular, while those inside the domain of s_ϵ are singular. Thus in the singular domain, the above equation can be written as

$$\vec{A}(x', y', z') + \int_{s_\epsilon} (\tilde{T} - \hat{\tilde{T}}) \vec{A} ds + \int_{s_\epsilon} \hat{\tilde{T}} \vec{A} ds = \int_{s_\epsilon} (\tilde{U} - \hat{\tilde{U}}) \hat{B} ds - \int_{s_\epsilon} \hat{\tilde{U}} \hat{B} ds \tag{5.79}$$

$\hat{\tilde{T}}$ is defined as $\nabla(\frac{1}{4\pi r})$ and $\hat{\tilde{U}}$ is $\frac{1}{4\pi r}$. In equation (5.79) the second term on the left hand side and the first term on the right hand side regularize the integral and reduce the order of the singularity. The remaining integrals are then integrated analytically. Thus the final form of the equation which is discretized in the boundary element formulation used in the dissertation is

$$\begin{aligned}\vec{A}(x',y',z') + \int_{s'} \tilde{T}\vec{A}ds + \int_{s_\epsilon} \hat{\tilde{T}}\vec{A}ds + \int_{s_\epsilon} (\tilde{T} - \hat{\tilde{T}})\vec{A}ds \\ = \int_{s^\epsilon} \tilde{U}\hat{B}ds + \int_{s_\epsilon} \hat{\tilde{U}}\hat{B}ds + \int_{s_\epsilon} (\tilde{U} - \hat{\tilde{U}})\hat{B}ds \end{aligned} \tag{5.80}$$

Discretization

For a typical eddy current geometry (Figure 5.1), only the boundary, or the surface, of the probe and conducting specimen are discretized. Four node isoparametric quadrilaterals are used for discretizing the surface. The associated shape functions are given in Appendix A. $\vec{A}$ and $\hat{B}$ are interpolated using the shape functions as,

$$\begin{aligned} A_k(x,y,z) &= \sum_{i=1}^{4} H_i(r,s)A_{ki} \\ \hat{B}_k(x,y,z) &= \sum_{i=1}^{4} H_i(r,s)\hat{B}_{ki} \qquad k = x,y,z \end{aligned} \tag{5.81}$$

Similarly, the derivatives of $\vec{A}$ are represented as

$$\begin{aligned} \frac{\partial A_k}{\partial x} &= \sum_{i=1}^{4} \frac{\partial H_i}{\partial x}A_{xi} \\ \frac{\partial A_k}{\partial y} &= \sum_{i=1}^{4} \frac{\partial H_i}{\partial y}A_{yi} \\ \frac{\partial A_k}{\partial z} &= \sum_{i=1}^{4} \frac{\partial H_i}{\partial z}A_{zi} \qquad k = x,y,z \end{aligned} \tag{5.82}$$

The Jacobian of the transformation is derived similarly to that in the finite element case (see chapter 3). The surface area for a 3D geometry is given by

$$ds = \sqrt{D} dr ds \tag{5.83}$$

where D is the determinant of the first fundamental magnitude. D is a 2×2 matrix formed by multiplying the reduced Jacobian RJ. Thus $D = RJ \times RJ^T$, where

$$RJ = \begin{bmatrix} \frac{\partial x}{\partial r} & \frac{\partial y}{\partial r} & \frac{\partial z}{\partial r} \\ \frac{\partial x}{\partial s} & \frac{\partial y}{\partial s} & \frac{\partial z}{\partial s} \end{bmatrix} \tag{5.84}$$

The next step is to integrate equation (5.77) over the domain surface and collocate it at every node point. Both two and three point Gauss quadrature rules are used for integrating. After collocating and integrating, the computation yields a global matrix equation

$$[V]\{A\} = [U]\{\hat{B}\} \tag{5.85}$$

where [V] and [U] are $3M \times 3M$ coefficient matrices and $\{A\}$ and $\{\hat{B}\}$ are the $3M \times 1$ vectors of the unknown functions. M is the number of surface nodes in the mesh which is normally much less than the number of volume nodes.

Linking process

The FEM and BEM global matrix equations are:

$$[G]\{A\} + [T]\{\hat{B}\} = \{Q\} \tag{5.86}$$

$$[V]\{A\} = [U]\{\hat{B}\} \tag{5.87}$$

Since $\hat{B}$ is to be eliminated,

$$\{\hat{B}\} = [U]^{-1}[V]\{A\} \tag{5.88}$$

This is substituted in equation (5.83) to obtain

$$[G]\{A\} + [T]\{[U]^{-1}[V]\}\{A\} = \{Q\} \tag{5.89}$$

Combining these two terms in the above equation, the final global system of equations is obtained:

$$[K]\{A\} = \{Q\} \tag{5.90}$$

where $[K] = [G] + [T][U]^{-1}[V]$.

The final global matrix is solved to obtain the final solution. It is relevant at this juncture to describe the nature of this global matrix generated by the FEM, BEM and the hybrid formulation.

In the domain FEM, the global matrix is the ideal matrix from a solution point of view. Though the number of rows and columns are large due to volumetric discretization, these matrices are normally symmetric. They are always sparse, banded and in general diagonally dominant. Thus most algorithms use compact storage schemes like *skyline storage* to store the non-zero terms of half the matrix (i.e upper or lower triangular matrix with the diagonal terms). The matrix is also well conditioned and a number of solution techniques are used to solve it.

The integral BEM, generates a smaller global matrix since only the surface is discretized. As it is based on the two point Green's function formulation, the matrix is always fully populated. There is no symmetry involved and it is not necessarily diagonally dominant. By averaging the off-diagonal terms, the matrix can be made

symmetric if required. If there are sharp corners in the geometry, then these could make the matrix ill-conditioned due to the singular integration.

In the hybrid formulation linking process between the finite and the boundary element matrix, the process involves two steps: 1) the surface finite element matrix is multiplied with the boundary element matrix (equation 5.89) and 2) the resultant of 1 is added to the global finite element matrix (equation 5.89). In step 1 the multiplication of two symmetric or unsymmetric matrices always results in an unsymmetric matrix. Thus, when added to the global finite element matrix it makes the final global matrix unsymmetric. Another disadvantage is that the sparsity of the finite element matrix is also lost. Thus the total matrix needs to be stored for obtaining the final solution.

A standard Gaussian elimination for complex matrices is used to solve this set of linear equations. Chapter 8 will present the results obtained form applying the formulation to an absolute eddy current probe over an aluminium block.

CHAPTER 6. POTENTIAL DROP METHODS: RESULTS

Chapters three and four discuss the finite element and boundary element formulation for the DCPD and ACPD methods of nondestructive testing. In this chapter, the results of the 2D and 3D simulations of the finite element and boundary element model on the various fatigue specimens are compared to existing data. The next chapter compares and contrast the two numerical techniques. All the calculations in the study are performed on the Stardent *GS 1000* computer.

ACPD Method

Only 2D simulations are reported for the ACPD method. For the measurement model, two simple geometries are considered. The first is a one dimensional crack with an infintesimal thickness and the second is a semi-circular crack with a finite aspect ratio (Figure 6.1). The initial step is to confirm the probe response as it scans across the specimen. This is achieved by comparing the normalized probe voltage of the finite and boundary element simulations to experimental data.

The discretization for the finite element simulation uses three node triangular elements while the boundary element simulation uses three node line elements. A 1.6 kHz alternating current input is the excitation source to generate the electric fields in the specimen.

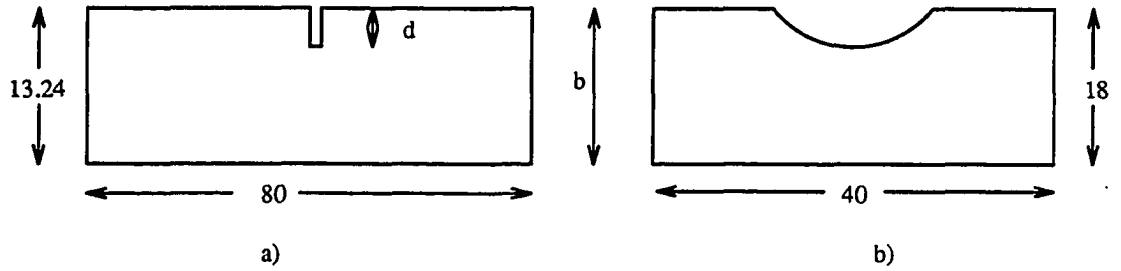

Figure 6.1: a) One dimensional crack specimen with an infinite aspect ratio crack and b) Semi-circular cracked specimen

Figure 6.2 is the plot of the normalized probe voltage as a function of the probe movement as it scans the crack from left to right. As one leg of the probe approaches the crack, there results a dip in the voltage which then jumps to a high level at the tip of the crack. As the other leg comes closer to the crack, the voltage drops and is then normalized to a constant level away from the crack. The finite and boundary element predictions [133] are very similar to the experimental data [116].

The frequency of the excitation is increased to reduce the skin depth in the specimen. Figure 6.3 and Figure 6.4 are the normalized voltages for four different voltages for the finite and boundary element models respectively. The skin depth reduces with increasing frequency, indicated by the drop in the voltage between the probe legs. This is a characterstic response of the probe used in the ACPD method.

All the figures confirm the validity of the numerical models. For a very low frequency, the skin depth is much greater than the crack depth and is called the *thick skin approximation.* Using equation (3.9), the crack depth can be predicted for different probe widths and constant frequency. The finite and boundary element

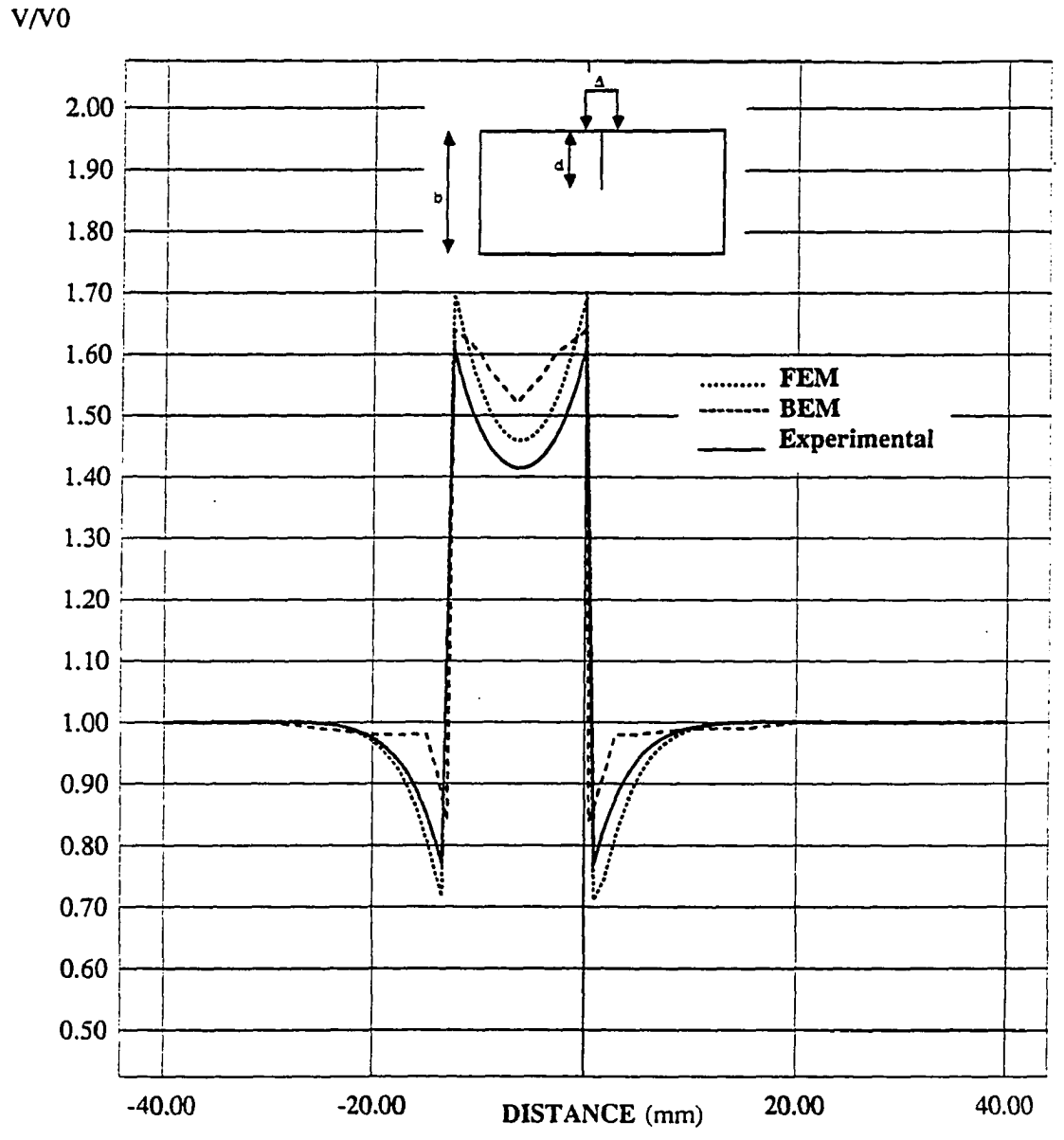

Figure 6.2: Normalized probe voltages for the infinitesimal thin crack for the FEM, BEM models and experimental data [116]

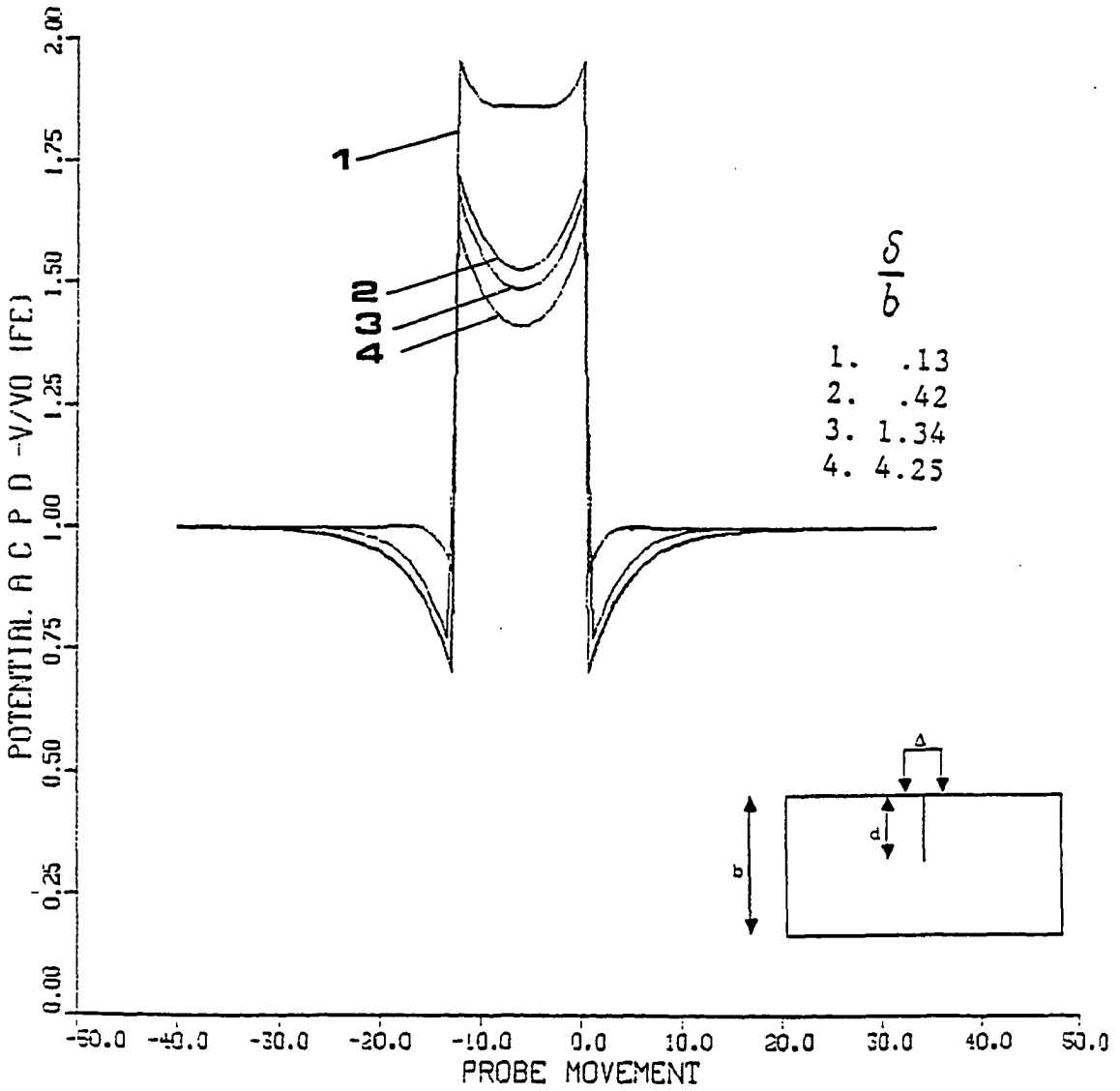

Figure 6.3: Finite element predictions of the normalized voltages for four different frequencies or four skin depth to specimen width ($\frac{\delta}{b}$) ratios

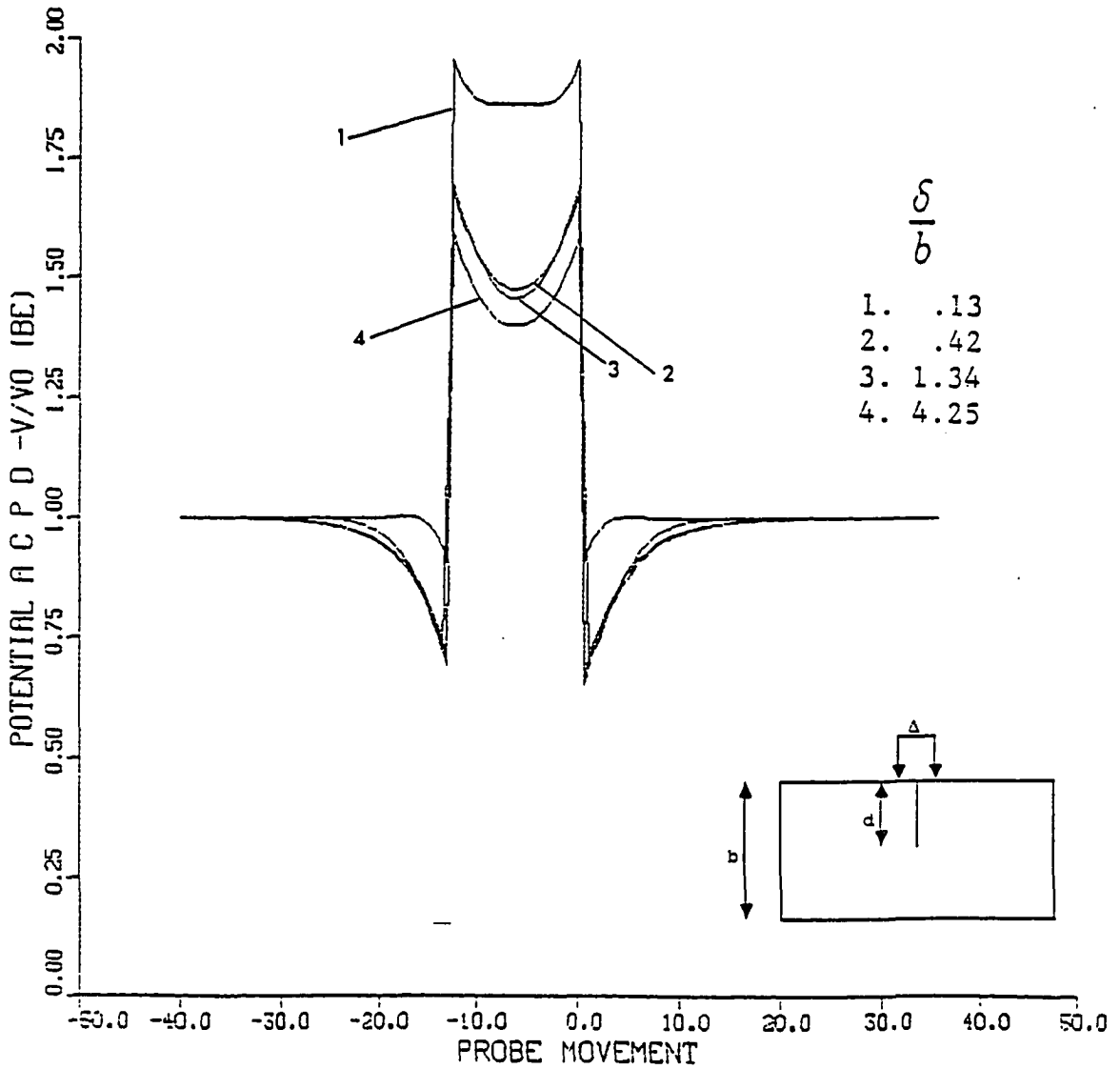

Figure 6.4: Boundary element predictions of the normalized voltages for four different frequencies or four skin depth to specimen width ($\frac{\delta}{b}$) ratios

predictions are shown in Figure 6.5. A maximum error of 6 % is achieved between the actual and numerically predicted crack depth.

Figure 6.6 is finite element representation of the current distribution in the material, clearly indicating the exponential decrease in the current magnitude and the perturbation due to the crack. The next two results are for the semi-circular crack. Figure 6.7 shows the potential value across the crack for the FEM, BEM models and experimental values [134]. The error calculated between the numerical and experimental data is less than 5 %. Finally to complete the study, the potential distribution in the specimen is plotted in Figure 6.8, demonstrating the shape of the crack. This is the result from the finite element simulation.

The modeling of the ACPD method demonstrated the usefulness of numerical modeling. The model not only helped in visualizing the voltage and current distribution in the specimen, but the crack depth is also predicted. Comparing the numerical predictions to experimental data, confirmed the validity of the numerical models. In the next section the DCPD method is modeled in both two and three dimensions.

DCPD Method

In the DCPD method, a direct current is applied to the specimen and the potential that develops across the crack is monitored. These potentials are plotted as *calibration curves* (see page 15) and used for predicting the fatigue crack length. Results from 2D and 3D simulations are presented below.

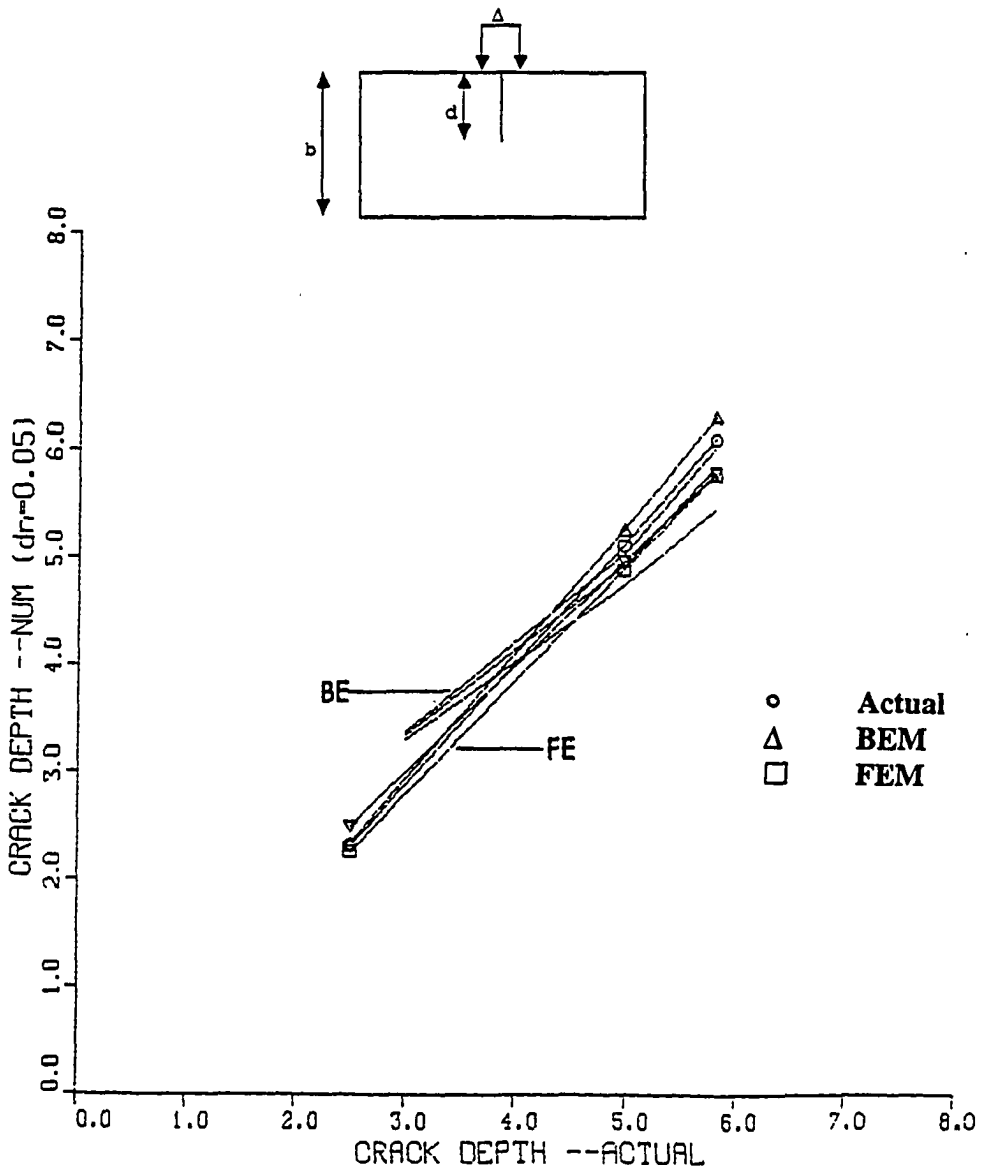

Figure 6.5: Finite element and boundary element predictions of the crack depth for three probe widths. Δ =12.5.29 and 58mm

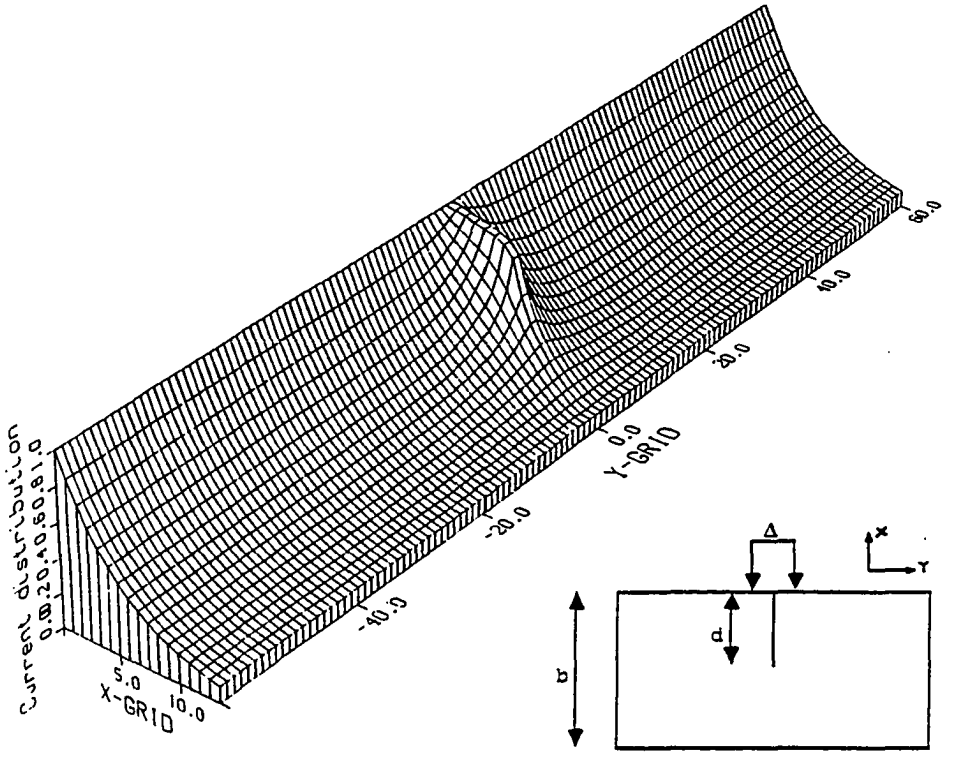

Figure 6.6: Finite element predictions of the current distribution in the specimen

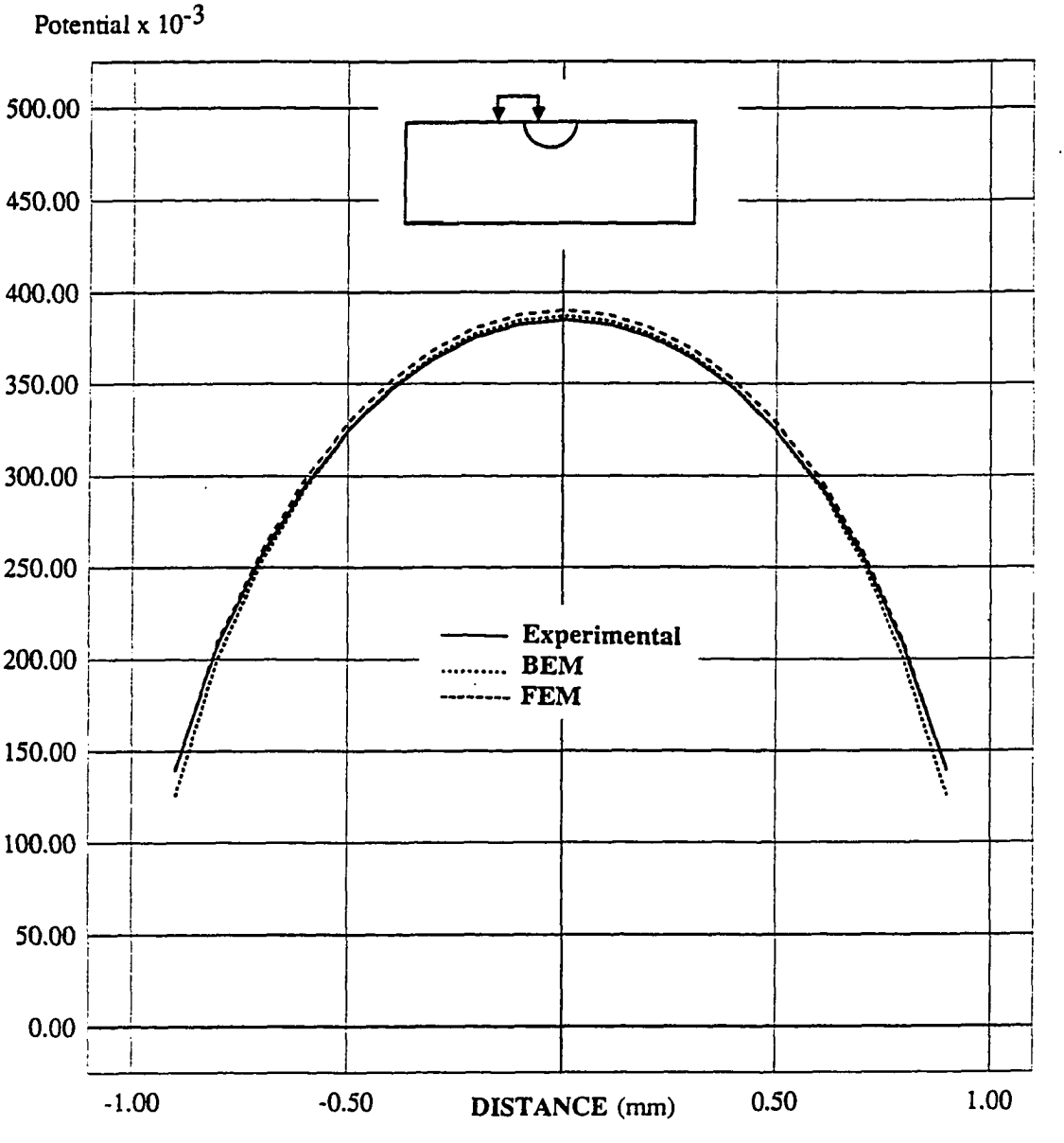

Figure 6.7: Finite element, boundary element and experimental data for the potential across a semi-circular crack

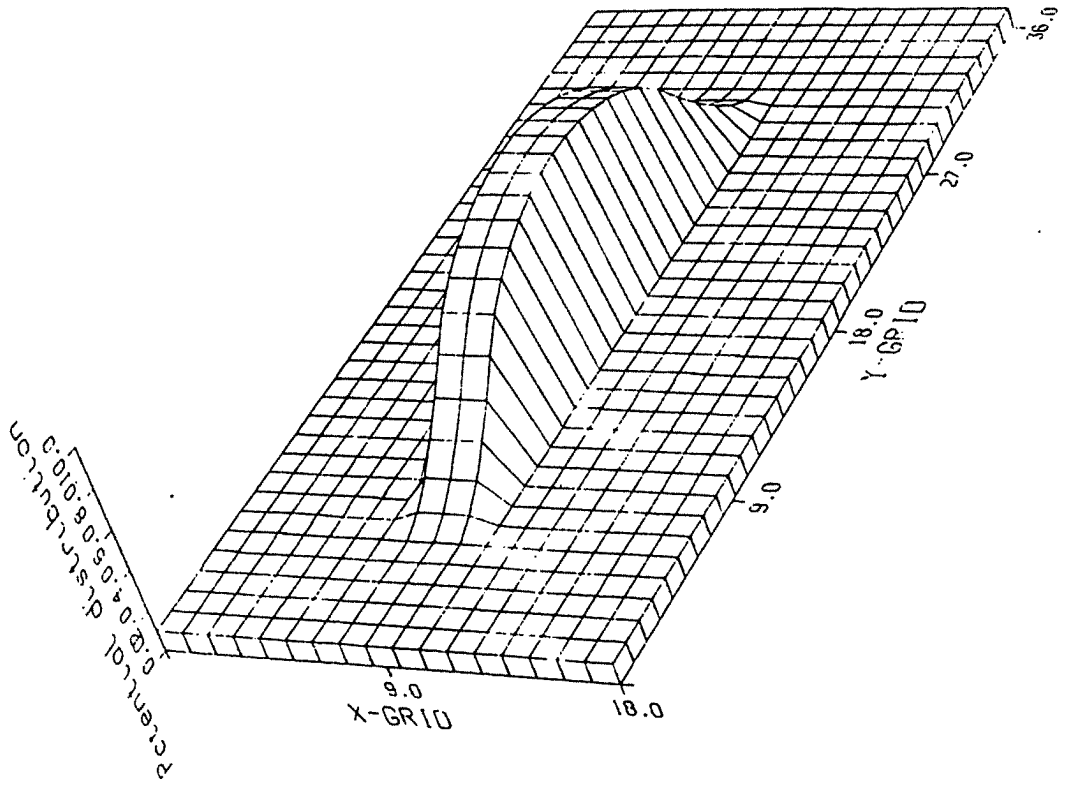

Figure 6.8: Finite element predictions of the potential distribution in the specimen

2D simulations

The compact tension (CT) and the single edge notch (SEN) specimen (Figure 3.2) are discretized in the 2D simulations. Figure 6.9 shows the finite element mesh for both the specimens. Only half the geometry is modeled due to symmetry. For both the specimens, the input is modeled as boundary conditions for the potential. In the CT specimen, a point on the left boundary is maintained at voltage V_1 with a reference voltage of $V = 0$ at the uncracked part of the specimen, while for the SEN specimen all the nodes on the left boundary of the specimen are maintained at voltage V_1.

Figure 6.10 and Figure 6.11 compare the calibration curves generated by the numerical models with experimental data for the SEN and CT specimen respectively. These curves depict the ratio of the potential as the crack increases, to the potential due to the initial crack, $(\frac{U}{U_0})$, as a function of the crack length to specimen width ratio $(\frac{A}{W})$ (Figure 3.2). Additionally, the data obtained from *Johnson's formula* (equation (3.2)) is also plotted in Figure 6.11 for the CT specimen. Again these plots confirm the numerical models.

Figure 6.12a shows the equi-potential contours obtained from the finite element model for the CT specimen while Figure 6.12b shows the equi-potential and equi-current contours for the SEN specimen. The effect of the crack, source position and other features are clearly demonstrated by the field plots.

The calibration curves are dimensionless quantities which make them universal. Researchers [41,101] have noted that these curves are independent of material properties, current input magnitude and thickness of the specimen. In the 2D analysis, the material property (conductivity) and voltage V_1 were changed to different values.

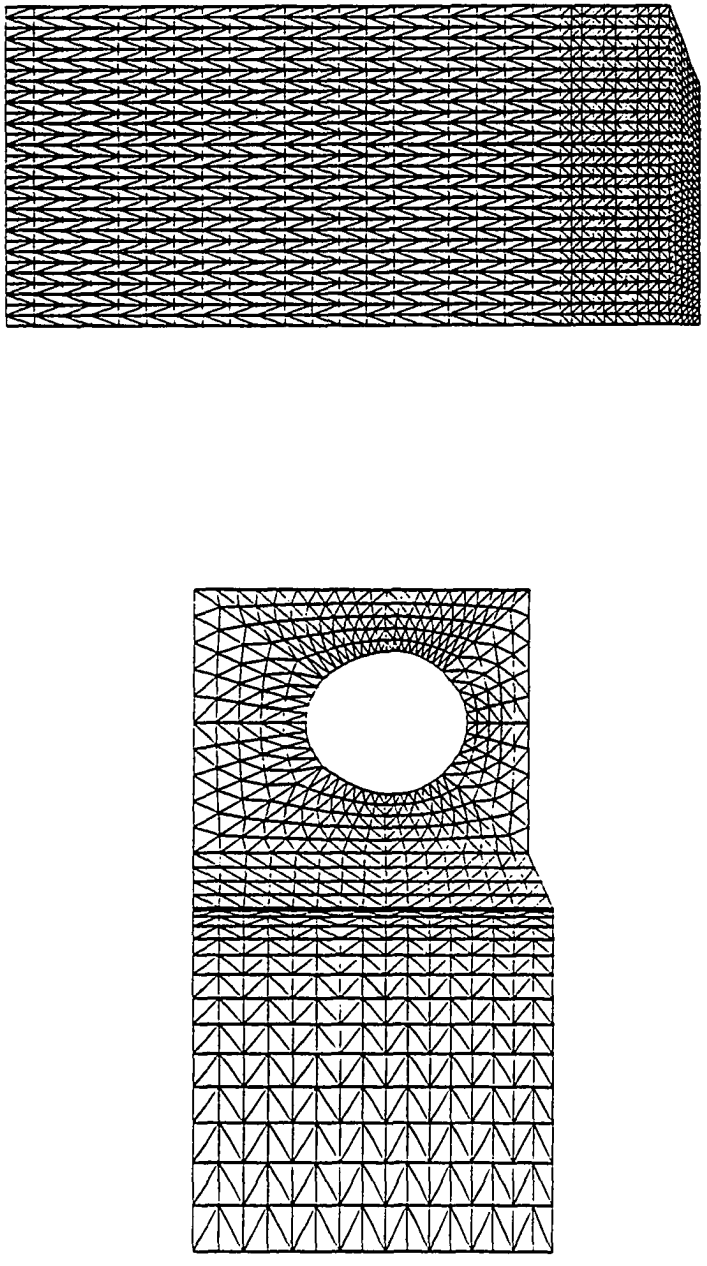

Figure 6.9: Two dimensional finite element mesh for a) SEN specimen and b) CT specimen

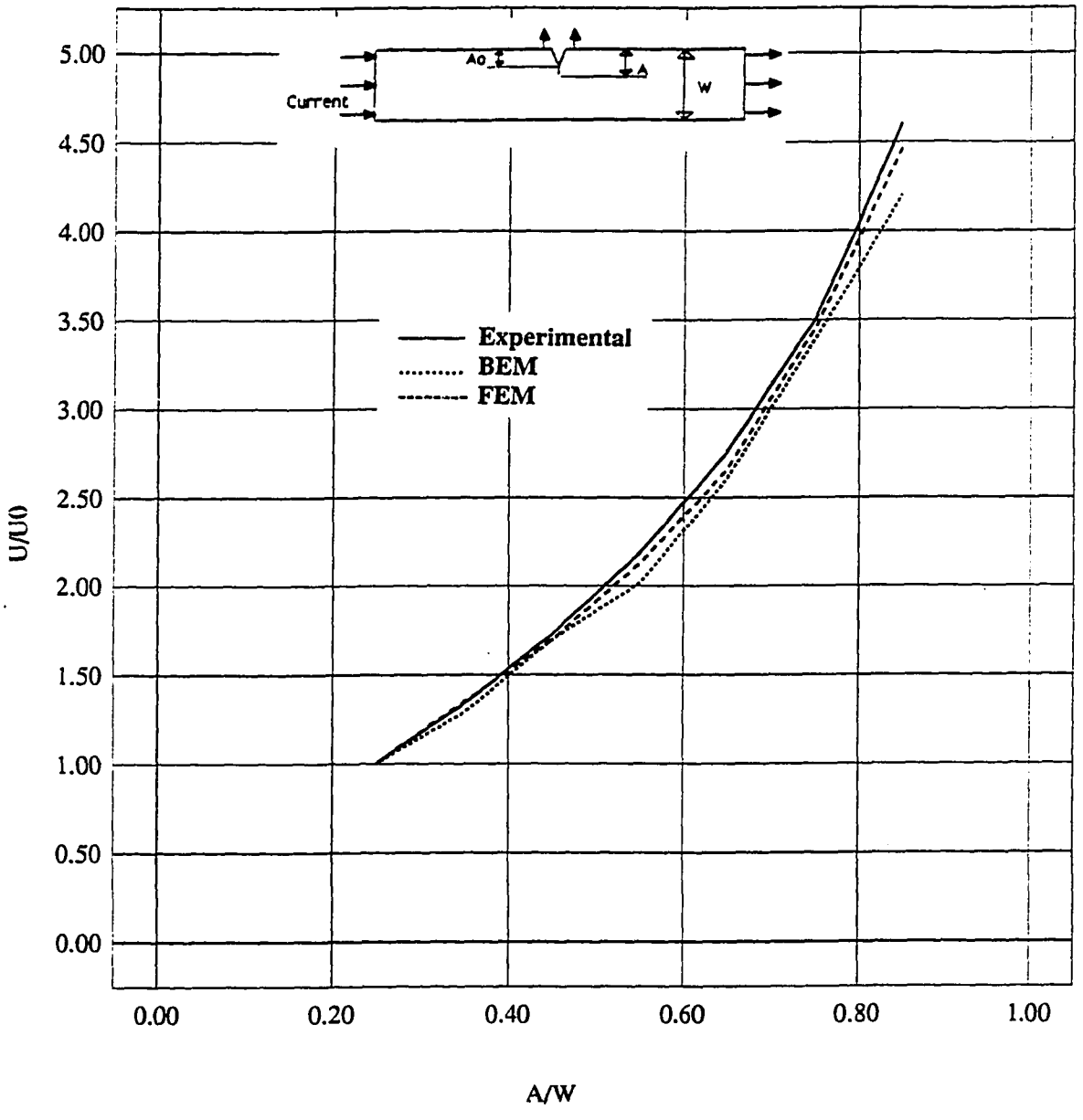

Figure 6.10: Calibration curves for the SEN specimen

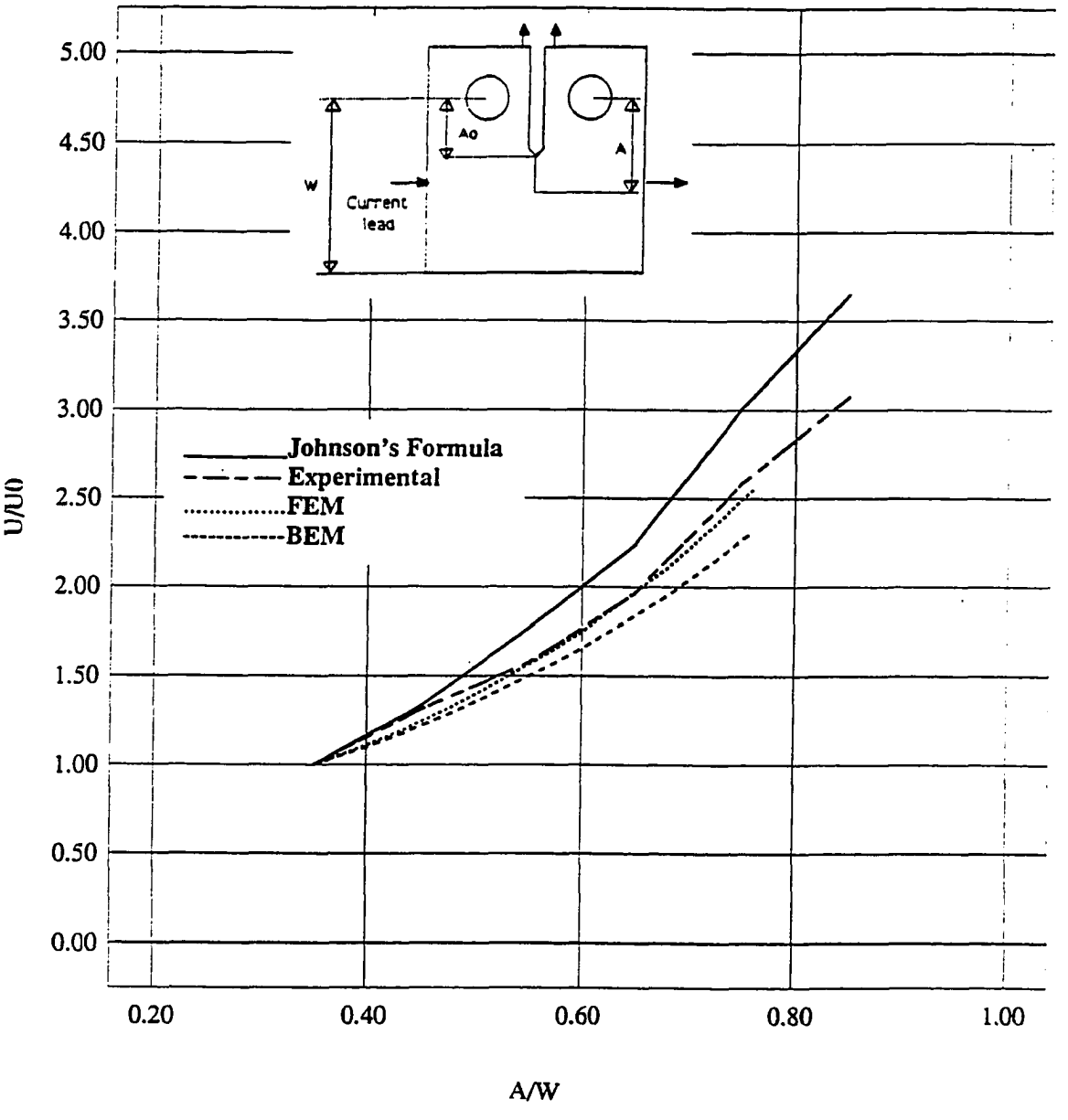

Figure 6.11: Calibration curves for the CT specimen

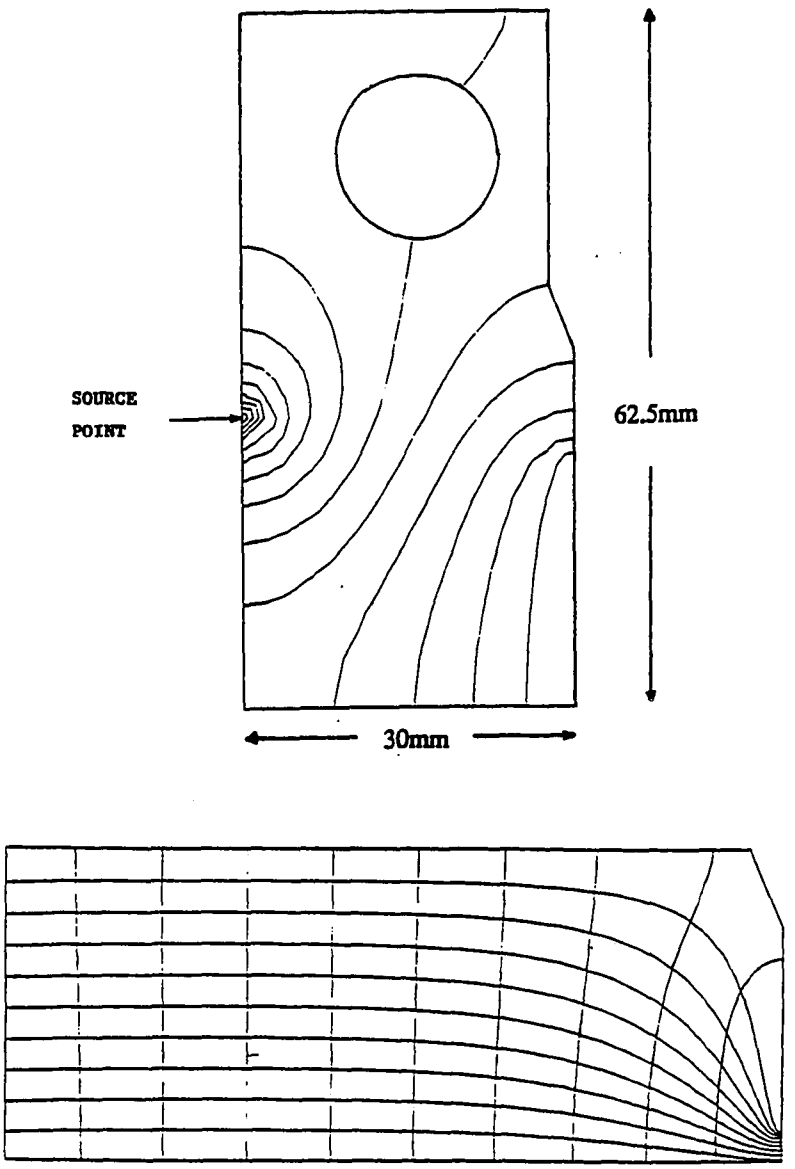

Figure 6.12: a) Equi-potential contours in the CT specimen from finite element data and b) Equi-potential and equi-current contours for the SEN specimen using finite element data

However, there were no changes observed in the calibration curves. To the best of the author's knowledge, a 3D numerical analysis using the DCPD method to see the effect of material thickness on the calibration curves has not been reported. The next section describes a 3D simulation of the CT specimen using the DCPD method.

3D simulations [135]

Figure 6.13 shows a CT specimen with the dimensions as shown. Again, symmetry of the specimen and test procedure allow for a quarter of the geometry to be modeled. As mentioned in an earlier chapter, the finite element model needs volumetric discretization which necessitates the use of eight node hexahedral elements. On the other hand, surface discretization, as required when using the BEM needs four node quadrilateral elements.

To validate the 3D finite and boundary element models, calibration curves for a 25.4mm specimen are compared to *Johnson's formula* and the 2D finite element prediction in Figure 6.14. These curves are comparable over a wide range of crack lengths.

To view the effect of sample thickness, Figure 6.15 plots the calibration curve for specimen thickness ranging from 6.25mm to 25.4mm. The last calibration plot compares the finite and boundary element predictions for two different specimen thicknesses (Figure 6.16).

The potential distribution on the top surface of the specimen is plotted for both the numerical models in Figure 6.17. The distributions are nearly identical in magnitude and shape. To complete this study the solution of the potential obtained by the finite element model is plotted for different thickness slices in Figure 6.18.

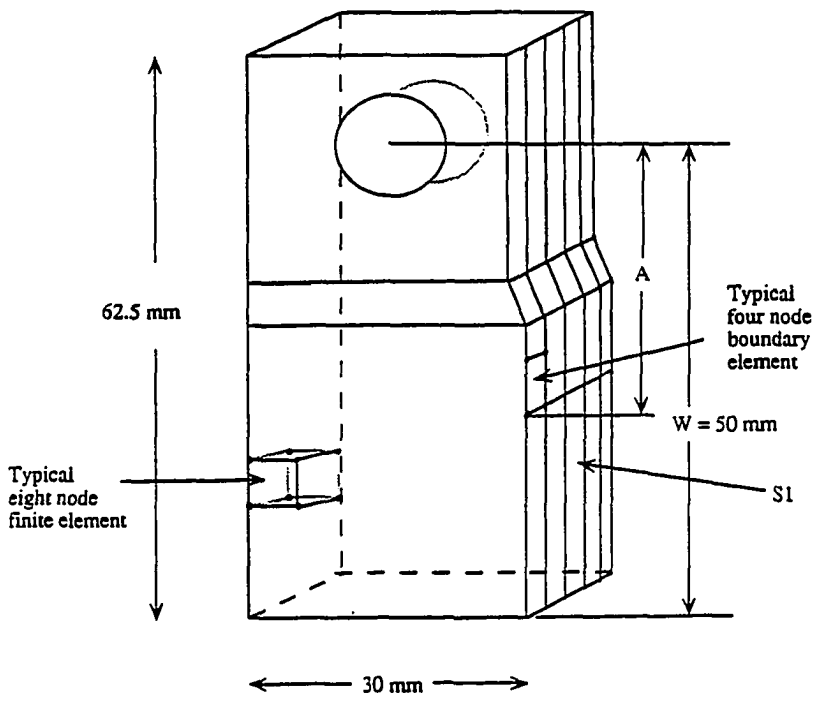

Figure 6.13: A quarter of the CT specimen used in the 3D modeling

The effect of the source point and crack is very clear in all the layers.

The next chapter will discuss these results in detail and the requisite computation resources. The finite element and boundary element model are compared and contrasted based on these results.

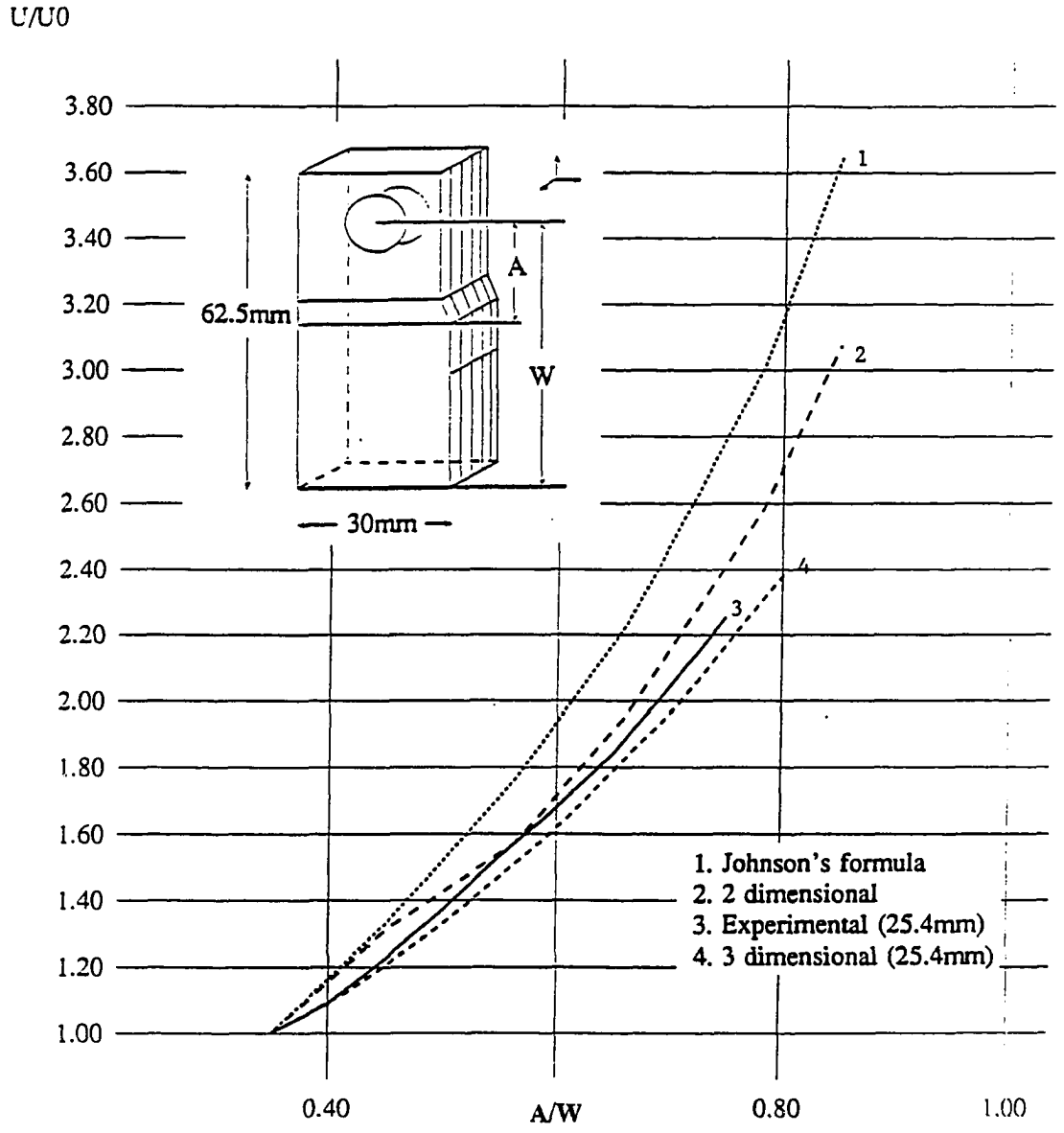

Figure 6.14: Calibration curves for the CT specimen comparing analytical, experimental [41] and numerical data

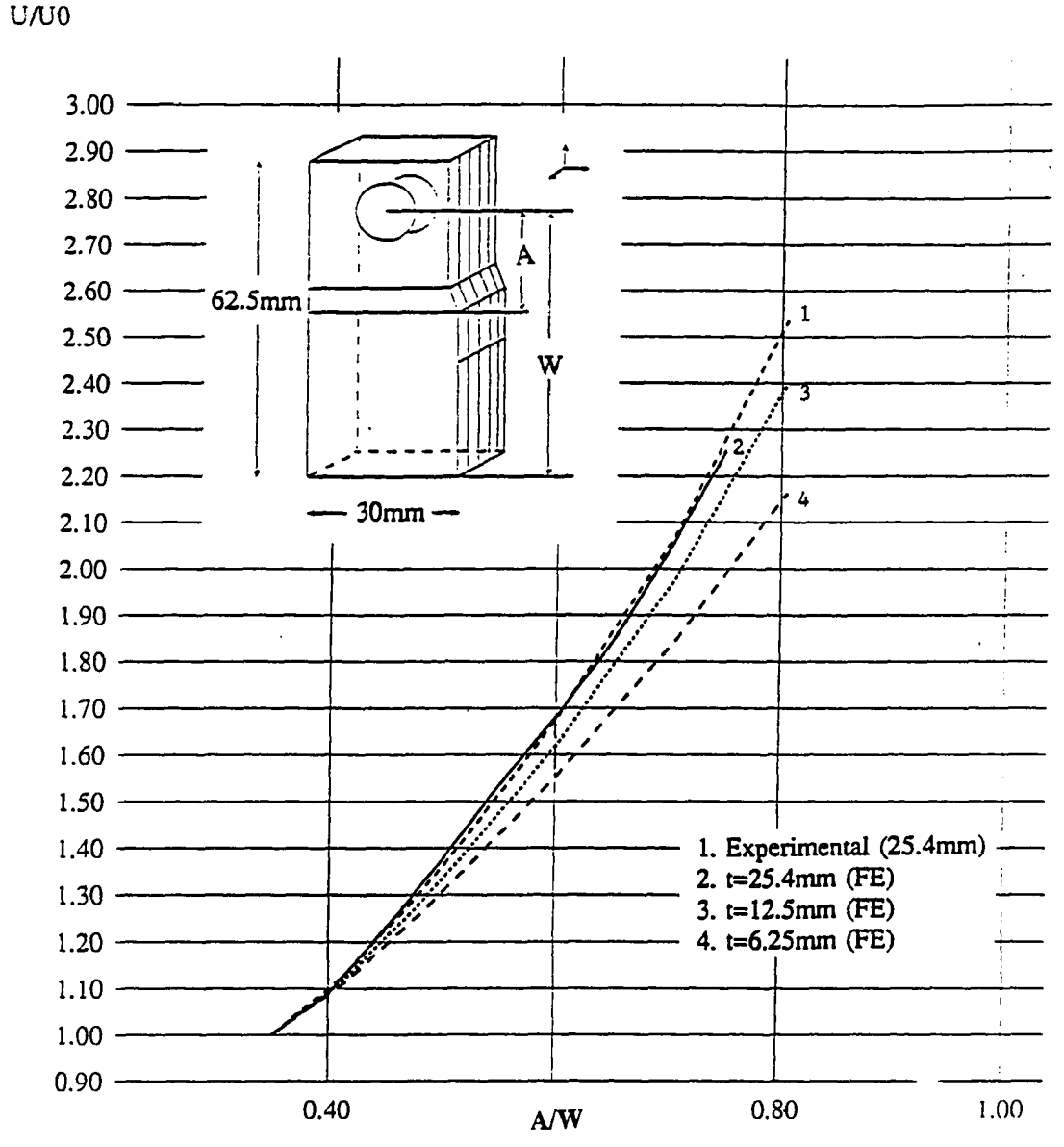

Figure 6.15: Finite element prediction of the calibration curves for range of specimen thickness

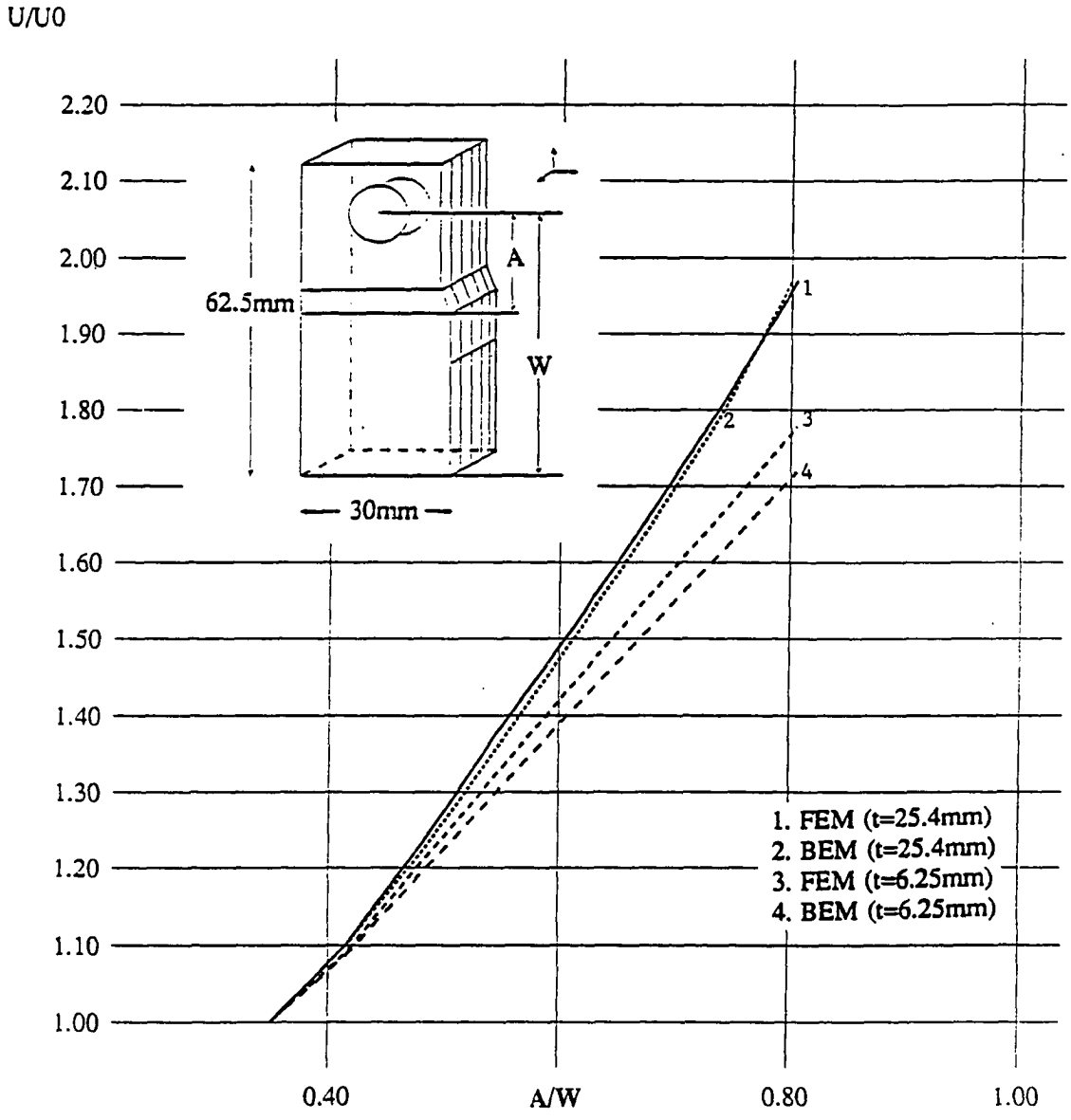

Figure 6.16: Finite element and boundary element predictions of the calibration curves for two different thickness

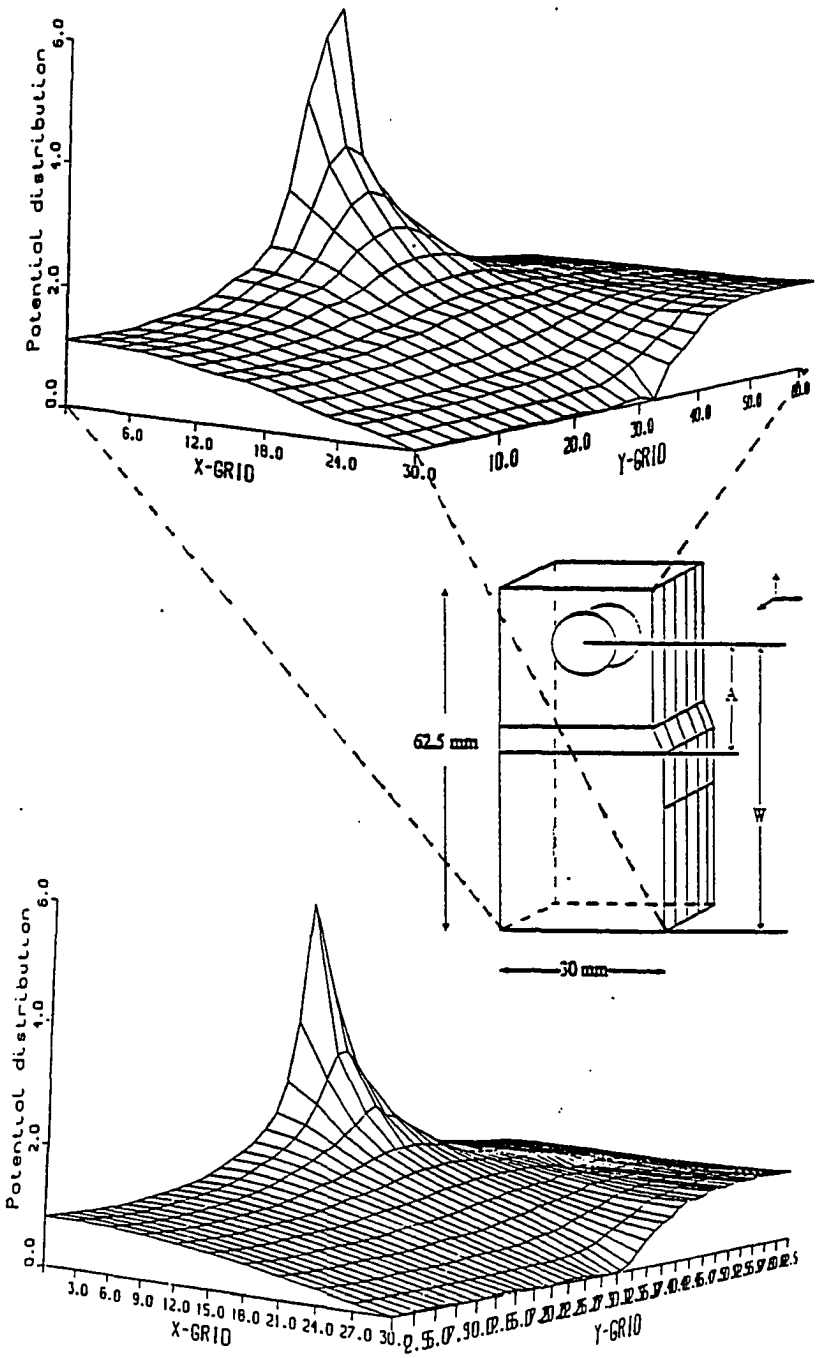

Figure 6.17: a) Finite element prediction of the potential distribution on the top surface and b) Boundary element predictions of the potential distribution on the top surface

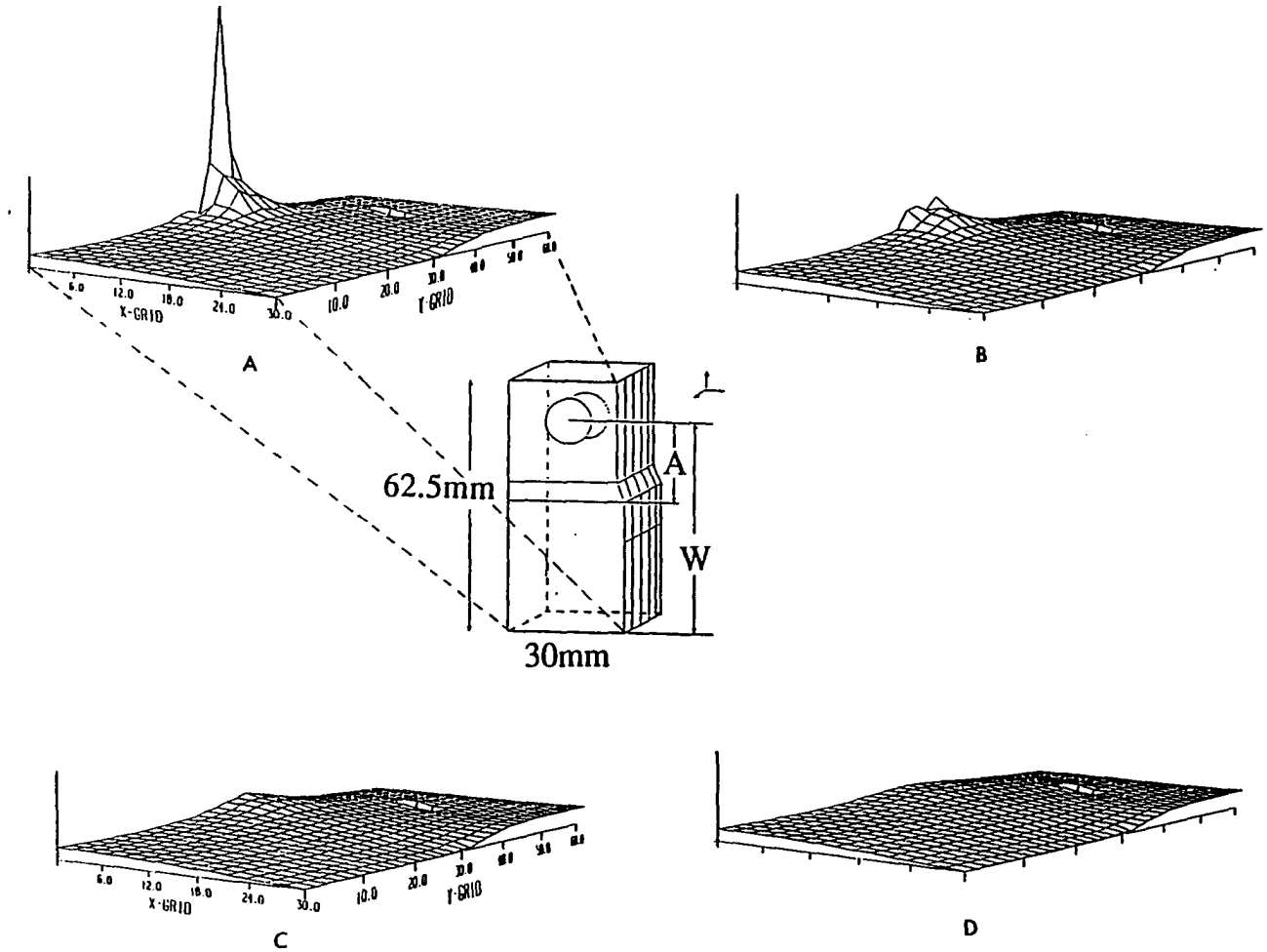

Figure 6.18: Potential distribution at different thickness slices in the sample a)top layer where the source is present b) second layer at a thickness of 6.25 mm c) third layer at a thickness of 12.5 mm and d) bottom layer at a thickness of 25.4 mm

CHAPTER 7. FINITE AND BOUNDARY ELEMENTS: ANALYSIS

One of the goals of this dissertation is to compare and contrast the FEM and BEM as applied to electromagnetic NDE. It is worth reiterating that an efficient forward numerical model is of extreme importance to the NDE community. The major benefits of the forward numerical model are able to:

- visualize the energy/defect interaction which helps in understanding a given phenomenon
- duplicate certain experiments which are difficult to replicate in a laboratory environment
- obtain the transducer response
- use the model as a test bed for generating data for the inverse problem [136]
- model complex shapes and geometries, non-linearities, anisotropy and other parameters

In today's computer aided design environment, effort is being devoted to incorporate NDE models at the design and manufacturing stage of product development in order to design and fabricate parts that would be easy to inspect and know apriori which type of NDE method could be applied at a later stage. Thus it is necessary to identify

and choose the best model for the application. This implies that the ideal numerical method has to be identified to satisfy this need. Modeling of the ACPD and DCPD method is the vehicle in this dissertation to highlight the issues involved in the FEM and BEM, two numerical models discussed in this dissertation.

When talking about the BEM and FEM, a particular consideration is that the BEM, which solves an integral equation for variables on the boundary, is of one dimension lower than the FEM. For 3D problems, the FEM discretizes the volume as compared to the BEM which discretizes the surface. In general, mesh generation for volume discretization is more complicated than surface discretization, especially for complex geometries. An important issue with respect to mesh generation is the degree of fineness of the mesh for both the FEM and BEM.

For the results obtained in chapter 5, the mesh density in all the situations was altered depending on the geometry and expected field gradient. In the initial meshes for both the 2D and 3D models, the nodes for the boundary element model correspond to the boundary nodes generated by the finite element mesh. Later, maintaining the same solution accuracy, the mesh was optimized by computing the difference in the solution as the number of nodes was decreased for both models in the 3D DCPD method simulation of the CT specimen. This resulted in 260 and 1548 nodes for the boundary element and finite element models respectively. As expected far fewer nodes were required for the boundary element model.

A distinctive characteristic of the BEM is the two point kernel function or the Green's function. This kernel depends on the problem dimension and type of PDE being solved. For Laplace's problem (DCPD method) in 2D, the Green's function is $\frac{1}{2\pi} \ln r$ while in 3D it is $\frac{1}{4\pi r}$. For more complicated integral equations, the generation

of this function is a task by itself. Since the Green's function is singular at $\vec{r} = 0$, this point is to be excluded from the integral equation. In other words, singular integration is to be performed. Normally the integral is regularized to reduce the order of the singularity, then integrated. This is done analytically, which is a tedious process,. making the implementation complex. On the other hand, the FEM is a standard technique and numerically does not vary either with the problem type or dimension. This makes it conducive to more general applications which as evidenced by the large number of commercial packages available in the market. The only limitation is the size of the problem to be handled which determines the required computer resources.

Another prominent feature of the BEM is the ease of handling infinite boundary problems. Though the DCPD and ACPD method are finite boundary problems, the hybrid model for eddy current applications involves an infinite boundary. The BIE equation for the boundary at infinity is dropped because the potential functions in the BIE satisfy radiation conditions. Thus only the surface discretization is necessary around the region of interest. An example where the infinite boundary is eliminated is the eddy current model where only a surface mesh is needed around the conductor and probe coil. The FEM requires discretization everywhere making it computationally expensive for 3D problems. Techniques such as ballooning [98], infinite elements [97] and others have been used by various researchers to handle infinite boundaries with finite elements.

From a qualitative point of view in NDE, researchers are interested in both the transducer response and the energy/defect interaction. For the 2D ACPD method, probe voltage as a function of scan distance is plotted in Figure 6.2 to 6.4. This is the voltage obtained at two points as the probe scans the specimen. Figure 6.6

shows the current distribution in the specimen from which one can visualize the perturbation due to the crack. The effect of the frequency and material properties on the magnitude of the current, and the probe's sensitivity to cracks, can also be clearly seen. Similarly, the potential distribution in Figure 6.8 determines the exact shape of the crack. In fracture mechanics, the calibration curves for the SEN and CT specimen provide information to predict the crack growth as shown in Figure 6.15 and 6.16. These depict the potential monitored at two locations where the probe straddles the crack. Again, the extent to which the fatigue crack perturbs the potential and the current in the specimen using the DCPD method is observed in Figure 6.12. Figure 6.12b clearly shows that current continuity is maintained with the current contours being concentrated in the uncracked portion of the crack. A highlight of the 3D DCPD modeling of the CT specimen is indicated in Figure 6.18. The potential distributions in the different layers in the CT specimen are nearly identical except close to the excitation point. This confirms that the calibration curves are independent of thickness.

The issue discussed in the above paragraph leads one to believe that, if only calibration curves are needed for a particular application, the BEM is better suited. In general, if the solution is required at specific points on the surface, the BEM is more efficient. In eddy current NDE, the probe response is interpreted as the impedance of the probe coil. Generally, the volume of the coil is much smaller than the volume of the conducting medium. Thus if one needs to compute only the probe impedance, the BEM is very attractive. If one requires the solution in the total domain or volume, the FEM is ideal. This is due to the fact that in the FEM, the solution already exists everywhere in the domain, thus requiring a minimum of post-processing. If an

infinite boundary problem is to be solved, the BEM has an inherent advantage. This is normally encountered in electromagnetic problems where the electric and magnetic fields around the region of interest need to be considered. Thus depending on the application, and the solution required, one can identify the type of numerical model to be used.

A major issue for all numerical methods is the computer resources required for a particular application. The next section discusses this issue for the two numerical methods.

Computer Resources

The two issues that need to be considered for any numerical method are a) computer memory storage and b) execution time or cpu time. After deciding on a formulation for a particular application and before implementing it on the computer, one needs to consider techniques that minimize the memory storage requirements and execute the algorithm in the shortest possible time. Achieving these criteria is not a simple task at all times.

Mesh optimization directly impacts the computer resource requirements. The growth of computer storage needed for the stiffness (global) matrix is the deciding factor in the overall storage requirements for both the numerical models. As discussed in Chapter 6, the FEM global matrix is banded, symmetric and sparse, while the BEM matrix is fully populated and non-symmetric. Table 7.1 summarizes the computer resources needed for the 2D modeling of the CT and SEN specimen using the DCPD method. Similarly Table 7.2 outlines the memory requirements and cpu time involved for modeling the 2D fatigue crack specimen using the ACPD method. For both cases,

Table 7.1: Computer resources for 2D SEN and CT specimen

	SEN		CT	
	FEM	BEM	FEM	BEM
Number of nodes	1116	38	972	68
Number of elements	2100	19	1720	34
Bandwidth	33	39	54	69
CPU time(seconds)	3.05	0.566	4.06	1.07
Total memory(words)	46K	3K	53K	9K

the finite element model uses three node triangular elements while the boundary element model uses the three node line elements.

It is obvious that the BEM is more economical for both cases. In the 3D modeling of the CT specimen, only the non-zero terms of the finite element stiffness matrix are stored, using the least computer storage. Figure 7.1 plots the increase in storage as the number of unknowns increases for the finite and boundary element models. For a finite bounded problem such as the DCPD and ACPD modeling, the FEM is attractive, if special storage techniques are implemented. If an infinite boundary problem is to be modeled, then the BEM will be more economical, since the number of unknowns needed for the finite element model will be much larger.

In the process of solving a set of linear equations, there is a close relationship

Table 7.2: Computer resources for 2D fatigue crack specimen

VARIABLES	FEM	BEM
Number of nodes	4097	278
Number of elements	7680	139
Bandwidth	18	278
CPU time(seconds)	22.5	4.6
Total memory(words)	75K	78K

between the storage of the global matrix and the solution algorithm. The stiffness matrices resulting from the finite element and boundary element formulations are symmetric and non-symmetric respectively. The final global matrix for the hybrid formulation is non-symmetric. If there are N variables to be solved, then a full storage requires N^2 matrix elements, while a *skyline storage* [140] scheme for a symmetric matrix needs $N^{1.7}$ matrix elements. An ideal and optimum matrix stores only the non-zero elements of the matrix which could be as low as $N^{1.5}$ matrix elements for a symmetric matrix.

In this research, all of these storage schemes have been used. For the 2D finite element programs, the global matrix is symmetric and banded. The matrix stored is $(N \times ((\frac{IB}{2}) + 1))$ where IB is the bandwidth. Storage of only the non-zero terms of the stiffness matrix was implemented in the 3D finite element modeling of the CT

specimen using the DCPD method. In the 3D hybrid formulation, skyline storage was used. Since boundary element matrices are always non-symmetric and fully populated, complete storage is the only option applicable. In 3D, it is common to have meshes with over 1000 nodes, and with three to four variables per node, optimum matrix storage is essential. Thus considerable effort must be devoted to incorporating such storage schemes in the finite element algorithm.

Execution times for the finite element model depend solely on the solution routine, while for the boundary element model they depend on the singular and regular integration and solution procedure. For the 3D modeling of the CT specimen, with identical tolerance for the finite and boundary element solution, the cpu time as a function of number of unknowns is plotted in Figure 7.2. The FEM curve shows a gradual increase in execution time which is attributed to the efficient preconditioning of the iterative, incomplete Cholesky conjugate gradient solver. The BEM model uses the direct Gaussian elimination. Again for finite boundary problems, using an efficient solver, the FEM is surprisingly fast. One can speculate that for infinite boundary problems, the BEM will be faster. Nevertheless, both these curves imply that mesh optimization is more crucial for boundary element models than finite element models.

In general, the solution of a linear system of equations is achieved by *direct* or *iterative* solvers. The most popular of *direct* solvers is the Gauss elimination scheme. It is fast and easy to implement, for well conditioned matrices. Also finite element matrices are diagonally dominant, a characteristic that speeds up the algorithm even further. A major drawback is that to solve with a *direct* solver the full stiffness matrix has to be stored in the computer core memory.

Iterative solvers are generally considered to reduce the core storage and decrease the solution or cpu time. Popular techniques include successive over relaxation (SOR), Gauss Seidel, conjugate gradient and others. With stable matrices and a realistic convergence criterion, the aim is to let the solution converge as fast as possible. (For N equations, number of iterations must be $\ll N$).

Since the incomplete Cholesky conjugate gradient (ICCG) algorithm was used in the 3D finite element model of the CT specimen, it was found that for a typical conjugate gradient iteration the storage needed was of $O(N)$. By preconditioning the matrix, one not only guarantees convergence but also drastically reduces the number of iterations (iterations $\ll N$). This impacts the execution time for each iteration and the total cpu time. Once again additional effort is required to implement these solution routines into the finite element programs to make them quick and efficient.

This chapter compares and contrasts the FEM and BEM as applied to the potential drop methods. The FEM and BEM are complementary techniques having their own advantages and disadvantages. With this information, a user can choose a particular model depending on the specific application of interest. The next chapter presents results of the hybrid finite boundary element model for eddy current NDE.

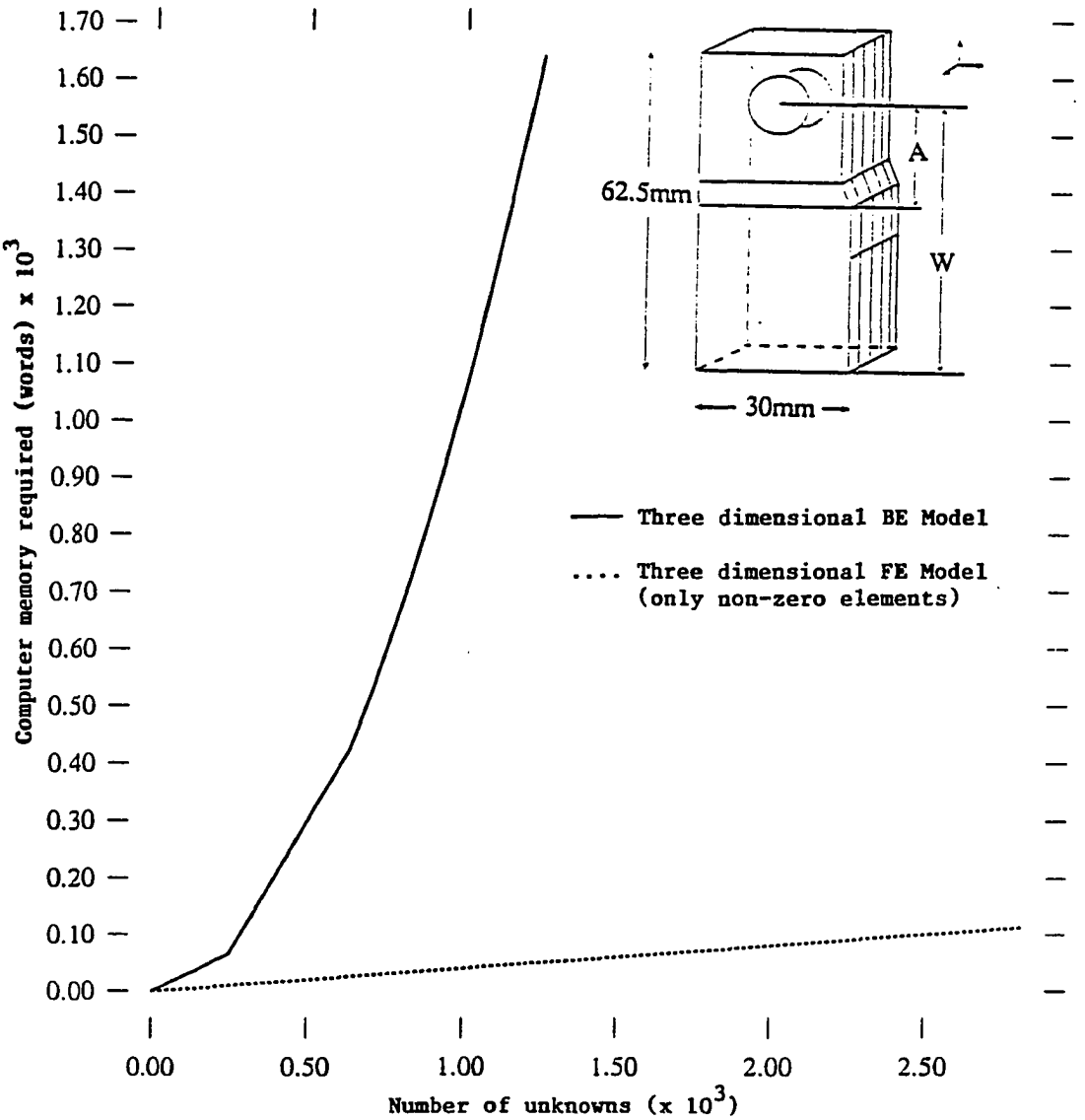

Figure 7.1: Computer memory requirements for the 3D finite and boundary element models (Note: only non-zero elements stored in the finite element model)

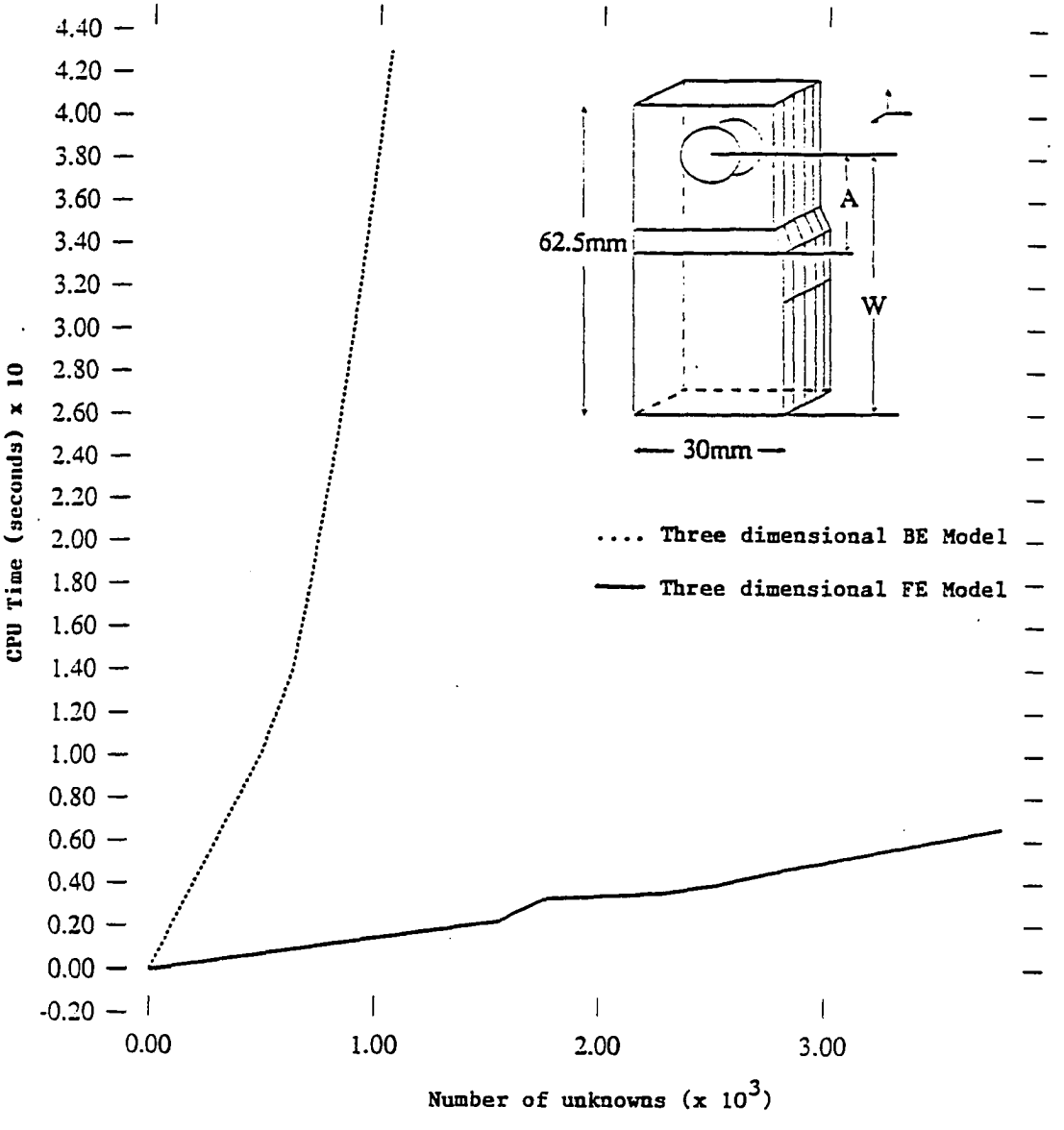

Figure 7.2: Execution times for the 3D finite and boundary element models (Note: The boundary element model uses Gaussian elimination whereas the finite element model uses the ICCG technique)

CHAPTER 8. EDDY CURRENT NDE: RESULTS

The latter part of this dissertation describes the feasibility of developing a 3D hybrid finite element-boundary element (FE/BE) model for eddy current NDE. Chapter 5 outlined the hybrid formulation in detail. To establish the validity of this model, the results are compared with 2D finite element calculations when applicable, and with published experimental data.

All the calculations in this study were performed on a *Project Vincent DEC 5000 workstation.* This includes mesh generation, global or stiffness matrix assembly and post processing of the data generated by the model. Two geometries are modeled for the feasibility study, a) an absolute eddy current coil in air (Figure 8.1) and b) an absolute eddy current coil over an aluminum block (Figure 8.2).

In practical eddy current testing, the transducer response is the change in probe or coil impedance as the probe scans the surface. The hybrid numerical model calculates the magnetic vector potential and the electric scalar potential everywhere in the domain. It is thus essential that the probe impedance be computed from the solution, $\vec{A}$ and ϕ. The next section describes the impedance calculation.

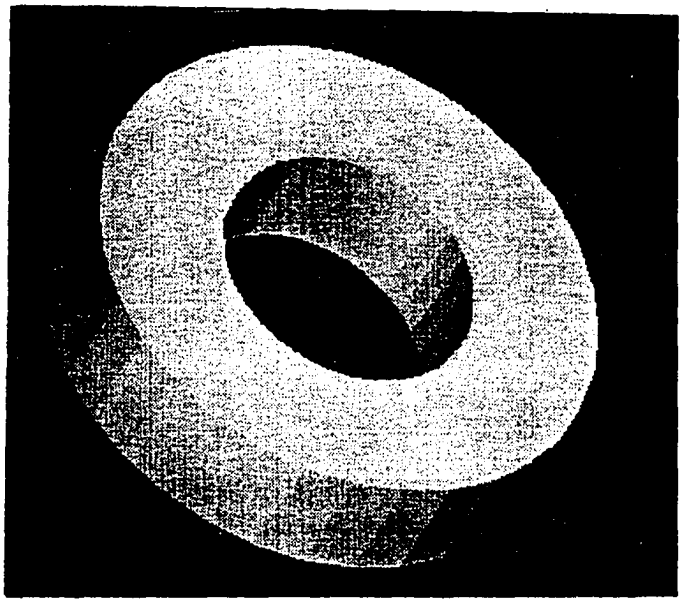

Figure 8.1: Absolute eddy current probe in air

Probe Impedance

The impedance of a circular coil of radius r_i can be calculated from the distribution of $\vec{A}$ [14]:

$$Z_i = \frac{j\omega 2\pi r_i A_i}{I_s} \tag{8.1}$$

where I_s is the source current in the probe . With discrete values of $\vec{A}$, this simple scheme is not applicable. The simplest way to overcome this problem is to assume an average value of $\vec{A}_i$ and r_i for each element in the coil. Thus for a coil of nn elements in the probe cros-section and Δ_i being the are of the ith element, the impedance can be calculated as

$$Z = \frac{j\omega 2\pi J_s}{I_s^2} \sum_{i=1}^{nn} r_{ci} A_{ci} \Delta_i \tag{8.2}$$

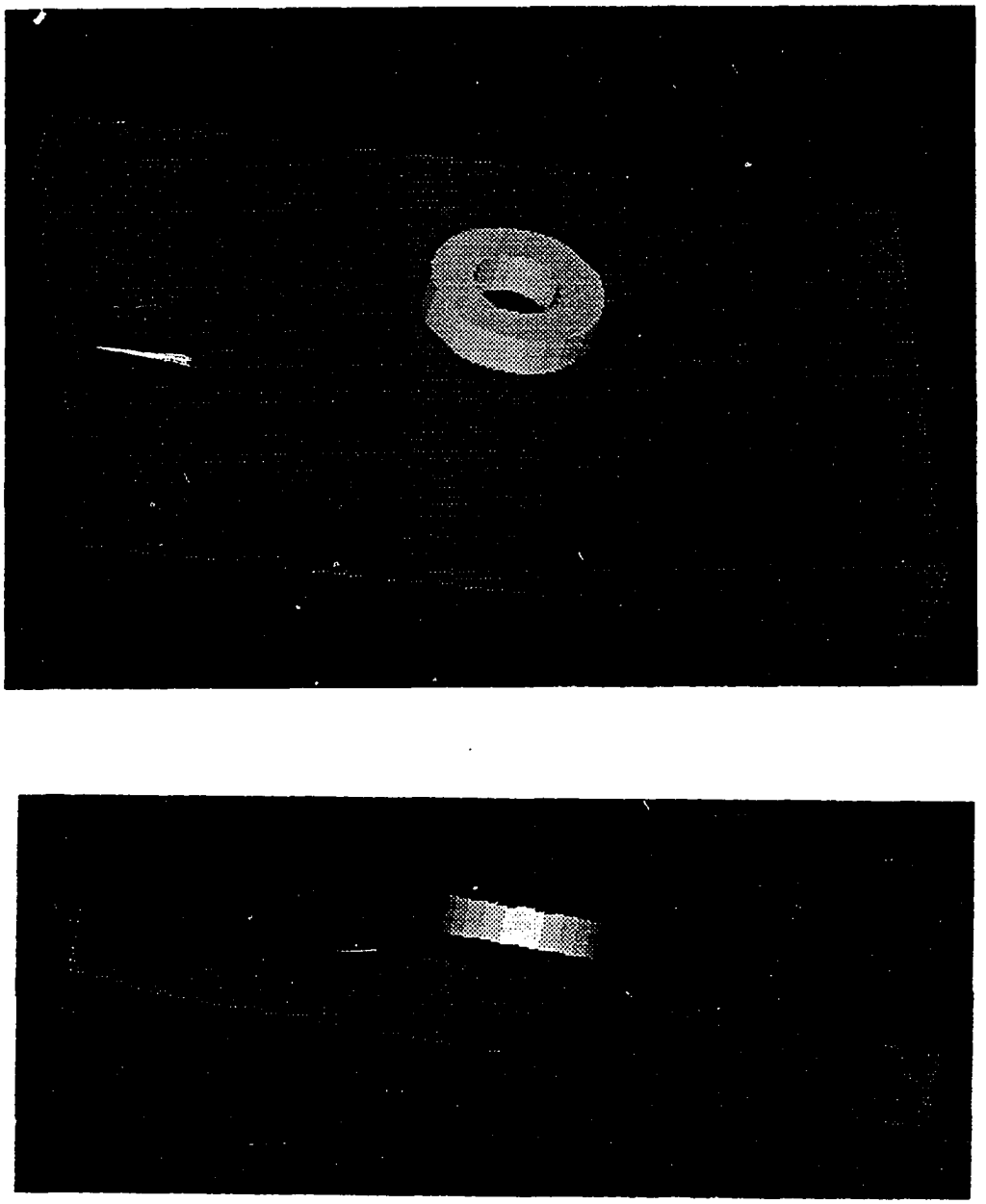

Figure 8.2: Two views of an absolute eddy current probe over an aluminum block a) top view and b) side view

with r_{ci} and $\vec{A_{ci}}$ being the centroidal values in each element. The self inductance of the probe can be calculated directly from equation (8.2) as

$$L_{probe} = \frac{2\pi J_s}{I_s^2} \sum_{i=1}^{nn} r_{ci} A_{ci} \Delta_i \tag{8.3}$$

In equation (8.1), $\vec{A}$ is implicitly assumed to be constant along the circumference of the coil. This implies that all the above equations are true for axisymmetric geometries only.

Another approach for calculating the impedance for 3D geometries is presented by Ida [15]. It is based on the energy of the system, and associates the system inductance with the stored energy and its resistance with the dissipated energy. The stored energy is expressed as

$$W = \frac{1}{2} \int_v \vec{B} \cdot \vec{H} \, dv \tag{8.4}$$

over the entire volume of the system. This equation is rewritten in terms of $\vec{B}$ for each element with volume v_i as

$$w_i = \frac{1}{2} \left(\frac{1}{\mu x} B_x^2 + \frac{1}{\mu_y} B_y^2 + \frac{1}{\mu_z} B_z^2 \right) v_i \tag{8.5}$$

For a domain with nn elements, the total energy is computed as

$$W = \sum_{i=1}^{nn} w_i = \frac{1}{2} \sum_{i=1}^{nn} \frac{1}{2} \left(\frac{1}{\mu x} B_x^2 + \frac{1}{\mu_y} B_y^2 + \frac{1}{\mu_z} B_z^2 \right) v_i \tag{8.6}$$

From this, the inductance of the probe coil is

$$L_{probe} = \frac{2W}{I_s^2} \tag{8.7}$$

The dissipated energy in the system is

$$P = \frac{J_{ei}^2 v_i}{\sigma} \tag{8.8}$$

where J_{ei} is the resultant eddy current density given by

$$\vec{J}_{ei} = -j\omega\sigma(\vec{A}_i + \nabla\phi_i) \tag{8.9}$$

Again for a discrete system with nn elements, the total dissipated energy is

$$P = \sum_{i=1}^{nn} \sigma\omega^2 v_i (A_{ci} + \nabla\phi_i)^2 \tag{8.10}$$

The probe resistance now becomes $R = \frac{P}{I_s^2}$ and the total coil impedance is

$$Z = \frac{1}{I_s^2}(P + j\omega 2W) \tag{8.11}$$

The general procedure for the hybrid finite-boundary element algorithm is shown in a flow chart in Figure 8.3. It consists of

- Boundary and finite element discretization
- Calculation of the boundary element *global* matrix
- Current distribution calculation for the volume elements
- Calculation of the finite element *stiffness* matrix
- Linking both formulations
- Solution algorithm to compute $\vec{A}$ and ϕ
- Post processing

The next section describes the results for the two cases.

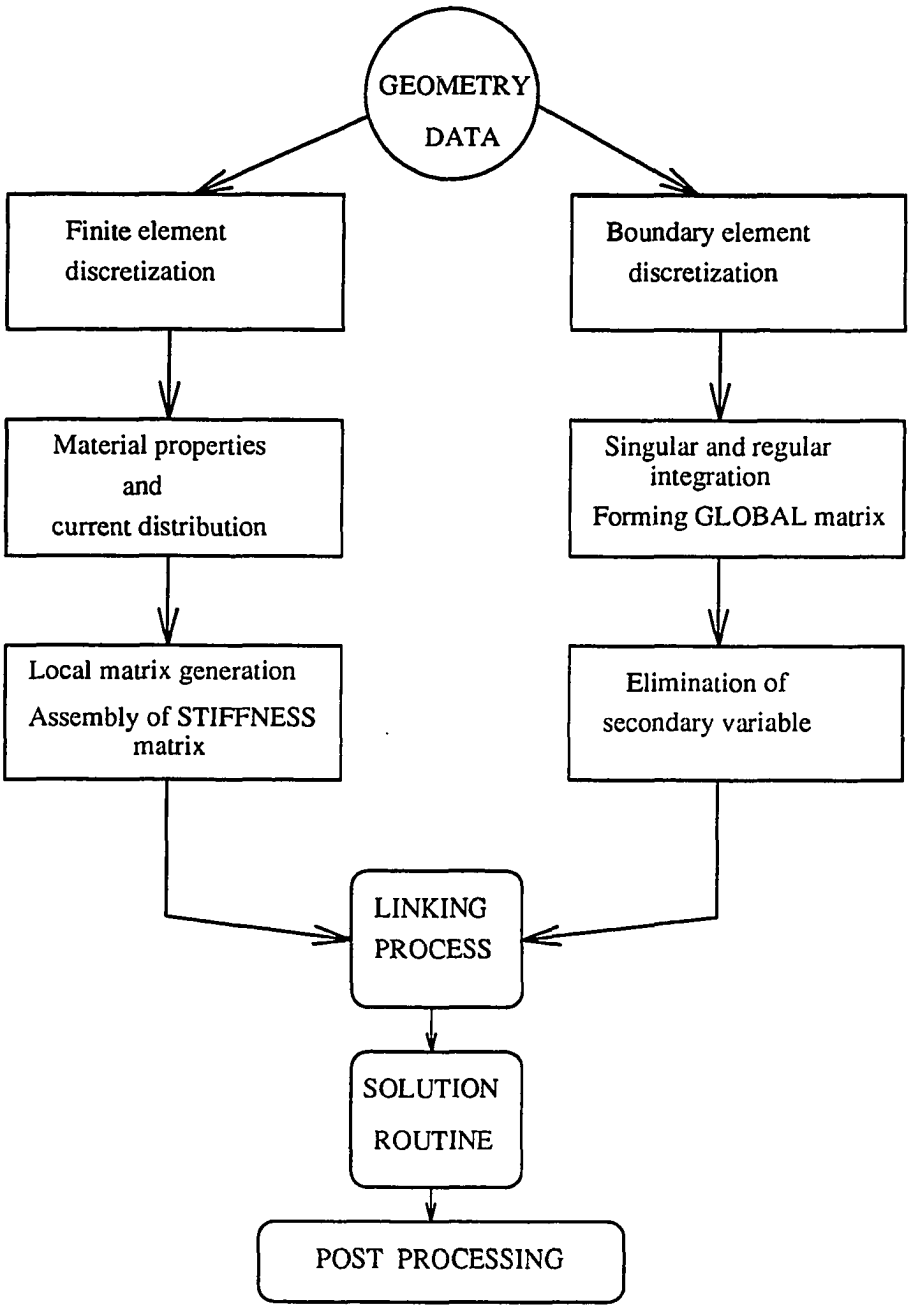

Figure 8.3: Hybrid finite-boundary element algorithm flow chart

Coil in Air

The coil geometry in Figure 8.1 has an inner diameter (I.D) of 12.4 mm, outer diameter (O.D) of 25 mm and is 6.25 mm thick. It is modeled as an ideal coil with $\sigma = 0.0\ S/m$ and $\mu_r = 1$.

Discretization

Discretization of the domain is a key step in the overall procedure. As mentioned in an earlier chapter, the discretization must be more dense where the field gradient is high and less dense everywhere else, to optimize the number of nodes and elements. The meshes utilized in this research were generated with an inhouse mesh generator.

The boundary element formulation described in this study uses four node quadrilateral elements to discretize the surface or boundary of the probe as shown in Figure 8.4. Volume discretization for the FEM uses eight node isoparametric brick elements with the surface nodes of both meshes coinciding.

Current distribution

The current in the coil is assumed to lie in the x-y plane with each element having two components of the current. Referring to Figure 8.5, the x and y components of the current are given by

$$J_x = J_0 \sin(\theta)$$
$$J_y = J_0 \cos(\theta) \tag{8.12}$$

where $J_0 = 1000 + j0.0\ \mathrm{A}/m^2$. The frequency of the excitation is 900 Hz. This information is introduced in the algorithm through the material property in the finite

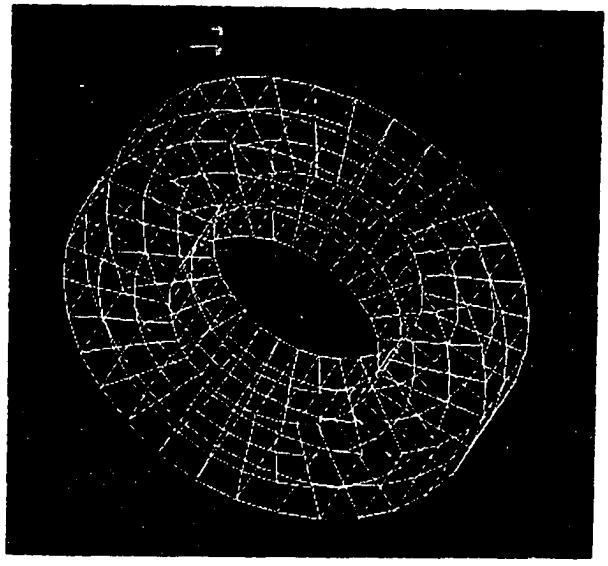

Figure 8.4: Surface mesh for the probe in air

element formulation.

Results

The inductance of the probe is computed using equation (8.3). For the given probe dimensions, the inductance in air is 220 mH [137]. Table 8.1 gives the computed value of the inductance for different levels of mesh discretization. These results clearly indicate that the inductance value is approaching the desired value as the number of elements and nodes in the mesh increases.

Coil Over a Block

The coil in air is now placed over an aluminum block with dimensions of 120 × 80 × 12.2 mm as shown in Figure 8.2. Conductivity of the block is 3.06×10^7 S/m

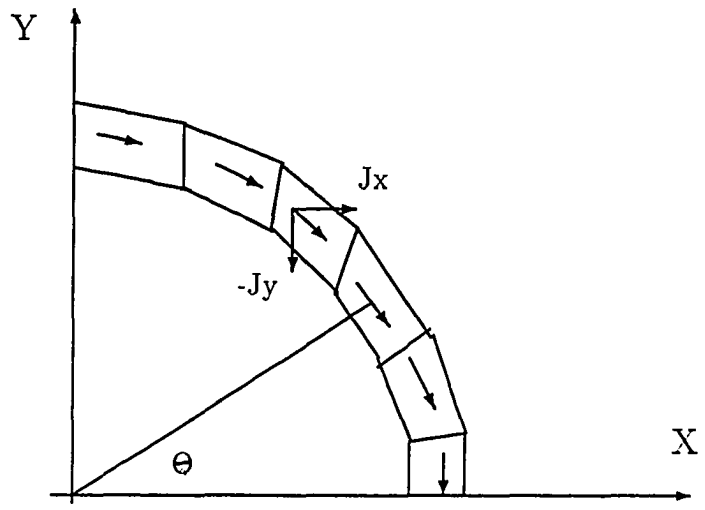

Figure 8.5: Specification of current density in the eddy current probe. Only a quarter of the probe coil is shown

Table 8.1: Computed probe inductance with increasing discretization

number of volume nodes	*Inductance (mH)*
96	48.4
128	68.3
144	157.87
192	186.4
216	194.17

Table 8.2: Discretization data for computing the lift-off characteristics

VARIABLES	BLOCK	PROBE
BEM nodes	54	142
BEM elements	66	130
FEM nodes	80	144
FEM elements	36	64

and the relative permeability is 1.

This model is tested for two cases:

1. Comparing lift-off characteristics with experimental data
2. Comparing the values of $\vec{A}$ and eddy current density in the block with 2D finite element data.

Discretization

The geometry is discretized differently for each of the above cases. For comparing the lift-off characteristics, the probe is discretized more densely than the block, as shown in Figure 8.6. Table 8.2 gives the discretization for case 1.

The change in inductance (ΔL) is computed as the probe is lifted off the aluminum block with $\Delta L = 0$ defined when the probe is resting on the block surface. Equation (8.3) is used for computing the inductance. The numerical and experimen-

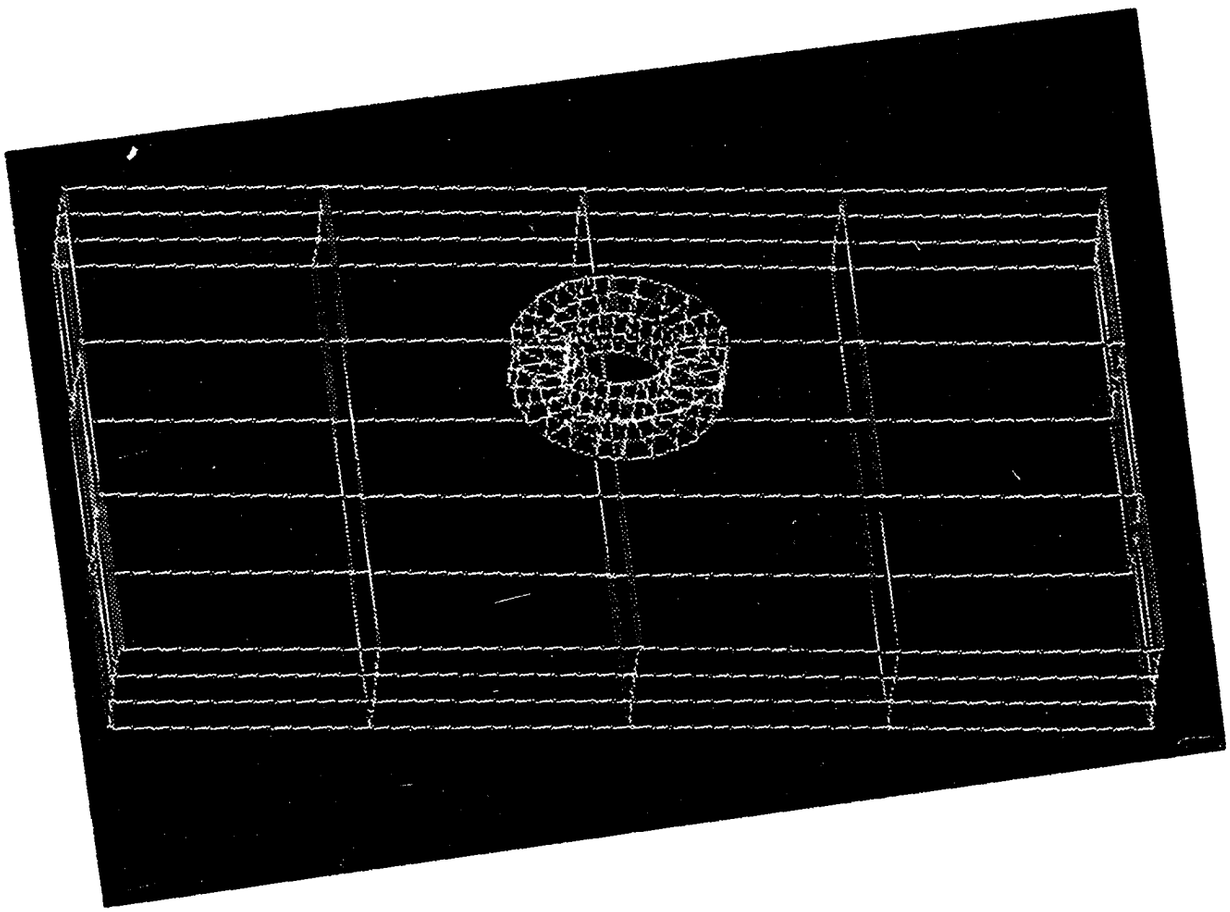

Figure 8.6: Surface mesh for computing the lift-off characteristics

Table 8.3: Discretization data for computing the eddy current density

VARIABLES	BLOCK	PROBE
BEM nodes	106	32
BEM elements	128	32
FEM nodes	175	32
FEM elements	96	8

tal data [137] relating to the change in inductance as a function of lift-off is plotted in Figure 8.7. The numerical values show the same trend, qualitatively. Two reasons can be attributed to the discrepancy, 1) insufficient discretization in the block and probe, and 2) calculation of the inductance using (8.3) is true only for axisymmetric geometries. Though the block is much larger than the probe, and at 900 Hz, the magnetic fields are localized, the geometry is still not axisymmetric. There is a certain error also introduced when calculating the centroidal values.

In the second case, the comparison is made for $\vec{A}$ and the eddy current density in the block. Since these quantities drop exponentially with depth in the block, the discretization is more dense in the upper layers of the block. In particular the skin depth at 900 Hz is 3.02 mm and so there are two elements per skin depth. This discretization is still not sufficient. Figure 8.8 shows the surface mesh for the probe and block while Table 8.3 gives details of the mesh.

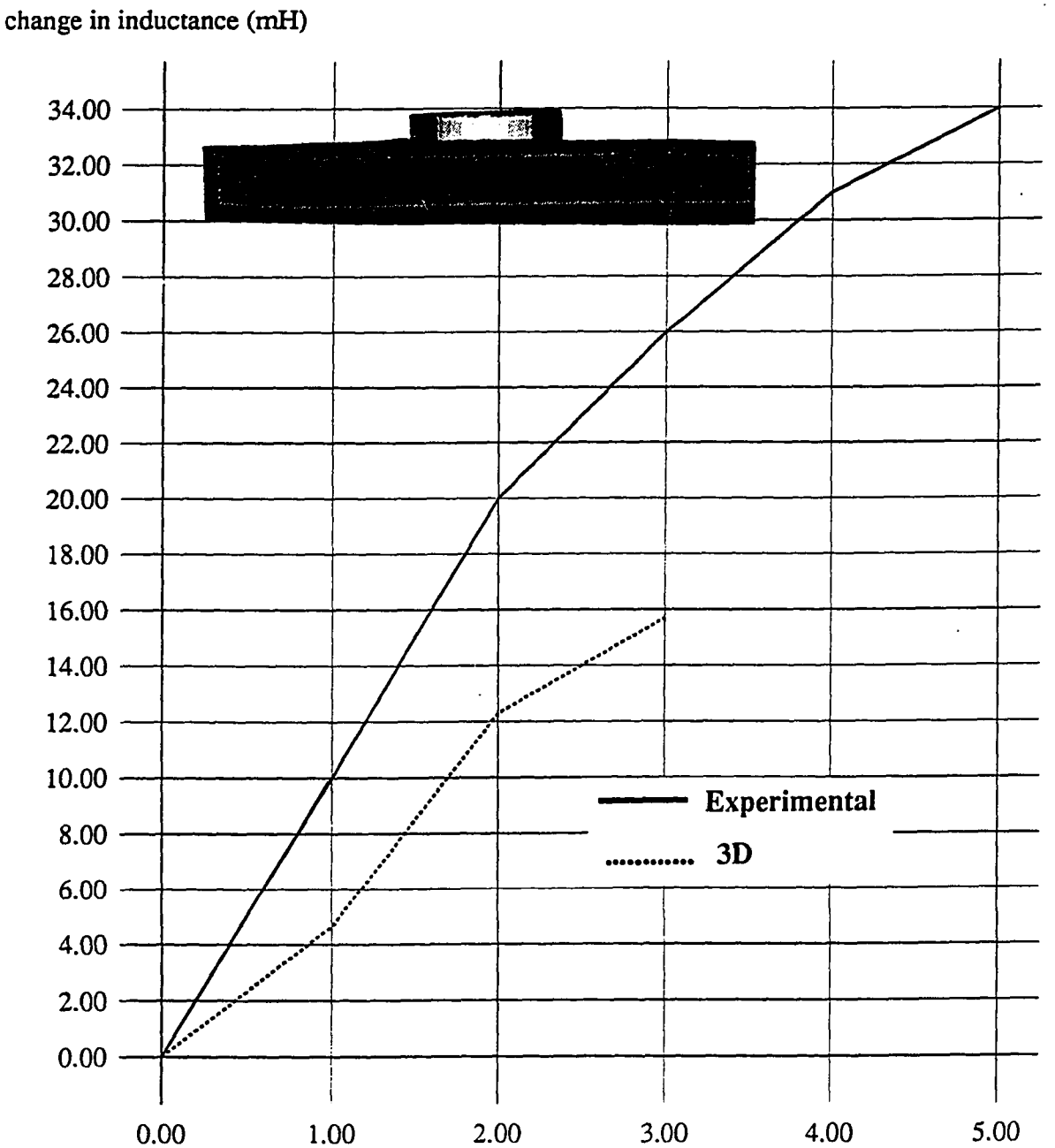

Figure 8.7: Lift-off characteristics for the absolute eddy current probe over the aluminum block

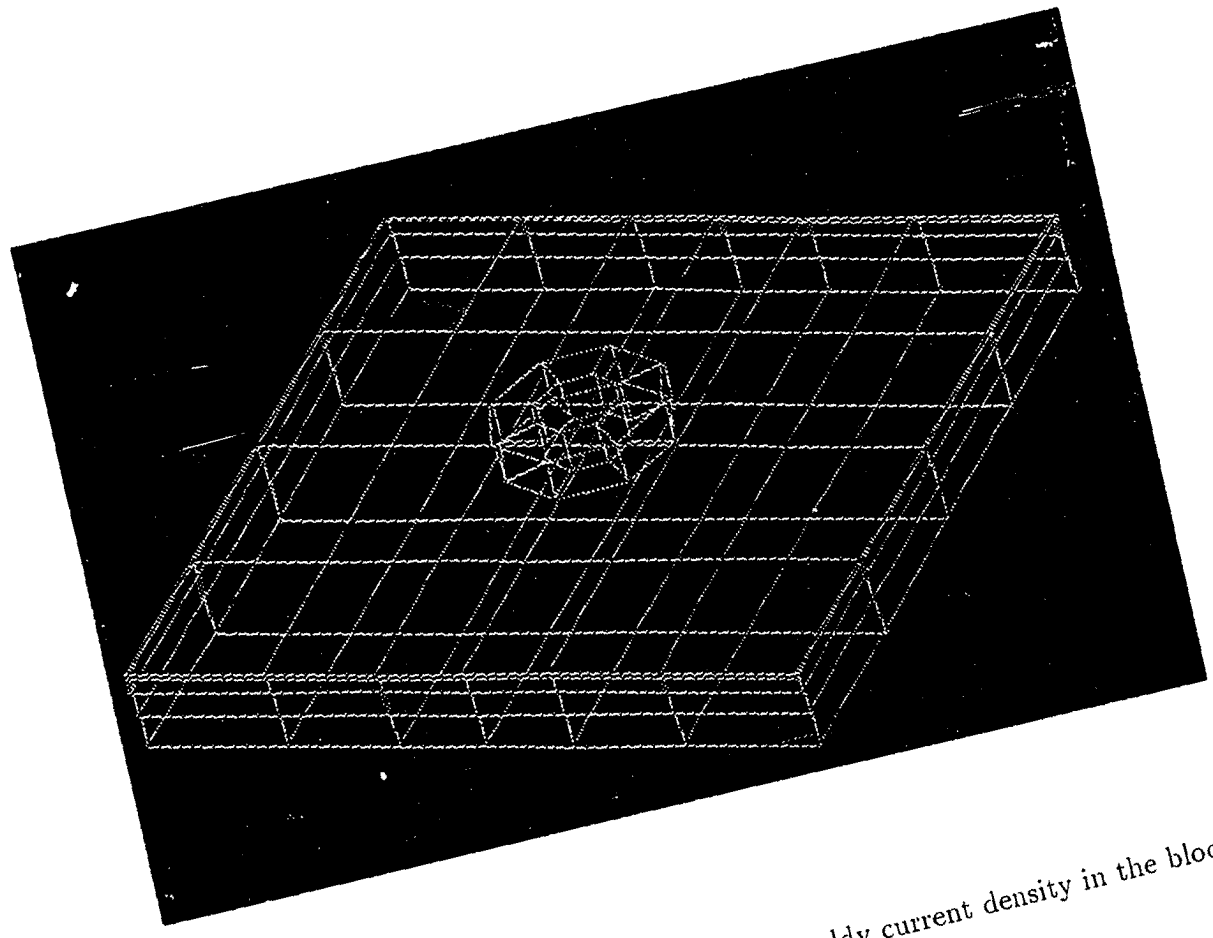

Figure 8.8: Surface mesh for comparing the eddy current density in the block

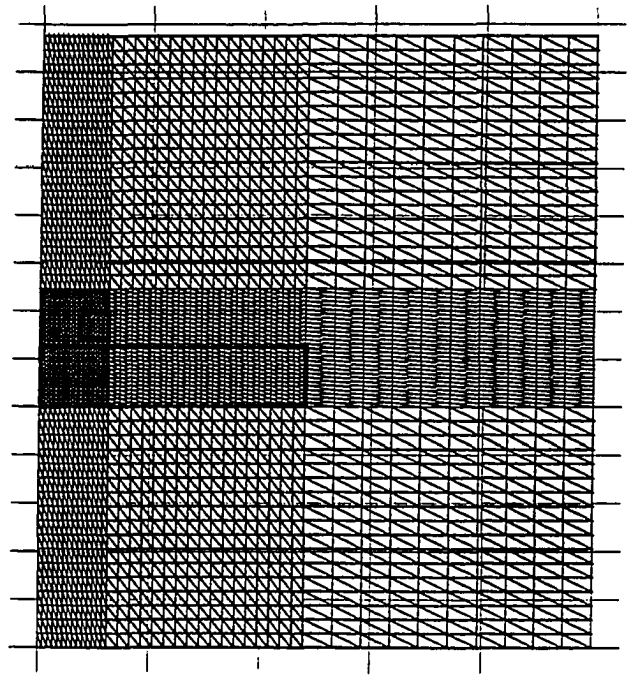

Figure 8.9: 2D mesh for probe over a block

An axisymmetric study of a probe over a block having the same dimensions is conducted. A 2D mesh using triangular elements showing the block, coil and boundary at infinity is seen in Figure 8.9. With one variable per node in the 2D case, a dense mesh is easily handled. The magnetic flux distribution around the coil is visualized in Figure 8.10.

The value of $\vec{A}$ at the tip of the probe, down the block, is plotted for the 2D and 3D case in Figure 8.11. The 3D curve shows a similar trend to the 2D case. One needs to keep in mind that the probe discretization is very coarse and the probe is not circular.

Finally the eddy current density for every element in the block is calculated using equation (8.9). Figure 8.12 plots the eddy current density as a function of the block

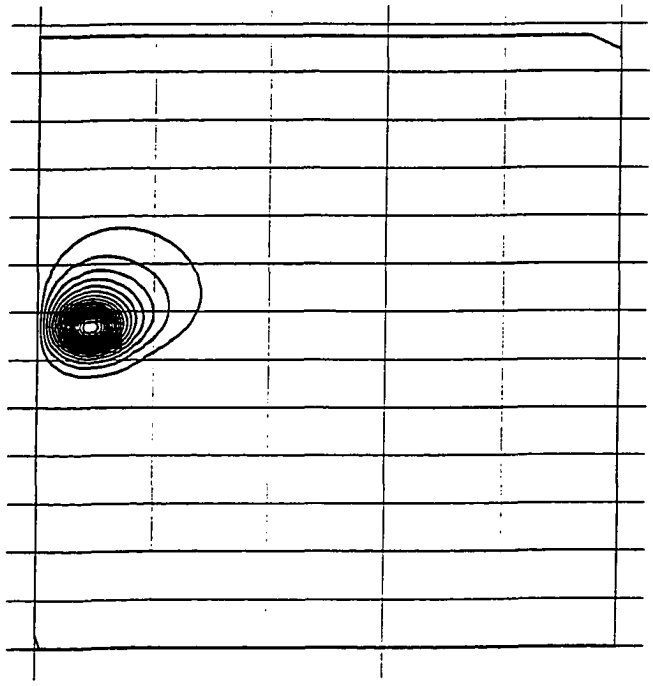

Figure 8.10: Flux plot for the absolute coil over the block

thickness. The two curves for the 2D mesh correspond to points under the probe and away from the probe as indicated on the figure. The 3D mesh has only one element under the coil and so the eddy current density is plotted for the element position down the block. Again, qualitatively the results show similar features.

Most of the meshes in this study have between 200 to 225 nodes. With four variables per node, the number of unknowns to be solved is 800 to 900. This is the upper limit that the workstation can handle in terms of the memory storage of the hybrid code without any problems. The cpu time for the entire algorithm to be executed for 225 nodes is around 28 minutes.

With the results presented above, one can confidently say that the feasibility study of the hybrid formulation was successful and that the hybrid model shows

promise for adaptation to various eddy current NDT situations.

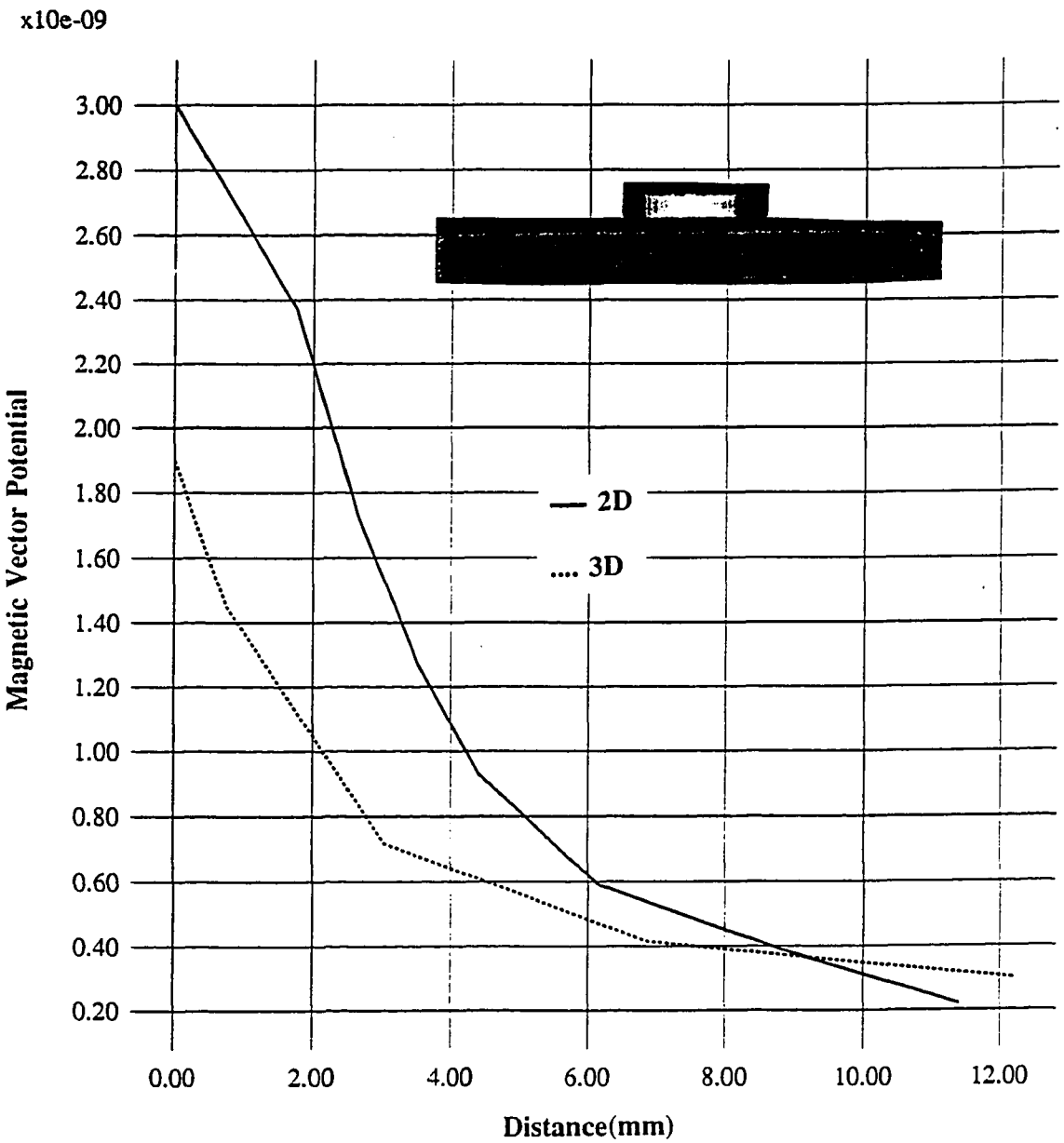

Figure 8.11: Comparison of vector potential values with 2D solution

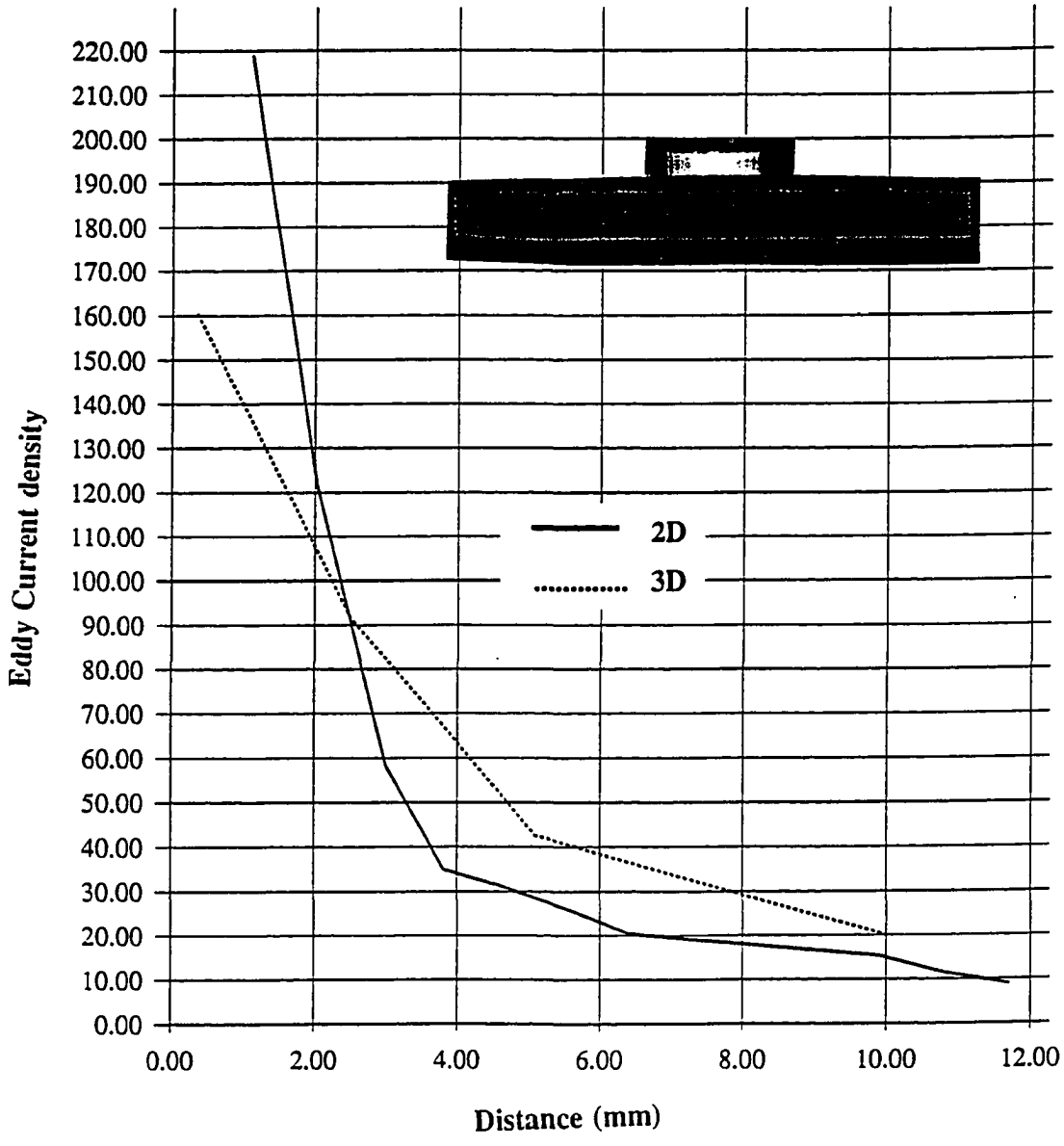

Figure 8.12: Comparison of eddy current density in the block

CHAPTER 9. CONCLUSIONS AND FUTURE WORK

The main goals of this dissertation are as follows:

- to develop a multiformulation strategy involving the FEM and BEM as applied to electromagnetic NDE. This involves developing and implementing finite element, boundary element formulation for specific applications, and then to compare and contrast the finite element and boundary element methods as applied to low frequency electromagnetic NDE
- to conduct a feasibility study of a three dimensional, hybrid finite element-boundary element model for eddy current NDE

This chapter ties together all the issues discussed in the earlier chapters and proposes directions for future work. Specifically, conclusions are drawn from the modeling of the fatigue crack specimens using the DCPD and ACPD methods regarding the advantages and disadvantages of using the finite and boundary element methods, and the feasibility of using the hybrid formulation for eddy current applications. Some practical issues regarding mesh generation, computer resource requirements and others are discussed. Finally future directions to modify and apply the 3D hybrid model to other situations are suggested.

Conclusions

To achieve the first goal, the following numerical models are developed:

- 2D finite and boundary element models of the CT and SEN specimen using the DCPD method.
- 3D finite and boundary element models of the CT specimen utilizing the DCPD method
- 2D finite and boundary element models for fatigue crack specimens using the ACPD method.

Conclusions drawn from the development of these models are discussed below. In the field of fracture mechanics, the fatigue crack growth is predicted via *calibration* curves generated for typical CT and SEN specimens using the DCPD method. These curves plot dimensionless quantities which are a function of the probe width and voltage input. Both the 2D finite and boundary element models predict curves comparable to analytical (Johnson's formula) and experimental data *with the numerical predictions closer to the experimental data than Johnson's formula.* This suggests that Johnson's formula is pessimistic or less accurate for the CT specimen. This can be attributed to the specimen clamping holes and a point excitation which makes the field non-uniform close to the crack. The potential distribution plots obtained from the finite element data show the uniformity of the potential close to the crack in the SEN specimen and non-uniformity for the CT specimen.

As mentioned earlier, this is the first time a 3D numerical model of the CT specimen using the DCPD method has been reported. Calibration curves for different

specimen thicknesses are predicted and compared to 2D and experimental data. Potential distribution plots are made at different thickness slices of the specimen from finite element data. The plots clearly indicate that the perturbations of the potential due to the crack are localized, close to the crack, implying that the thickness of the specimen does not affect the calibration curves. *Thus one can conclude that a 2D numerical model is sufficient, within tolerable limits to predict fatigue crack growth behavior.*

After solving Laplace's equation, the scalar Helmholtz equation representing the ACPD method is solved by modeling an infinitesimal thin crack and a circular crack. Finite and boundary element models predict the potential across the probe as the probe scans the specimen. Using these data, the models predict the crack length for the infinitesimal thin crack. Finite element data are used to visualize the current distribution in the thin crack specimen and construct the shape of the semi-circular crack. The Green's function, a modified Bessel function of the second kind, order zero, is successfully implemented in the boundary element algorithm.

The above sequence of work can lead to three major conclusions from the user's point of view:

1. *If one is interested in the solution at specific points on the boundary of the domain, then the boundary integral equation with the corresponding Green's function should be developed for the specific boundary conditions.* Using the BEM, the BIE can be solved to obtain the solution. This is true for both 2D and 3D problems.

2. *On the other hand if the solution is needed everywhere in the domain to study the energy/defect interaction and obtain the transducer response, then the finite*

element model is the obvious choice. This is due to the fact that the volumetric discretization allows the solution to be obtained in the total domain.

3. For 3D boundary value problems with the boundary at infinity, the BEM or a hybrid method combining the finite element and boundary element formulation should be utilized. *This would enable the modeling of complex 3D structures with sufficient discretization to produce realistic data.*

The comparison of the FEM and BEM utilizing the 2D and 3D models of the CT and SEN specimen, using the DCPD and ACPD methods, leads one to believe that in general, *the FEM and BEM are complementary techniques* each with their own advantages and disadvantages. The contrasting features are best highlighted in Table 9.1. The discussion of matrix features, size and type of integrals involved for a given problem are key in deciding the computer resource requirements. Thus, one can conclude that the *decision to use a particular modeling technique depends on a number of related factors such as application, geometry, available computer resources and others.*

Another key issue to be considered while comparing the BEM and FEM, or for that matter any numerical algorithm, is that of computer resources. Computer memory storage and the cpu time are the resources to be optimized. For the BEM, the cpu time depends on the numerical integration of the kernels and the solution of the linear equations. By using solvers from established mathematical packages such as *LINPACK*, the solution time is optimized. Regarding the numerical integration, an adaptive integration scheme is utilized. This uses lower quadrature order for planar elements with higher order of integration for corner or complex shaped elements.

Table 9.1: Complementary features of the FEM and BEM

FEM	*BEM*
Domain method	Integral method
Volume discretization	Surface discretization
No singular integrals	Singular integrals in the Green's function
Symmetric, Sparse and banded matrix	Non-symmetric and fully populated matrix
Handles anisotropy and non-linearity	Restricted to linear medium

In the finite element algorithm, both the issues of computer memory and cpu time are critical. As implemented in the 3D finite element modeling of the CT specimen, only the non-zero terms of the symmetric global matrix are stored. Similarly in the 3D hybrid code, the *skyline* storage is used for the finite element matrix which reduces the burden on the core memory storage. An efficient ICCG iterative solver reduces the cpu time drastically by reducing the number of iterations. *This leads one to conclude that for the FEM, a lot of effort has to be devoted to store the global matrix in a compact form and use the most efficient solver for the set of linear equations to make the algorithm competitive with other 3D numerical techniques.*

A key ingredient to optimize computer resources is the mesh generator or the discretization scheme. All the meshes in this research are generated with the mesh density varying with the field gradient to produce sufficient number of nodes and

elements according to the *users intuition.* As mentioned earlier, these meshes are all generated from an in-house mesh generator. *With 3D modeling of complex structures, this approach is insufficient and one needs to be familiar with and use commercial mesh generators.* These generators are adaptive in nature, produce optimal meshes and are in general interactive. The only drawback is the length of the learning curve for the user, and the interface to extract the data needed for inputting to the finite and boundary element algorithms.

To pursue the second goal of this dissertation, a hybrid 3D finite-boundary element model is developed. To the author's knowledge, the chosen formulation has not been applied to electromagnetic NDE applications. The magnetic vector potential and the electric scalar potential are the variables in the 3D formulation. The vector potential is chosen as it offers generality and the convenience of continuity over material interfaces and discontinuities. The hybrid technique has no restriction on any parameters. The number of nodes, elements, material properties, frequency, geometry etc are not restricted by any means and therefore the model is general. *The hybrid finite-boundary element (FE/BE) formulation for eddy current NDE derives benefits from both techniques.* Major advantages of this formulation are:

- *this general purpose formulation is applicable to most quasi-static electromagnetic phenomena* which includes modeling of power devices such as transformers, motors and other electrical engineering applications.

- the boundary element formulation for the exterior represents exactly the boundary at infinity. *Thus only discretizing around the region of interest is needed.*The BIE derived for the curl-curl equation makes the linking process between the two formulations straightforward. Identifying the Green's function is relatively

easy as it corresponds to the 3D free space Green's function.

- the finite element formulation discretizes the curl-curl equation which handles non-linear magnetic permeability and anisotropy. *Imposing the Coloumb gauge guarantees the uniqueness of the magnetic vector potential.* The scalar potential is essential for modeling multiple materials or interfaces with different conductivities or zero conductivity regions. *This enables modeling a wide class of materials and problems.*

- *With finite elements, discretizing the volume of the probe coil and the conductor, one can study the energy/defect interaction and also obtain the transducer response. This was the main criterion that the model was required to fulfill.*

One disadvantage of the hybrid FE/BE method is that the final global matrix is non-symmetric and loses the sparsity pattern of the finite element matrix.

The results obtained for the coil in air modeled zero conductivity regions, and the table of inductance calculations for increasing discretization showed the value converging to the desired inductance. Modeling of the probe over an aluminum block, handles materials with different conductivity. Predictions of the lift-off characteristics are a measure of change in flux linkage as the probe is lifted off the block. Similarly eddy current density plots are not measurable experimentally, but are of significant importance to the understanding of the physical phenomenon. *The results from the 3D hybrid FE/BE algorithm compared to experimental data confirmed the feasibility of using the hybrid formulation for eddy current NDE and other applications.*

Most 3D finite, boundary element or hybrid models solving vector boundary value problems are executed on a supercomputer to handle reasonably sized meshes.

This feasibility study, conducted on a workstation confirmed the qualitative nature of the results as an initial step to validate the formulation. It is planned, as discussed in the following pages, to utilize a supercomputer or parallel machine in further development of the 3D hybrid FE/BE model.

Future Work

Suggestions for future research based on this dissertation can be grouped into two major categories:

1. modifications to the 3D hybrid finite-boundary element model to test the formulation more rigorously
2. ideas for utilizing the FEM or the BEM as applied to electromagnetic NDE

The implementation of the formulation on the workstation precluded the author from testing the algorithm on more dense discretizations due to the limitation of the computer. In order to obtain more data with the same or other geometries using the hybrid FE/BE formulation, the following suggestions are made:

- Increase discretization for both the finite and boundary element formulations.
- Execute the algorithm on a supercomputer or transfer the code to a parallel machine such as the Mas-Par at the *Scalable Computing Lab* at Ames Laboratory. Some effort will be needed to rewrite part of the code to benefit from the parallel architecture. However the limitations of storing large stiffness matrices and solving the system of equations can be overcome.

- Investigate if the energy method is applicable to the hybrid code for computing the probe impedance for 3D geometries.

- Use computer graphics to plot the eddy current density or flux contours for any of the 3D geometries for better visualization.

It is essential that some *resources* need to be devoted to utilize the benefits of existing commercial mesh generators. A general purpose interface routine could be developed for the *IDEAS* package to extract the mesh information needed for the finite and boundary element software.

To compute probe impedance values needed for *probability of detection* models or other *CAD* models, a boundary element formulation for eddy current analysis should be considered.

With parallel machines being more easily accessible than before, considerable efforts need to be channeled to modify both, the boundary and finite element models to be executed on these machines.

Finally, from the experience gained in this research, one can conclude that for a particular application, a user must identify his or her *needs* very thoroughly. Then, the user must take into account the available computer resources, the time required to solve the given problem and the post-processing needs. With this background information, the user can make an intelligent guess as to which numerical model would best satisfy the given specifications.

To conclude this dissertation, the author tried to fulfill his goal of using the dissertation as a platform to increase the awareness of the benefits of numerical modeling in electromagnetic NDE.

BIBLIOGRAPHY

[1] W. Lord, "Partial differential equations and the NDE inverse problem," Review of Progress in Quantitative NDE, D.O. Thompson and D.E. Chimenti Eds.. Plenum Press, New York, 1988, pp. 425-430.

[2] W. Lord, "Forward and Inverse NDE problems," Proceedings of the ISMM International Symposium on Computer Applications in Design, Simulation and Analysis, Acta Press, 1988, pp. 113-116.

[3] L. Udpa and W. Lord, "Diffusion, waves, phase and eddy current imaging," Review of Progress in Quantitative NDE, D.O. Thompson and D.E. Chimenti Eds., Plenum Press, New York, 1984, pp. 499-506.

[4] M.V.K. Chari and P. Silvester, "Analysis of turboalternator magnetic fields by finite elements," *IEEE Transactions on Power Apparatus and Systems*, vol. PAS-90, No. 2, March/April 1971, pp. 454-459.

[5] M.V.K. Chari, A. Konrad, M.A. Palamo and J. D'Angelo, "Three dimensional vector potential analysis for machine field problems," *IEEE Transactions on Magnetics*, vol. MAG -18, No. 2, March 1982, pp. 436-446.

[6] N. Ida and W. Lord, "Simulating electromagnetic NDT probe fields," *IEEE Computer Graphics Applications*, May/June 1983, pp. 21-28.

[7] R. Ludwig and W. Lord, "A finite element study of ultrasonic wave propagation and scattering in an aluminum block," *Materials Evaluation*, January 1988, pp. 108-113.

[8] S. Nath, "Remote field eddy current phenomena," M.S. Thesis, Colorado State University, 1988.

[9] W. Lord and R. Palanisamy, "Development of theoretical models for NDT eddy current phenomena," Eddy Current Characterization of Materials and Structures, G. Birnbaum and G. Free, Eds, ASTM, Philadelphia, 1981, pp. 5-21.

[10] T.G. Kincaid and M.V.K. Chari, "The application of finite element method analysis to eddy current nondestructive evaluation," *IEEE Transactions on Magnetics*, vol. MAG-15, No. 6, November 1979, pp. 1956-1960.

[11] R. Palanisamy and W. Lord, "Finite element modeling of electromagnetic NDT phenomena," *IEEE Transactions on Magnetics*, vol. MAG-15, No. 6, November 1979, pp. 1479-1481.

[12] R. Palanisamy and W. Lord, "Prediction of eddy current probe signal trajectories," *IEEE Transactions on Magnetics*, vol. MAG-16, No.5, September 1980. pp. 1083-1085.

[13] W. Lord, "Development of finite element model for eddy current NDT phenomena," EPRI Report, NP-2026, September 1981.

[14] R. Palanisamy, "Finite Element Modeling of Eddy Current Nondestructive Testing Phenomena," Ph.D. Dissertation, Colorado State University, 1980.

[15] N. Ida, "Three Dimensional Finite Element Modeling of Electromagnetic Nondestructive Testing Phenomena," Ph.D. Dissertation, Colorado State University, 1983.

[16] O. Biro and K. Preis, "Finite element analysis of 3-D eddy currents," *IEEE Transactions on Magnetics*, vol. 26, No. 2, March 1990, pp. 418-423.

[17] D. Rodger and J.F. Eastham, "Multiply connected regions in the $A - \xi$ three dimensional eddy current formulation," *IEE Proceedings*, Pt A, vol. 134, No. 1, January 1987, pp. 58-66.

[18] Z. Ren and A. Razek, "New technique for solving three dimensional multiply connected eddy-current problems." *IEE Proceedings*, vol. 137, Pt. A, No. 3, May 1990, pp. 135-140.

[19] A. Nicolas, "3D eddy current solution by BIE techniques," *IEEE Transactions on Magnetics*, vol. 24, No.1, January 1988, pp.130-133.

[20] R. Beissner, "Boundary integral model of eddy current flaw detection in three dimensions," *Journal of Applied Physics*, vol. 60, No. 1, July 1986, pp. 352-356.

[21] D. Rodger, "Differential methods, finite elements and applications," Industrial Applications of Electromagnetic Computer Codes, Y.R. Crutzen et al. Eds, Kluwer Academic, Dordrecht, 1990, pp. 51-79.

[22] A. Bossavit and J. C. Verite, "A mixed FEM-BIEM method to solve eddy current problems," *IEEE Transactions on Magnetics*, vol. MAG-18, No. 2, March 1982, pp. 431-435.

[23] O. Biro and K. Preis, "On the use of magnetic vector potential finite element analysis of three dimensional eddy currents," *IEEE Transactions on Magnetics*, vol. 25, No. 4, July 1989, pp. 3145-3159.

[24] R.L. Ferrari, "Complementary variational formulation for eddy current problems using the field variables E and H directly," *IEE Proceedings*, vol. 132, Pt. A, No. 4, July 1985, pp. 157-164.

[25] R. Albanese and G. Rubinacci, "Integral formulation for 3D eddy current computation using edge elements," *IEE Proceedings*, vol. 135, Pt. A, No. 7, September 1988, pp. 457-462.

[26] N.A. Demerdash and T.W. Nehl, "An evaluation of the methods of finite elements and finite differences in the solution of nonlinear electromagnetic fields in electrical machines," *IEEE Transactions on Power Apparatus and Systems*, vol. PAS-98, No. 1, January/February 1979, pp. 74-87.

[27] T. Tortschanoff, "Survey of numerical methods in field calculations," *IEEE Transactions on Magnetics*, vol. MAG-20, No. 5, September 1984, pp. 1912-1917.

[28] M.D.R. Beasley et al., "Comparative study of three methods for computing electric fields," *IEE Proceedings*, vol. 126, No. 1, January 1979, pp. 126-134.

[29] A. Krawczyk and J. Turkowski, "Recent developments in eddy current analysis," *IEEE Transactions on Magnetics*, vol. MAG-23, No. 5, September 1987, pp. 3032-3037.

[30] P. Girdino, P. Molfino and G. Molinari, "The versatiality of a multiformulational approach in the solution of electromagnetic field problems," *IEEE Transactions on Magnetics*, vol. MAG-23, No. 5, September 1987, pp. 3284-3289.

[31] S.J. Salon and J.M. Schneider, "A comparison of boundary integral and finite element formulation of the eddy current problem," *IEEE Transactions on Power Apparatus and Systems*, vol. PAS-100, No. 4, April 1981, pp. 1473-1479.

[32] G. Molinari, "Guidelines for an effective usage and procedures of validation," Industrial Application of Electromagnetic Computer Codes, Y.R.Crutzen et al. Eds, Kluwer Academic, Dordrecht, 1990, pp. 101-120.

[33] C.W. Trowbridge, "Electromagnetic computing: The way ahead?," *IEEE Transactions on Magnetics*, vol. 24, No. 1, January 1988, pp. 13-18.

[34] C.W. Trowbridge, "Overview of the 'state of the art' in electromagnetic analysis and design," Industrial Application of Electromagnetic Computer Codes. Y.R.Crutzen et al. Eds, Kluwer Academic, Dordrecht, 1990, pp. 1-27.

[35] O.C. Zienkiewicz, Finite element method, 3rd edition, McGraw Hill, 1977.

[36] P. Silvester and M.V.K. Chari, "Finite element solution of saturable magnetic field problems," *IEEE Transactions on Power Apparatus and Systems*, vol. PAS-89, No. 7, September- October 1970, pp. 1642-1648.

[37] O.W. Anderson, "Transformer leakage flux program based on the finite element method," *IEEE Transactions on Power Apparatus and Systems*, vol. PAS-92. March/April 1973, pp. 682-689.

[38] M.V.K. Chari, "Finite element solution of the eddy current problem in magnetic structures," *IEEE Transactions on Power Apparatus and Systems*, vol. PAS-93. No. 1, January-February 1974, pp. 62-72.

[39] O.W. Anderson, "Finite element solution of complex potential electric fields," *IEEE Transactions on Power Apparatus and Systems*, vol. PAS-96, No. 4. July/August 1977, pp. 1156- 1161.

[40] J.R. Brauer, "Finite element analysis of electromagnetic induction in transformers," Presented at the IEEE Winter Power Meeting, New York, January 1977.

[41] R.O. Ritchie and K.J. Bathe, "On the calibration of the electric potential technique for monitoring crack growth using finite elements," *International Journal of Fracture*, vol. 15, No. 1, February 1979, pp. 45-55.

[42] G.H. Aronson and R.O. Ritchie, "Optimization of the electric potential technique for crack growth monitoring in compact test pieces using finite elements," *Journal of Testing and Evaluation*, vol. 7, No. 4, July 1979, pp. 209-215.

[43] J.H. Hwang and W. Lord, "Finite element modeling of magnetic field/defect interaction," *Journal of Testing and Evaluation*, vol. 3, No. 1, January 1975. pp. 21-25.

[44] W. Lord and J.H. Hwang, "Defect characterization from magnetic leakage fields," *British Journal of Nondestructive Testing*, January 1977, pp. 14-18.

[45] S.R. Satish and W.Lord, "A variable reluctance probe for the detection of magnetite buildup in steam generator tubing," presented at the DARPA/AF Review of Progress in Quantitative NDE, Boulder, Colorado, August 1981.

[46] S.R. Satish and W. Lord, "Hall plate measurements of magnetite buildup in pressurized water reactor steam generators," *IEEE Transactions on Instrumentation and Measurement*, vol. IM-32, No. 3, September 1983, pp. 414-418.

[47] W. Lord, "Flux distribution-pipeline flaws," AGA Final Report, Project Pr 179-713, 1988.

[48] M.V.K. Chari, "Finite element solution of magnetic and electric field problems in electrical machines and devices," Finite Elements in Electrical and Magnetic Field Problems, Eds. M.V.K. Chari and P. Silvester, John Wiley and Sons. New York, 1979, pp.87-108.

[49] W. Lord, Electromagnetic Methods of Nondestructive Testing, Gordon and Breach, London, 1985.

[50] W. Lord, "Eddy current methods of flaw detection and their modeling," Electromagnetomechanical Interaction in Deformable Solids and Structures, edited by Y. Yamamoto and K. Miya, North Holland Press, 1987, pp. 202-214.

[51] W. Lord and R. Palanisamy, "Magnetic probe inspection of steam generator tubing," *Materials Evaluation*, vol. 38, No. 5, May 1980, pp. 38-40.

[52] R. Palanisamy and W. Lord, "Finite element simulation of support plate and tube defect eddy current signals in steam generator NDT," *Materials Evaluation*, vol. 39, No. 7, June 1981, pp. 651-655.

[53] R. Palanisamy and W. Lord, "Finite element analysis of eddy current phenomena," *Materials Evaluation*, vol. 38, No. 10, October 1980, pp. 39-43.

[54] N. Ida and W. Lord, "3-D finite element modeling of eddy current NDT phenomena," *IEEE Transactions on Magnetics*, vol. 21, 1985, pp. 2635-2643.

[55] W. Lord et al., "A finite element study of the remote field eddy current phenomenon," *IEEE Transactions on Magnetics*, vol. 24, No. 1, January 1988, pp. 435-438.

[56] Y.S. Sun et al., "3-D finite element modeling of the remote field eddy current effect," Review of Progress in Quantitative NDE, Eds. D.O. Thompson and D. Chimenti, Plenum Press, New York, vol. 9A, 1989, pp. 319-326.

[57] D.L. Atherton, B. Szpunar and S. Sullivan, "The application of the finite element calculation of the remote field inspection technique," *Materials Evaluation*, vol. 45, September 1987, pp. 1083-1086.

[58] H. Hoshikawa et. al., "Study of the remote field eddy current testing," Electromagnetomechanical Interaction in Deformable Solids and Structures, edited by Y. Yamamoto and K. Miya, North Holland Press, Amsterdam, 1987.

[59] R. Ludwig and X.W. Dai, "Numerical and analytical modeling of pulsed eddy currents in a conducting half space," *IEEE Transactions on Magnetics*, vol. 26, 1990, pp. 299-307.

[60] D. Rodger, T. Karaguler and P.J. Leonard, "A formulation for 3D moving conductor eddy current problems," *IEEE Transactions on Magnetics*, vol. 25, No. 5, September 1989, p. 4147-4149.

[61] D. Rodger, P.J. Leonard and T. Karaguler, "An optimal formulation for 3D moving conductor eddy current problems with smooth rotors," *IEEE Transactions on Magnetics*, vol. 26, No. 5, September 1990, pp. 2359-2363.

[62] Y.K. Shin and W. Lord, "Numerical modeling of probe velocity effects for eddy current and flux leakage NDE," Review of Progress in Quantitative NDE, Eds. D.O. Thompson and D. Chimenti, vol. 10A, Plenum Press, New York, 1991, pp. 921-926.

[63] N. Ida, R. Palanisamy and W. Lord, "Eddy current probe design using finite element analysis," *Materials Evaluation*, vol. 41, November 1983, pp. 1389-1394.

[64] J.F. Cardenas-Garcia et. al., "Finite element modeling of 3D capacitive array sensors for NDE applications," Review of Progress in Quantitative NDE, Eds. D.O. Thompson and D. Chimenti, vol. 10A, Plenum Press, New York, 1991, pp. 927-934.

[65] R.F. Harrington, "The method of moments in electromagnetics," *Journal of Electromagnetic Waves and Applications*, vol. 1, No. 3, 1987, pp. 181-200.

[66] C.A. Brebbia, The Boundary Element Method for Engineers, Pentech Press, London, 1978.

[67] J.Simkin, "A comparison of integral and differential equation solution of field problems," *IEEE Transactions on Magnetics*, vol. Mag-18, No. 2, March 1982, pp. 401-405.

[68] I.D. Mayergoyz, "Boundary integral equation of minimum order for the calculation of three dimensional eddy current problems," *IEEE Transactions on Magnetics*, vol. Mag-18, No. 2, March 1982, pp. 536-539.

[69] J.H. McWhirter et.al.,"Computational methods for solving static field and eddy current problems via Fredholm integral equations," *IEEE Transactions on Magnetics*, vol. Mag-15, No. 3, May 1979, pp. 1075-1074.

[70] M.H. Lean and A.Wexler, "Accurate field computation with the boundary element method," *IEEE Transactions on Magnetics*, Mag-18, No. 2, 1982, pp. 331-335.

[71] M.H. Lean and A. Wexler, "Accurate numerical integration of singular boundary element kernels over boundaries with curvature," *International Journal of Numerical Methods in Engineering*, vol. 21, No. 2, 1985, pp. 211-228.

[72] M.H. Lean, M. Freidman and A. Wexler, "Application of the boundary element method in electrical engineering problems," Developments in Boundary Element Methods - I, P.K. Banerjee and R.Butterfield Eds., Applied Science Publishers, London, 1979, pp. 207-250.

[73] M.H. Lean, "Application of boundary integral equation methods to electromagnetics," *IEEE Transactions on Magnetics*, vol. Mag-21, No. 5, September 1985. pp. 1823-1828.

[74] C.W. Trowbridge, "Applications of integral equation methods to the numerical solution of magnetostatic and eddy-current problems," Finite Elements in Electrical and Magnetic Field Probles, Eds., M.V.K. Chari and P. Silvester. John Wiley and Sons, New York, 1979, pp.191-213.

[75] W.M. Rucker and K.R. Richter, "Three dimensional magnetostatic field calculations using the boundary element method," *IEEE Transactions on Magnetics*. vol. Mag-24, No. 1, January 1988, pp. 23-26.

[76] W.M. Rucker and K.R. Richter, "A BEM code for 3-D eddy current calculations," *IEEE Transactions on Magnetics*, vol. 26. No. 2, March 1985. pp. 462-465.

[77] K.R. Richter and W.M. Rucker, "Numerical foundations, integral methods and applications," Industrial Application of Electromagnetic Computer Codes, Y.R. Crutzen et al. Eds, Kluwer Academic, Dordrecht, 1990, pp. 29-50.

[78] H.Tsuboi, "On the boundary integral expression for 3-D eddy current analysis," *COMPEL*, vol. 9, Supplement A, 1990, pp. 37-40.

[79] H. Tsuboi and M. Tanaka, "Three dimensional eddy current analysis by the boundary element method using vector potential," *IEEE Transactions on Magnetics*, vol. 26, No. 2, March 1990, pp. 454-457.

[80] A. Nicolas, "3D eddy current solution by the BIE techniques," *IEEE Transactions on Magnetics*, vol. 24, No. 1, January 1989, pp. 130-133.

[81] R.E. Beissner, "Boundary element model of eddy current flaw detection in three dimensions," *Journal of Applied Physics*, 60(1), July 1986, pp. 352-356.

[82] R.E. Beissner, "Scalar potential model of eddy current interaction with three dimensional flaws," *Journal of Nondestructive Evaluation*, vol. 7, Nos. 1/2, 1988, pp. 15-21.

[83] R.E. Beissner, "Boundary element modeling in eddy current NDE: a review," *Electrosoft*, vol. 2/3, June/September 1991, pp. 122-141.

[84] W. Scott Dunbar, "The volume integral method of eddy current modeling," *Journal of Nondestructive Evaluation*, vol. 5, No. 1, 1985, pp. 9-14.

[85] A.H. Kahn, "Boundary integral equation methods for two dimensional models of crack field interactions," *Journal of Nondestructive Evaluation*, vol. 7, Nos. 1/2, 1988, pp. 3-14.

[86] H.Tsuboi, T. Misaki and T. Kikuta, "Computation of three dimensional electromagnetic field in eddy current testing of steel pipes," *IEEE Transactions on Magnetics*, vol. 24, No. 6, November 1988, pp. 3168-3170.

[87] M.P. Connolly, D.H. Michael, R. Collins, "The inversion of surface potential measurements to determine crack size and shape," *Journal of Applied Physics*, 64(5),1, September 1988.

[88] R.K. Livesly, J.J. Modi and T. Smithers, "The use of parallel computation for finite element calculations," Parallel Computing, M. Feilmeier and G. Joubert and U. Schendel, Eds., Elsevier Science Publishers, London, 1986, pp. 149-156.

[89] N. Ida, "Finite element computation on SIMD and MIMD parallel computer," *COMPEL*, vol. 9, Supplement A, 1990, pp. 177-180.

[90] C.F. Bryant et. al., "Parallel processing and the integration of analysis and design in electromagnetics computation," *COMPEL*, vol. 9, Supplement A, 1990, pp. 171-176.

[91] B.H. McDonald and A. Wexler, "Finite element solution of unbounded field problems," *IEEE Transactions on Microwave Theory and Techniques*, vol. MTT-20, No. 12, December 1972, pp.

[92] J. D'Angelo, "Hybrid finite element/boundary element analysis of electromagnetic fields," Topics in Boundary Element Research, Edited by C. Brebbia, Springer-Verlag, Heidelberg, July 1989, pp. 151-180.

[93] S.J. Salon and J. D'Angelo, "Applications of the hybrid finite element-boundary element method in electromagnetics," *IEEE Transactions on Magnetics*, vol. 24, No. 1, January 1988, pp. 80-85.

[94] J.M. Schneider, The Finite Element-Boundary Integral Hybrid Method and its Applications to Two-Dimensional Electromagnetic Field Problems, Ph.D. Dissertation, Rensselear Polytechnic Institute, 1982.

[95] J.P. Peng and S.J. Salon, "Hybrid finite element boundary element solutions using half space Green's functions," *Journal of Applied Physics*, 55(6), March 1984, pp. 2198-2200.

[96] F. Matsuoka, "Calculation of a three dimensional eddy current by the FEM-BEM coupling method," Electromagnetomechanical Interactions in Deformable Solids and Structures, edited by Y. Yamamoto and K. Miya, North Holland Press, Amsterdam, 1987, pp. 169-174.

[97] P. Bettess, "Infinite elements," *International Journal of Numerical Math in Engineering*, vol. 11, 1977, pp. 53-64.

[98] P. Silvester et al., "Exterior finite elements for 2-dimensional field problems with open boundaries," *IEE Proceedings*, 124, 1977, pp. 1743-1747.

[99] M.V.K. Chari, "Electromagnetic field computation of open boundary problems by a semianalytical approach," *IEEE Transactions on Magnetics*, vol. 23, No. 5, September 1987, pp. 3566-3568.

[100] T. Nakata, James and James, eds, 3-D Electromagnetic Field Analysis, *COMPEL*, vol. 9, supplement A, 1990.

[101] H.H. Johnson, "Calibrating the electric potential drop method for studying slow crack growth," *Materials Research and Standards*, vol. 5, No. 9, September 1965, pp. 442-445.

[102] K.H. Schwalbe and D. Hellman, "Application of the electric potential method to crack length measurements using Johnson's formula," *Journal of Testing and Evaluation*, vol. 9, No. 3, May 1981, pp. 218-221.

[103] R.O. Ritchie, G.G. Garretti and J.F. Knott, "Crack growth monitoring: Optimization of the electrical potential technique using an analogue method," *International Journal of Fracture Mechanics*, vol. 7, 1971, pp. 462-467.

[104] C. P. You and J.F. Knott, "Electrolytic tank simulation of the potential drop technique for crack length determinations," *International Journal of Fracture*, vol. 23, 1983, pp. R139-R141.

[105] D.P. Romilly, "Development of the DC potential drop method for one and two dimensional crack growth monitoring," *Experimental Techniques*, May/June 1990, pp. 22-27.

[106] Che-Yu Li and R.P. Wei, "Calibrating the electric potential method for studying slow crack growth," *Journal of Testing and Evaluation*, vol. 6, No. 8, August 1966, pp. 392-394.

[107] G. Clark and J.F. Knott, "Measurement of fracture cracks in notched specimens by means of theoretical electrical potential calibrations," *Journal of Mechanics and Physics of Solids*, vol. 23, No. 4/5, August/October 1975, pp. 265-276.

[108] M.E. Orazem and W. Ruch, "An improved analysis of the potential drop method for measuring crack lengths in compact tension specimens," *International Journal of Fracture*, vol. 31, 1986, pp. 245-252.

[109] W.D. Dover et al., "AC field measurement - Theory and practice," The Measurement of Crack length and Shape during Fracture and Fatigue, Ed. C.J. Beevers, Engineering Materials Advisory Sevices, West Midlands, U.K, 1980, pp. 222-260.

[110] W. Dover et al., "The use of AC field measurements to determine the shape and size of a crack in a metal," Eddy Current Characterization of Materials and Structures, Eds. G. Birnbaum and G. Free, ASTM, 1981, STP 722, pp. 401-427.

[111] R. Collins, W.D. Dover and D.H. Michael, "The use of AC field measurements for nondestructive testing," Nondestructive Testing, vol. 8, Ed. R.S. Sharpe, Academic Press, London, Chapter 5, 1985.

[112] R. Collins, D. Mirshekhar-Syahkal and D.H. Michael, "The mathematical analysis of electromagnetic fields around surface cracks in metals," Review of Progress in Quantitative NDE, Eds. D.O. Thompson and D.E. Chimenti, Plenum Press, New York, vol. 2B, 1983, pp. 1255-1268.

[113] M.C. Lugg and D.A. Topp, "ACFM technology applied to the measurement of coating thickness and displacement," *British Journal of NDT*, vol. 33, No. 1, January 1991, pp. 4-6.

[114] R. Collins, D.H. Michael and K.B. Ranger, "The AC field around a plane semi-elliptical crack in a metal surface," Proceedings of the 13th Symposium on Nondestructive Evaluation, San Antonio, Texas, 1981, pp. 470-479.

[115] D.H. Michael, R.T. Waechter and R. Collins, "The measurement of surface cracks in metals by using AC electric fields," Proceedings of Royal Society, London, vol. A381, 1982, pp. 139-156.

[116] D. Mirshekhar-Syahkal, R. Collins and D.H. Michael, "Developments in surface crack detection by the AC field technique," Review of Progresss in Quantitative NDE, Eds. D.O. Thompson and D.E. Chimenti, Plenum Press, New York, vol. 4A, 1985, pp. 349-357.

[117] D.H.Michael and R. Collins, "The AC field around a plane crack in a metal surface when the skin depth is large," *Journal of Nondestructive Evaluation*, vol. 3, No. 1, 1982, pp. 19-24.

[118] D.H. Michael et al., "Thick skin modeling for surface breaking cracks," Review of Progress in Quantitative NDE, D.O. Thompson and D.E. Chimenti Eds., Plenum Press, New York, vol. 7A, 1988, pp. 191-197.

[119] A.M. Lewis, D.H. Michael, M.C. Lugg and R. Collins, "Thin skin electromagnetic fields around surface breaking cracks in metals," *Journal of Applied Physics*, vol. 64, No. 8, October 1988, pp. 3777-3783.

[120] M. McIver, "Characterization of surface breaking cracks in metal sheets by using AC electric fields," Proceedings Royal Society, London, vol. A421, 1989 , pp. 179-194.

[121] H. Takahashi and K. Miya, "Crack shape recognition based on AC potential," *Electrosoft*, vol. 2/3, June/September 1991, pp. 104-121.

[122] C.A. Balanis, Advanced Engineering Electromagnetics, John Wiley & Sons, New York, 1989.

[123] R.B. Guenther and J.W. Lee, Partial Differential Equations of Mathematical Physics and Integral Equations, Prentice-Hall, New York, 1988.

[124] T.J. Rudolphi, Class notes EM526, Boundary Element Method, Iowa State University, Spring 1990.

[125] C.F. Bryant, C.R.I. Emson and C.W. Trowbridge, "A comparison of Lorentz gauge formulation in eddy current computations," *IEEE Transactions on Magnetics*, vol. 26, No. 3, March 1990, pp. 430-433.

[126] T. Morisue, "Magnetic vector potential and electric scalar potential in three dimensional eddy current problems," *IEEE Transcations on Magnetics*, vol. MAG-18, No. 2, March 1982, pp. 531-535.

[127] S. Hasebe and Y. Kano, "About treatment of gauge of A in 3-D magnetostatic analysis," *IEEE Transactions on Magnetics*, vol. MAG-23, September 1987, pp. 3305-3307.

[128] C.S. Biddlecombe et al.,"Methods for eddy current computation in three dimensions," *IEEE Transactions on Magnetics*, vol. MAG-18, No. 2, March 1982, pp. 492-497.

[129] C.R.I. Emson and J. Simkin, "An optimal method for 3-D eddy currents," *IEEE Transactions on Magnetics*, vol. MAG-19, 1983, pp. 2443-2446.

[130] T. Nakata et al.,"Comparison of various methods for 3-D eddy current analysis," *IEEE Transactions on Magnetics*, vol. 24, No. 6, November 1988, pp. 3159-3161.

[131] M. Sarma, "Potential functions in electromagnetic field problems," *IEEE Transactions on Magnetics*, vol. MAG 6, No. 3, September 1970, pp. 513-518.

[132] N.A. Demerdash, T.W. Nehl and F.A. Fouad, "Finite element formulation and analysis of three dimensional magnetic field problems," *IEEE Transactions on Magnetics*, vol. MAG-16, No. 5, September 1980, pp. 1092-1094.

[133] S. Nath, W. Lord and T.J. Rudolphi, "Hybrid numerical methods for electromagnetic NDE," Review of Progress in Quantitative NDE, D.O. Thompson and D.E. Chimenti Eds, Plenum Press, New York, vol. 10A, 1990, pp. 317-324.

[134] S. Nath, "Boundary integral and finite element simulation of potential drop NDE measurements," *Electrosoft*, vol. 2, No. 2/3, June/September 1991, pp. 92-103.

[135] S.Nath, T.J. Rudolphi and W. Lord, "Comparative study of the finite element and boundary element analyses of the DC potential drop method," *Materials Evaluation*, vol. 50, No. 1, January 1992, pp. 51-55.

[136] Z. You, "Finite element analysis of ultrasonic imaging," Ph.D. Dissertation, Iowa State University, 1991.

[137] S.K. Burke, "A benchmark problem for computation of ΔZ in eddy current nondestructive evaluation (NDE)," *Journal of Nondestructive Evaluation*, vol. 7, Nos. 1/2, 1988, pp. 35-41.

[138] T.Onuki and H.Shimamoto, "Hybrid boundary element and finite element analysis for eddy current problems," Proceedings of the First Joint Japan/US Symposium on Boundary Element Methods, October 1988, pp. 347-354.

[139] T. Onuki, "Hybrid finite and boundary element method applied to electromagnetic problems," *IEEE Transactions on Mangnetics*, vol. 26, No. 2, March 1990, pp. 582-587.

[140] J.E. Akin, Application and Implementation of Finite Element Methods, Academic Press, New York, 1982.

APPENDIX A. SHAPE FUNCTIONS FOR ISOPARAMETRIC ELEMENTS

- 3 node triangular element for 2D finite elements

$$N_1(r,s) = 1 - r - s$$
$$N_2(r,s) = r$$
$$N_3(r,s) = s$$

- 4 node quadrilateral element for 2D finite elements and 3D boundary elements

$$N_1(r,s) = \frac{1}{4}(1-r)(1-s)$$
$$N_2(r,s) = \frac{1}{4}(1+r)(1-s)$$
$$N_3(r,s) = \frac{1}{4}(1+r)(1+s)$$
$$N_4(r,s) = \frac{1}{4}(1-r)(1+s)$$

- 8 node box elements for 3D finite elements

$$N_1(r,s,t) = \frac{1}{8}(1+r)(1-s)(1-t)$$
$$N_2(r,s,t) = \frac{1}{8}(1+r)(1+s)(1-t)$$
$$N_3(r,s,t) = \frac{1}{8}(1-r)(1+s)(1-t)$$
$$N_4(r,s,t) = \frac{1}{8}(1-r)(1-s)(1-t)$$
$$N_5(r,s,t) = \frac{1}{8}(1+r)(1-s)(1+t)$$

$$N_6(r,s,t) = \tfrac{1}{8}(1+r)(1+s)(1+t)$$
$$N_7(r,s,t) = \tfrac{1}{8}(1-r)(1+s)(1+t)$$
$$N_8(r,s,t) = \tfrac{1}{8}(1-r)(1+s)(1+t)$$

APPENDIX B. DIRAC DELTA FUNCTION $\delta(\vec{r})$ AND ITS PROPERTIES

Definition:

$$\delta(\vec{r}) = 0 \qquad \vec{r} \neq 0$$

$$\int f(\vec{r})\delta(\vec{r})d\tau = f(0)$$

Special case :

$$\int \delta(\vec{r})d\tau = 1$$

If the origin is shifted, then the shift property of the delta function results as:

$$\delta(\vec{r_1} - \vec{r_2}) = 0 \qquad r_1 \neq r_2$$

$$\int f(\vec{r_1})\delta(\vec{r_1} - \vec{r_2})d\tau = f(\vec{r_2})$$

$$\delta(\vec{r_1} - \vec{r_2}) = \delta(\vec{r_2} - \vec{r_1})$$

In general $\delta(\vec{r})$ is not really a function, since it is undefined (infinite) at $\vec{r} = 0$. It is therefore defined as a *distribution* [123].

APPENDIX C. DERIVATION OF THE GREEN'S FUNCTION FOR THE ACPD METHOD IN 2 DIMENSIONS

The governing equation for the ACPD method in 2D is the scalar Helmholtz equation given by

$$\nabla^2 \vec{E} - k^2 \vec{E} = 0 \tag{C.1}$$

where $k^2 = j\omega\mu\sigma$. From equation (4.1), the Green's function satisfies

$$LG(\vec{r_1}, \vec{r_2}) = \delta(\vec{r_1} - \vec{r_2}) \tag{C.2}$$

where L is the Sturm Liouville operator. Thus

$$G(\vec{r_1}, \vec{r_2}) = L^{-1}\delta(\vec{r_1} - \vec{r_2}) \tag{C.3}$$

For this particular case, $L = \nabla^2 - k^2$, thus

$$(\nabla^2 - k^2)G(\vec{r_1}, \vec{r_2}) = \delta(\vec{r_1} - \vec{r_2}) \tag{C.4}$$

Integrating both sides over a small volume gives:

$$\begin{aligned} \int_v \nabla^2 - k^2)G(\vec{r_1}, \vec{r_2})dv &= \int_v \delta(\vec{r_1} - \vec{r_2})dv \\ \int_v \nabla^2 - k^2)G(\vec{r_1}, \vec{r_2})dv &= 1 \end{aligned} \tag{C.5}$$

Condsider equation (B.4), and using the cylindircal coordinate system (r, θ, z), gives:

$$\begin{aligned} \nabla^2 G &= \frac{1}{r}\frac{\partial}{\partial r}(r\frac{\partial G}{\partial r}) + \frac{1}{r^2}\frac{\partial^2 G}{\partial \theta^2} \\ &= \frac{\partial^2 G}{\partial r^2} + \frac{1}{r}\frac{\partial G}{\partial r} + \frac{1}{r^2}\frac{\partial^2 G}{\partial \theta^2} \end{aligned} \tag{C.6}$$

In 2D, it is assumed that G is constant in the θ direction, and $\frac{\partial^2 G}{\partial \theta^2} = 0$. Thus for this case,

$$\begin{aligned} \frac{\partial^2 G}{\partial r^2} + \frac{1}{r}\frac{\partial G}{\partial r} - k^2 G = 0 \qquad & r \neq 0 \\ \frac{\partial^2 G}{\partial r^2} + \frac{1}{r}\frac{\partial G}{\partial r} - k^2 G = \infty \qquad & r = 0 \end{aligned} \tag{C.7}$$

For $r \neq 0$,

$$r^2\frac{\partial^2 G}{\partial r^2} + r\frac{\partial G}{\partial r} - r^2 k^2 G = 0 \tag{C.8}$$

The solution of the above equation is given as [123]

$$G(\vec{r_1}, \vec{r_2}) = AI_0(rk) + BK_0(rk) \tag{C.9}$$

where I_0 and K_0 are the modified Bessel functions. To determine the constants A and B by considering the asymptotic behaviour of the functions I_0 and K_0.

The asymptotic limits for I_0 and K_0 are :

As $r \to 0$, $K_0 \to \infty$ and $I_0 \to 1$ and as $r \to \infty$, $K_0 \to 0$ and $I_0 \to \infty$

Thus as $r \to 0$, $A = 0$. Thus the solution is

$$G = BK_0(rk)$$

From applying appropriate boundary conditions and further limit analysis, $B = \frac{1}{2\pi}$.

The Green's function for the ACPD method in 2D is

$$G(\vec{r_1}, \vec{r_2}) = \frac{1}{2\pi}K_0(rk) \tag{C.10}$$

APPENDIX D. NUMERICAL INTEGRATION

The need for numerical integration is to find the elemental contribution in the finite and boundary element formulation using isoparametric elements.

An integral evaluated using Gauss quadrature is written as

$$\int_a^b f(x)dx = \sum_i w_i f'(x_i) \tag{D.1}$$

where w_i are a set of special weights attached to the quadrature points x_i. These weights and points are well documented in the literature.

For a linear element the minimum number of quadrature points is one and for a second order element at least two quadrature points are necessary. In this dissertation, the two point quadrature scheme is used. It can be written as

$$\int_{-1}^{1}\int_{-1}^{1}\int_{-1}^{1} f'(r,s,t)drdsdt = \sum_{k=1}^{2}\sum_{j=1}^{2}\sum_{i=1}^{2} w_i w_j w_k f'(r',s',t') \tag{D.2}$$

where s,t and q are the quadrature points in the three directions. w_i, w_j and w_k are the correponding weights. Thus a total of eight quadrature points are needed to integrate over each element. Table C.1 and Table C.2 give the quadrature points and weights.

Table D.1: Two point Gauss quadrature weights and points

Weights	Gauss Points
1.0	-.577350269189626
1.0	+.577350269189626

Table D.2: Three point Gauss quadrature weights and points

Weights	Gauss Points
.555555555555556	-0.774596669241483
.888888888888889	0.0
.555555555555557	+0.774596669241483